AD/A-006 728

ELECTRICAL DISCHARGES IN WATER. A HYDRODYNAMIC DESCRIPTION

K. A. Naugolnykh, et al

Foreign Technology Division
Wright-Patterson Air Force Base, Ohio

23 December 1974

Unclassified

Security Classification

AD/A006728

DOCUMENT CONTROL DATA - R & D

(Security classification of title, body of abstract and indexing annotation must be entered when the overall report is classified)

1 ORIGINATING ACTIVITY (Corporate author) Foreign Technology Division Air Force Systems Command U. S. Air Force	2a. REPORT SECURITY CLASSIFICATION Unclassified 2b. GROUP

3. REPORT TITLE

ELECTRICAL DISCHARGES IN WATER. A HYDRODYNAMIC DESCRIPTION

4. DESCRIPTIVE NOTES (Type of report and inclusive dates)

Trahslation

5. AUTHOR(S) (First name, middle initial, last name)

K. A. Naurol'nykh, N. A. Roy

6. REPORT DATE	7a. TOTAL NO. OF PAGES	7b. NO OF REFS
1971	212	76

8a. CONTRACT OR GRANT NO b. PROJECT NO c. d.	9a. ORIGINATOR'S REPORT NUMBER(S) FTD-HC-23-2049-74 9b. OTHER REPORT NO(S) (Any other numbers that may be assigned this report)

10. DISTRIBUTION STATEMENT

Approved for public release;
distribution unlimited.

11. SUPPLEMENTARY NOTES	12. SPONSORING MILITARY ACTIVITY
	Foreign Technology Division Wright-Patterson AFB Ohio

13. ABSTRACT

09,20

i

DD FORM 1473

Unclassified

Security Classification

EDITED TRANSLATION

FTD-HC-23-2049-74 23 December 1974

ELECTRICAL DISCHARGES IN WATER. A HYDRODYNAMIC DESCRIPTION

By: K. A. Naugol'nykh, N. A. Roy

English pages: 205

Source: Elektricheskiye Razryady v Vode (Gidrodinamicheskoye Opisaniye) 1971, pp. 1-155

Country of Origin: USSR
Translated under: F33657-72-D-0854
Requester: AFWL/IN
Approved for public release;
distribution unlimited.

PREPARED BY:

TRANSLATION DIVISION
FOREIGN TECHNOLOGY DIVISION
WP-AFB, OHIO.

U. S. BOARD ON GEOGRAPHIC NAMES TRANSLITERATION SYSTEM

Block	Italic	Transliteration	Block	Italic	Transliteration
А а	*А а*	A, a	Р р	*Р р*	R, r
Б б	*Б б*	B, b	С с	*С с*	S, s
В в	*В в*	V, v	Т т	*Т т*	T, t
Г г	*Г г*	G, g	У у	*У у*	U, u
Д д	*Д д*	D, d	Ф ф	*Ф ф*	F, f
Е е	*Е е*	Ye, ye; E, e*	Х х	*Х х*	Kh, kh
Ж ж	*Ж ж*	Zh, zh	Ц ц	*Ц ц*	Ts, ts
З з	*З з*	Z, z	Ч ч	*Ч ч*	Ch, ch
И и	*И и*	I, i	Ш ш	*Ш ш*	Sh, sh
Й й	*Й й*	Y, y	Щ щ	*Щ щ*	Shch, shch
К к	*К к*	K, k	Ъ ъ	*Ъ ъ*	"
Л л	*Л л*	L, l	Ы ы	*Ы ы*	Y, y
М м	*М м*	M, m	Ь ь	*Ь ь*	'
Н н	*Н н*	N, n	Э э	*Э э*	E, e
О о	*О о*	O, o	Ю ю	*Ю ю*	Yu, yu
П п	*П п*	P, p	Я я	*Я я*	Ya, ya

*ye initially, after vowels, and after ъ, ь; e elsewhere. When written as ё in Russian, transliterate as yё or ё. The use of diacritical marks is preferred, but such marks may be omitted when expediency dictates.

* * * * * * * * * * *

GRAPHICS DISCLAIMER

All figures, graphics, tables, equations, etc. merged into this translation were extracted from the best quality copy available.

RUSSIAN AND ENGLISH TRIGONOMETRIC FUNCTIONS

Russian	English
sin	sin
cos	cos
tg	tan
ctg	cot
sec	sec
cosec	csc
sh	sinh
ch	cosh
th	tanh
cth	coth
sch	sech
csch	csch
arc sin	$\sin^{-1}$
arc cos	$\cos^{-1}$
arc tg	$\tan^{-1}$
arc ctg	$\cot^{-1}$
arc sec	$\sec^{-1}$
arc cosec	$\csc^{-1}$
arc sh	$\sinh^{-1}$
arc ch	$\cosh^{-1}$
arc th	$\tanh^{-1}$
arc cth	$\coth^{-1}$
arc sch	sech^{-1}
arc csch	csch^{-1}

---

rot	curl
lg	log

TABLE OF CONTENTS

FTD-HC-23-2049-74

ACADEMY OF SCIENCES USSR

ACOUSTIC INSTITUTE

K. A. Naugol'nykh, N. A. Roy

Electrical Discharges in Water

(A Hydrodynamic Description)

Nauka Press

Moscow, 1971

UDC 537.528

Electrical discharges in water. K. A. Naugol'nykh, N. A. Roy, Nauka Press, 1971, 155 pp.

This monograph is dedicated to an investigation of the hydrodynamic phenomena during electrical discharges in a liquid. The book is based primarily on the studies of the authors and their colleagues in this area. This monograph presents a qualitative picture of the phenomena during an electrical discharge in water in their actual sequence. Means of initiating an electrical discharge in a liquid are described. The physical processes taking place in the discharge channel and the properties of the matter in it are examined. Experimental information on the electrical characteristics of a discharge and the rates of expansion of the channel are presented. Theoretical models of a discharge as a hydrodynamic phenomenon are examined and the results of calculations are compared with experimental data.

This book is intended for scientific workers - physicists and specialists using electrical discharges in a liquid as sources of pressure pulses. Fifteen tables, 90 illustrations, 76 bibliographical references.

Editor in Chief

Doctor Physical-Mathematical Sciences
Yu. P. Rayser

CHAPTER 1

IN PLACE OF AN INTRODUCTION

1. An Electrical Discharge in a Liquid - A Process With a High Concentration of Energy.

The development of technology has brought to the attention of physics the task of investigating processes with great concentrations of energy, high pressures and temperatures. A pulsed electrical discharge in a liquid is one such process. The high temperature and pressure arise as a result of the rapid release of energy of a condenser in the discharge channel. These qualities of pulsed electrical discharges in liquids are used widely in the development of new technological processes of machining different materials and in the creation of new means of energy conversion.

In 1944 B. R. Lazarenko and N. I. Lazarenko [1] mentioned the possibility of using pulsed electrical discharges in a liquid for machining metal. At the present time this method has obtained wide use in many branches of industry. The electrosparking of metals basically makes use of the ability of pulsed discharges in a liquid to create a dense high-temperature plasma. The liquid here primarily functions to inhibit expansion of the channel, as a consequence of which the density of the energy released in the channel is increased and, consequently, the temperature and pressure of the plasma in the channel are raised. The physical foundations of electrosparking of metal have been studied intensively [2].

Thanks to the high temperature and pressure of the plasma in the channel pulsed electrical discharges in water may serve as a source of high intensity light [3].

At different times many investigators have turned their attention to the ability of pulsed electrical discharges in water

to create high pressures. The fact that a discharge in a liquid may have destructive force was recorded in 1767-1769 by Lane and Priestly [4, 5]. The possibility of creating cumulative jets under the influence of the pressure arising during an electrical discharge in a liquid was mentioned in 1944 by Pokrovskiy and Stanyukovich [6]. Prungel [7] in 1948 undertook the first attempt to measure the electromechanical efficiency of a discharge in water. The possible applications of an electrical discharge in seismic surveying were mentioned in 1952 by Vogel [8] and in 1955 by Mazov and Meyer [9]. The active popularization of the applications of this phenomenon by Yutkim [10] led to the wide application of pulsed electrical discharges in water for performing such classic manufacturing processes as stamping, grinding, fettling, and so forth.

Pulsed electrical discharges in water are used as powerful sound sources, useful in hydroacoustic and hydrogeological research [11, 12].

In practice discharges with highly distinctive parameters are used. The principal parameters - the energy of the discharge and its duration - may vary within a very wide range. While in the case of electrosparking of metals the discharge energy amounts to a few joules, in manufacturing processes and in devices in which a discharge serves as a source of pressure pulses, the energy of one discharge reaches 10^3 - 10^5 J. The durations of the discharges also may differ significantly. Usually, discharges are used at close to critical conditions since these conditions provide for the most rapid transmission of the energy of the storage device into the discharge channel, and, as will be shown below, the greatest electroacoustic efficiency. The duration of a discharge in this case is determined approximately by the value $2\pi\sqrt{LC}$, where L and C are respectively the inductance and capacitance of the discharge circuit. Discharge durations lie in the range from tenths to hundreds of microseconds. The pulsed electrical strengths developed during discharge reach values on the order of 10^2 - 10^5 kW.

Depending on the energy of a discharge and its duration, the energy densities in the discharge channel may also differ significantly, in some cases reaching values of 10^2 - 10^3 J/cm^2, which in all is only one order of magnitude below the energy density in the case of explosions of solid explosives. The pressure in the channel is raised to several thousand atmospheres, and the temperature - to several tens of thousands of degrees. In some cases, when the magnetic energy density is on the same order of magnitude as the gas kinetic energy density of the particles in the channel, the influence of magnetic pressure on the channel (the pinch effect) may prove to be significant. In practice, primarily discharges with moderate energy densities are used in a channel, the expansion of the channel causing a disturbance of the density of the surrounding liquid, small in comparison with the equilibrium state, and the magnetic pressure is small in comparison with the kinetic gas pressure.

The physical phenomena which appear during an electrical discharge in a liquid had not been studied sufficiently. In particular, the hydrodynamic characteristics of discharges, a knowledge of which is important for practical applications, have been studied insufficiently. The present monograph is dedicated to the investigation of electrical discharges from the hydrodynamic point of view.

In this study, basically, we examine electrical discharges in water with moderate energy densities in the channel, since this case is the most interesting for many applications of an electrical discharge as a source of pressure pulses.

A quantitative picture of the phenomena during an electrical discharge in water in their actual sequence is presented in the next section of this chapter.

The means of initiating an electrical discharge in a liquid used experimentally are described in Chapter 2.

The processes which take place in the discharge channel and the properties of the matter in it are examined in Chapter 3. Experimental information on the electrical characteristics of the discharge and the rates of expansion of the channel, and also estimates of the pressures and temperatures in the discharge channel, are presented. The properties of the low temperature dense plasma formed in the discharge channel are examined and an energy balance equation is derived. The specific form of this equation depends on the form of the equation defining the pressure in the channel as a function of the radius of the channel and its derivatives. In order to determine this relationship in different cases, hydrodynamic problems of the expansion of a cavity in a liquid are examined in Chapter 4.

On the basis of the results of the third and fourth chapters, theoretical models of an electrical discharge in water are constructed in Chapter 5.

The results of calculations are compared with experiments in Chapter 6.

This monograph is based primarily on the studies of the authors and their colleagues: D. P. Frolov, M. I. Charushina, A. I. Ioffe, V. Ye. Gordueyev, K. P. Krivosheyev, V. I. Nemchenko, B. N. Drapezo, N. G. Kozhelupova, and R. A. Volchenkova, who took part in the study in different stages. The authors extend them their most sincere thanks. The authors also thank L. M. Kvasova for her help in preparing the manuscript for printing.

2. Physical Phenomena During an Electrical Discharge in Water.

The principle phenomena characteristic of electrical discharges in a liquid are described briefly in this section. First we consider the so-called pre-discharge stage, during the course of which the discharge channel closing the gap between the electrodes is

formed, and then consider the phenomena which take place during the release of the energy of the condenser in the discharge channel, and finally, the pulsations of the gas bubble after the discharge.

A typical process of the initiation of a discharge is the breakdown of theelectrode gap in a liquid under the influence of the electric voltage appearing on the electrodes when a charged condenser is connected with them. In the voltage range used in practice (1-100 kV), two breakdown mechanisms are known: the streamer, or leader meachanism, corresponding to high voltages, and the thermal mechanism which takes place in the case of low voltages. The most favorable conditions for the appearance of a leader breakdown occur in the case of high voltage non-uniform fields between a positive point and a negative plane. As a result of the breakaway of the Townsend ionization rushing to the point, leaders are formed, growing in the direction ofthe ionization centers on which the Townsend ionization was formed. This process is reminiscent of gas breakdown. The set of leaders on the positive point have the form of a brush corona. The closure of the electrode gap by one of the leaders leads to the completion of the process of their formation of the discharge channel. This mechanism provides for the breakdown of electrode gaps several centimeters in length with voltages of several tens of kilovolts. The breakdown lag, that is, the time between the moments of switching on the voltage and forming the channel, in the case of leader breakdown is practically independent of the amount of hydrostatic pressure, at least up to 1000 atm.

In the case of low voltages the leader mechanism of breakdown is replaced by the thermal mechanism. Heating and evaporation of the water near the electrodes takes place under the influence of conduction current. As a result, a gas "bridge", along which the breakdown of the electrode gap takes place, is formed between the electrodes. Distinctive features of this mechanism of a discharge initiation are the great breakdown delay, reaching a value of several milliseconds, the short length of the gaps which can be

broken down, and the great increase in the breakdown lag with an increase in hydrostatic pressure.

A discharge may be initiated, if technological factors require it, also with the use of auxilliary means.

After the formation of a channel an intense discharge current, reaching tens and hundreds of kiloamps, heats the plasma even at the initial stage of the discharge to a temperature on the order of 10^4 °K. During the discharge process, while the current is flowing, the plasma temperature varies insignificantly, dropping after the end of the discharge.

Heating the plasma produces an increase in pressure in the channel. Under the influence of the elevated pressure the channel expands. The pressure in the channel passes through a maximum during the discharge process: in the initial stage of the discharge the pressure in the channel increases, in spite of the increase in its volume, and drops only toward the end of the discharge. A pressure in the channel at the maximum reaches a value on the order of 10^3 atm in the case of a moderate energy density in the channel.

The plasma density during the discharge process varies insignificantly and is maintained at a level of 10^{20} particles/cm^{-3}. This takes place because the decrease in plasma density due to the expansion of the channel is compensated by the arival of new particles as the result of the evaporation of water from the channel wall.

The resistance of the channel in the initial stage of the discharge drops because of the increase in the cross section of the channel and because of a certain increase in the specific conductance of the plasma. Toward the end of the discharge the resistance of the channel increases in spite of the continuing expansion of the channel.

This takes place because of the cooling of the plasma and deionization caused by this process.

The expansion of the channel continues even after energy ceases to be released, first under the influence of the pressure which is elevated in comparison with the hydrostatic pressure, and then as a result of the inertia of the flowing liquid. In the post-discharge state, the channel is converted into a gas bubble. The expansion of the bubble continues until the kinetic energy of the flow is completely converted into the potential energy of the bubble, the pressure in which is significantly less than the hydrostatic pressure. Then, reverse motion of the liquid takes place under the influence of the hydrostatic pressure. The potential energy again is converted into the kinetic energy of the converging flow. When the cavity is slammed shut the pressure of the gas in it increases sharply. Under the influence of this pressure the liquid is thrown back, and the process is repeated in the form of several successive damping pulsations. The period of the pulsations and

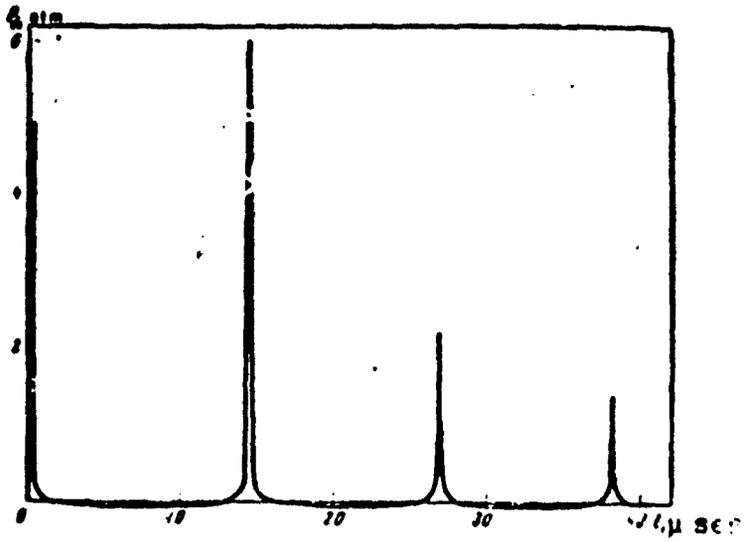

Figure 1.1. Profile of compression wave emitted by an electrical discharge in a liquid.

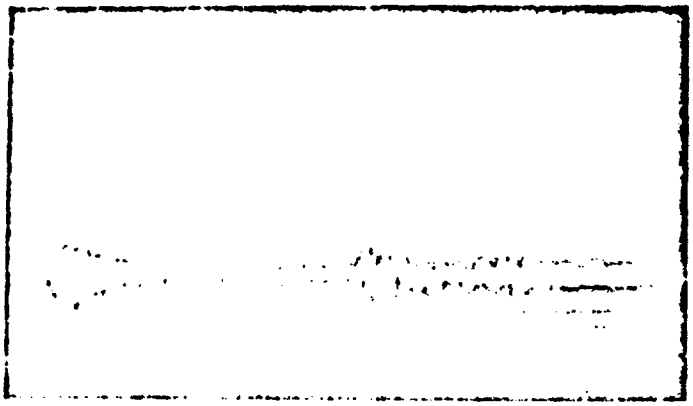

Figure 1.2. Oscillogram of compression wave at a distance of 1 m from a discharge.

the maximum bubble radius are determined by the amount of energy released in the channel.

The expansion of the channel in the discharge stage and the subsequent pulsations of the bubble are accompanied by the emission of compression and rarefaction waves. Compression waves are emitted in the discharge stage and during the following bubble welding, when the high pressure in the channel and then in the compressed bubble causes compaction of the adjacent layers of liquid. Compression waves alternate with relatively long rarefaction waves, which are emitted in stages when the pressure in the bubble is lower than the hydrostatic pressure. A typical profile of a compression wave arising in a liquid as a result of an electrical discharge is shown in Figs. 1.1 and 1.2.

In the case of the intensive release of energy the rate of expansion of the channel may become comparable to the speed of sound in the liquid and even exceed it. In these cases a compression wave propagating in a liquid is converted into a shock wave in the immediate vicinity of the channel or even is emitted immediately in the form of a shock wave. The energy released in the discharge channel basically is expended in the work performed by the channel during expansion (around 50%), and in heating the matter in the discharge channel.

The work performed by the channel is subdivided into the compression wave energy emitted in the discharge stage (up to 20%), and the gas bubble pulsation energy, equal to the potential energy of the bubble at the moment of maximum volume (up to 30%). The pulsation energy gradually is consumed in the emission of compression and rarefaction waves and in other losses.

Fig. 1.1 shows a schematicized profile of a pressure wave, and Fig. 1.2 a profile recorded experimentally at a distance of 1 m from a discharge channel 0.9 μf in capacity at 30 kV; the length of the channel is 6 cm; the inductance of the discharge circuit is 3 μH; the time markings are 1 msec; the amplitude of the compression pulse emitted by the discharge in the direction perpendicular to the channel is 9 atm. In the channel of this discharge, the conditions of which are close to critical, around 350 J of energy m about 10 μsec was released. Pulses, reflected from the tank wall and from the free surface of the water, are seen on the experimental curve after the compression pulses.

REFERENCES

1. *Лазаренко Б. Р., Лазаренко Н. И.* Электрическая эрозия металлов. М., Госэнергоиздат, 1944.
2. Физические основы электроискровой обработки материалов. Сборник статей. М., изд-во «Наука», 1966.
3. *Early H. C., Martin E. A.* — Commun. and Electronics, 1956, 1, 788.
4. *Lane T.* — Philos. Trans., 1767, p. 451.
5. *Priestly J.* — Philos. Trans., 1769, p. 57.
6. *Покровский Г. И., Станюкович К. П.* — Изв. АН СССР, серия физ., 1944, 8, 214.
7. *Frungee F.* — Optik, 1948, 3, 124.
8. *Vogel C. B.* — Geophysics, 1952, 17.
9. *Малов М. Р., Мещер Г. И.* — Труды лаборатории аэрометодов АН СССР, 1955, 4, 119—122.
10. *Юшкин Л. А.* Электрогидравлический эффект. М., Машгиз, 1955.
11. Bur. Ships J., 1962, 3, 4.
12. *Rechen E. V.* Marine Sciences Instrument., 3 Proc. 3 Nat. Marine Sci. Symps. N. Y. Plenum Press, 1956.

CHAPTER 2

DISCHARGE INITIATION

1. Introduction.

Discharge initiation is understood as meaning the process of creating a current conducting channel, closing an electrode gap, in a liquid. This process may be based upon different physical phenomena. The principal one is the breakdown of the liquid under the influence of voltage applied to the electrodes. With sufficiently high electric intensities, the breakdown of a liquid, similar to the breakdown of a gas, is characterized by the formation of leaders which develop from one electrode to another. In the case of low field intensities and in liquids having sufficiently high conductivity, a gas cavity, along which electric breakdown then takes place, first forms between the electrodes.

In addition to these phenomena other means may also be used for initiating a discharge, for example, the vaporization of small wet metal wires with which the electrodes are connected preliminarily. For discharge initiation it is possible to use preliminary breakdown of the electrode gap under the influence of high voltage from an auxilliary source, and also breakdown along a gas bubble artificially formed between the electrodes.

The variety of methods of initiating discharges stems from the necessity of creating discharges in different conditions, namely: under different initial working voltages, in liquids with different conductances and under different hydrostatic pressures, and also from the necessity of forming discharge channels with different parameters. The latter is important for matching the resistance of the channel with the resistance of the conducting circuit in order to create insignificant losses in transmitting energy from the condenser to the channel.

In addition, when using electrical discharges as sources of compression pulses it is necessary that the mean resistance of the channel with respect to time be close to the critical resistance of the discharge circuit. Fulfilling this condition, as will be shown below, provides for the maximum efficiency of the discharge. For investigative purposes sometimes it is necessary to obtain a channel of a certain form, for example cylindrical; this is easy to do by initiating discharges with wires.

The method of initiation used usually must provide for a brief initiation process in comparison with the duration of the discharge itself for stability of the discharge and for low energy consumption.

In the following sections we shall consider several methods of initiating discharges in water.

2. Initiating discharges by high voltage breakdown in weakly conducting water.

The conductance of water exerts significant influence on the processes of discharge initiation. In cases important for practical purposes conductances may vary within quite wide limits: from a value on the order of 10^{-4} (ohm x cm)$^{-1}$ for tap water to a value on the order of 10^{-2} (ohm x cm)$^{-1}$ for sea water. Discharges in weakly conducting water are used most widely. Discharge initiation in this case usually is primed by means of electrode gap breakdown under the influence of high voltage applied to electrodes. The voltages used here reach 100 kV. The mechanism of breakdown under the action of high voltages comes down to the formation and development of leaders up to the point where one of them closes the electrode gap.

For leader formation it is necessary that the field strength at the electrode surface exceed a threshold value on the order of several tens of kilovolts per centimeter. Point - plane or point -

point type electrodes, creating an intensely non-uniform field, are used to create the maximum possible field strengths. The field strength at a point with a radius of curvature r which is less than the length of the electrode gap l, may be found according to the approximation formula

$$E \approx \frac{2u}{r \ln \frac{4l}{r}} \qquad (2.1)$$

- for point-plane type electrodes and according to the formula

$$E \approx \frac{u}{r \ln \frac{2l}{r}} \qquad (2.2)$$

- for point-point type electrodes.

These formulas show that the field strength at a point is determined primarily by the radius of curvature of the point r and by the voltage u, it being higher for the case of electrodes of the point-plane type.

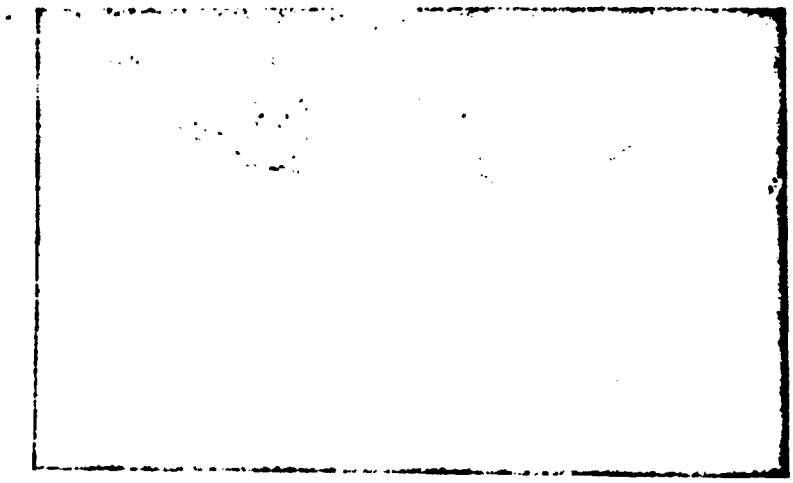

Figure 2.1. Discharge channel.

The minimum field strength, calculated according to formula (2.1), at which leaders still appear, proves to be approximately equal to 36 kV/cm and corresponds to the case of a positive point in the negative plane [1]. This result is obtained in experiments with a point in the form of a rod insulated with a vacuum rubber

Figure 2.2. Discharge channel.

Figure 2.3. Development of streamers in tap water. Positive electrode point, negative plate. u_0 = 108 kV, electrode gap 17.5 cm.

tube 8 mm in diameter with a tip sharpened into a cone with an angle of 30°. The radius of curvature of the point was 0.5 - 4 mm and the water contact area was 0.8 - 4 cm^2. The voltages used were in the 16 - 100 kV range, and the capacitance of the storage device varied within the limits of 0.01 - 10 μf. The reliability of the minimum amount of field strength corresponding to the threshold of the appearance of leaders is unknown for other conditions, not so much because of the approximate nature of the calculating formula, but because of distortions of the field at the electrode point introduced by different factors. The degree of surface roughness of the electrode plays a significant role in the process of leader formation. A [illegible] in leader formation was observed after

polishing the tip [2]. It is possible that a gap film, the breakdown of which also is an indicator of leader formation, is formed during the delay as a result of water being heated by the current on the electrode. The presence of roughness facilitates the formation of gas bubbles at individual points. Insulation of the lateral surface of the point plays a significant role in the process of leader formation. Insulation is necessary in order to exclude

Figure 2.4. Development of streamers in tap water. Positive electrode point, negative plate. u_0 = 108 kV, electrode gap 16.5 cm.

Figure 2.5. Development of a streamer in tap water. Negative electrode point, positive plate. u_0 = 108 kV, electrode gap 1.5 cm.

contact of the high voltage electrodes with other parts of the device. The presence of insulation creates field distortion due to the appearance of charges settling on the surface of the insulating dielectric. The formation of a leader therefore takes place, as a rule, not on the point, where the theoretical field strength is at a maximum, but at the border of the electrode with the insulation. This phenomenon is seen clearly in a photograph of a discharge between electrodes in the form of two rods 10 mm in diameter and with an electrode gap of 2.5 cm. The voltage on the electrodes

before breakdown is 50 kV (Figs. 2.1 and 2.2 [2]). This effect leads to the destruction of the insulation and limits the service life of the electrode.

Electrode polarity has a marked influence on leader formation. The pre-leader time - the time of the formation of a leader for a negative point in the positive plane - is somewhat less than in the case of a positive point if the field strengths do not exceed 85 kV/cm. In the case of high field strength, approximately 350 kV/cm, the situation is the reverse. In this case, the time of leader formation is not more than 0.5 sec for a positive point, and for a negative one, 1 - 2 μsec [1].

The development of leaders in the gaps between a point in a plane takes place significantly differently depending on what polarity the point has [3].

In the case of a positive point, the Townsend ionizations rushing to the point from the individual centers of ionization, "mark out" the path for the growth of leaders. Figs. 2.3 and 2.4 show photographs of the streamer picture which appears in an electrode gap 17.5 and 16.5 cm long formed by a positive tip and a negative grinded plane in tap water. The working voltage of the storage device is 108 kV, and the capacitance is 0.1 μf. The positive electrode was the end of an RK-3 cable with the outer insulation and braiding removed; the diameter of the high voltage insulation is 9 mm and the diameter of the inner wire is 1.37 mm.

In the case of a negative point the electric field "blows out" electrons from the point, evidently, significantly more uniformly. A negative space charge is formed around the point, lowering the field strength in the area of the negative electrode. This effect hinders leader formation. In this situation the presence of a positive surface charge on the electrode insulation plays an important role.

The field picture changes sharply thanks to these charges. Great field gradients appear in the direction from the point to the insulation surface, and a leader is formed in this direction. A leader, spreading along the insulation surface of a negative electrode point, is shown in the photograph given in Fig. 2.5. This photograph was taken in conditions differing from the conditions which obtained in the case of the photographs in Figs. 2.3 and 2.4 only by the fact that the electrode polarity is changed and the inner electrode distance is decreased to 1.5 cm.

Thus, the most favorable conditions for the appearance of leaders, necessary for closing an electrode gap, exists on a positive high voltage point. The dynamics of the growth of leaders in the electrode gap formed by a positive point and a negative plane depends on the amount of voltage, the capacitance of the storage device, and the amount of point area in contact with the water. Information on the development of leaders usually is obtained by means of photographing leaders by the self-exposure method, examples of which are the photographs in Figs. 2.3 - 2.5; by high speed motion picture photography, an example of which is shown in Fig. 2.6; by photography with the use of image conversion [4]; by motion picture photography with direct illumination [5] and by oscillography of the discharge current and voltage in the electrode gap.

The following basic rules will be established according to the results of an experimental investigation of the development of leaders.

The magnitude of the strength at a point, depending on the voltage and radius of curvature of the point surface, in contact with the water, determines the number of leaders which appear. The higher the field strength, the greater is the number of leaders which develop. A quantitative idea of the dependence may be obtained according to photographs of the brush corona on Fig. 2.3, taken at 10[illegible] kv and on Fig. 2.7 and 2.8, where the corona on the

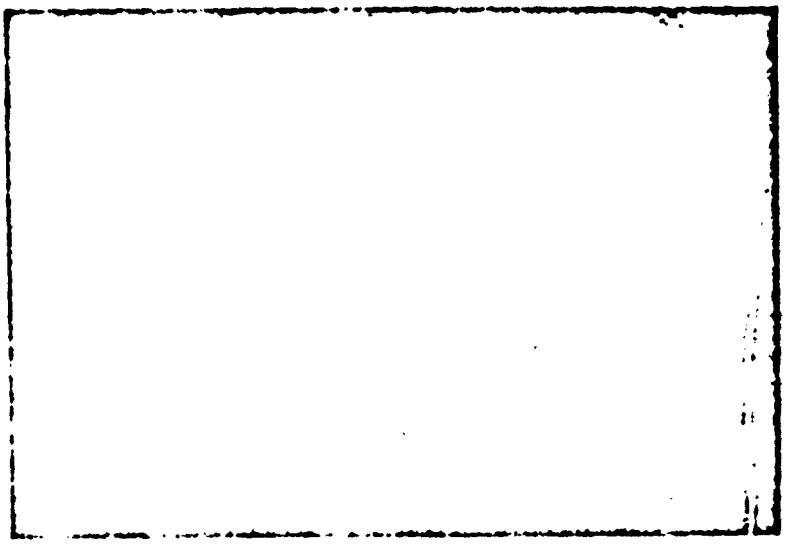

Figure 2.6. Photographs of streamer development.

same electrodes is depicted, but with a voltage of 30 kV, a condenser capacitance of 0.33 μf and electrode gaps of, respectively, 10 and 9 cm. In these photographs it is obvious that at 36kV the number of leaders is significantly less than at 108 kV. This is explained by the fact that with an increase in field strength avalanches are formed on nucleii having a higher ionization potential.

After the formation of the leaders, their development is determined by the field strength at their heads. When the field strengths prove to be lower than a certain critical value, the formation of avalanches ceases and the growth of the leader stops. The field strengths at the head of a leader drop for two reasons: due to a voltage drop along the length of the leader and due to a decrease in voltage on the electrodes as a consequence of the discharge of the condenser. Therefore, the higher is the voltage on the condenser, and the greater its capacitance, the greater is maximum length of leaders. For example, in the case of a capacitance 0.1 μf and voltages of 10, 30 and 100 kV, the maximum length of the leaders formed on a positive electrode made of a

RK-3 cable, is equal, respectively, to 1, 4 and 15 cm. If we leave the voltage equal to 30 kV, then with condenser capacitances of 0.1, 0.2, 0.4, 0.9 and 1.6 μf the maximum leader length will be, respectively, 4, 4.5, 5, 5.5 and 6 cm. The maximum leader length passes through a maximum if the voltage is increased, maintaining the energy of the storage device constant. In this case, the effect of the increasing voltage first is neutralized, and then is cancelled by the effect of the reduction in the constant time of the condenser discharge due to the reduction in capacitance and also due to the reduction in the resistance of the electrode gap because of the increase of coronal branching.

Kuzhekin [1] obtained empirical formulas characterizing the growth of positive leaders, valid for the following conditions: voltage range u = 15 - 100 kV, condenser capacitance range C = 0.1 - 10 μf, point area S = 0.8 - 4 cm^2. The point is made in the form of a rod 8 mm in diameter, sharpened into a cone with an angle of 30°, and a radius of curvature of the tip of the cone r = 0.5 - 4 mm. The conductivity of water $\sigma \sim 10^{-4}$ $(ohm \times cm)^{-1}$, and the negative electrode is a plate.

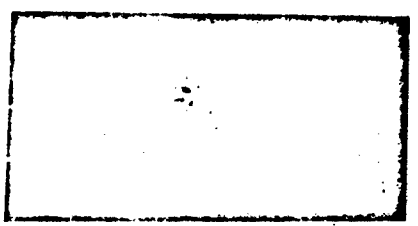

Figure 2.7. Brush corona. Positive electrode - point.

For these conditions the maximum length of the leaders, and, consequently, the maximum disruptive length of the electrode gap is determined by the formula

$$l_{max} = \sqrt{\frac{2.5 C_0^2 \left(\frac{u^2}{u_0^2} - 4\frac{u}{u_0} + \ln 12 \frac{u^2}{u_0^2}\right)}{4 \left(\ldots\right) a}} + 1.25^2 - 1.25 \text{ [cm]}. \qquad (2.3)$$

Here $u_0 = 18 \times 10^3 \ln 4l/r$ is the voltage corresponding to the minimum field strength at which leaders still appear (36 kV/cm); a is a constant equal to 3600 sec x V^2/cm; l is the distance between electrodes.

The length of a gap requiring not more than 10% of the energy of the storage device for its own disruption is determined by the formula

$$l_{\Delta W=10\%} = \sqrt{\frac{0,035C(u-u_0)^2}{\sqrt{S_{a3}}} + 1,25^2} - 1,25 \text{ [cm]}. \qquad (2.4)$$

These formulas give incorrect results if, in particular, the amount of point area is less than the lower limit of the above-mentioned range of variation of S, for example, in the case of an electrode made of an RK-3 cable, when the area amounts to several square millimeters.

Let us consider the development of leaders in time. As high-speed motion picture photography shows [2], the "growth" of leaders takes place with interruptions. The interruptions result, evidently,

Figure 2.8. Brush corona. Positive electrode - point.

from two causes: The leader head running into gas bubble - cavitation nucleii, increases the radius of curvature of the leader head and thus reduces the field strength on it, and lags in avalanch formation due to the temporary absence of centers of ionization with sufficiently low ionization potentials in the liquid near the leader head. The number of interruptions and their duration depend on the amount of voltage - with an increase in voltage these values decrease. As a result, the average rate of growth of a leader,

determined as the ratio of the length of the disruptive distance to the amount of breakdown lag, depends on the voltage. The average rate of leader growth thus determined also depends upon the lag in leader formation on an electrode, which, in turn, is determined not only by the voltage, but also by the form of the electrode and its structure.

We shall now cite some experimental data on the dependence of the average rate of leader "growth" on the voltage for two types of formation of a positive electrode-point. One of these was made from a rod 8 mm in diameter, insulated with a vacuum tube. The end of the rod was sharpened into a cone with an angle of 30° and a radius of curvature of 0.5 - 4 mm. The average speed at 20 kV was 2×10^4 cm/sec and at 100 kV - 5×10^6 cm/sec [1].

The other electrode was the end of an RK-3 cable. The maximum disruptive distance l, corresponding to the breakdown lag τ, and the average rate of leader growth l/τ with different values of the working voltage are given in Table 2.1. In obtaining these data the amount of condenser energy was held constant and equal to 45 J [6].

TABLE 2.1

u, kv	l, cm	t, τsec	l/τ, cm/sec
52	5	2,5	$2 \cdot 10^6$
30	5	4	$1,3 \cdot 10^6$
21,2	2,5	15	$1,7 \cdot 10^6$
15	1,2	22	$5,5 \cdot 10^4$

The data in Table 2.1 testify to the fact that in case of an electrode-point, made in the form of the end of an RK-3 cable having a substantially smaller area of electrode-water contact than in the preceding case, the average rate of leader growth for the same voltage values prove to be somewhat higher. This effect, evidently, is due to the significantly shorter lag in leader formation on the electrode with the smaller radius of curvature.

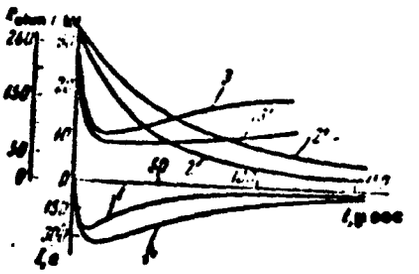

Figure 2.9. Electrical characteristics of a discharge in the absence of absence of breakdown. Length of electrode gap 6 cm, voltage 30 kV.

1,2,3 - current, voltage and resistance in the case of a condenser discharge equal to 0.4 μf; 1', 2', 3' correspond to a condenser discharge of 0.9 μf.

The lifetime of the leaders, if the electrode gap exceeds the maximum length of the leaders, is not limited by the time of their growth. Leaders exist even after reaching the maximum length, the total life time sometimes exceeding the time of leader growth by two orders of magnitude. For illustration, Figs. 2.9 and 2.10 show oscillograms of discharge current and voltage on electrodes, recorded in the case of the discharges of condensers 0.4 and 0.9 μf in capacitance at 30 kV in the case where the leader development is not completed by the breakdown of the electrode gap (Fig. 2.9), with a gap length of 6 cm; and when a channel is formed (Fig. 2.10), with a gap length of 5 cm [3].

In addition, Figs. 2.9 and 2.11 show the time dependences of the electrode gap resistance, calculated according to the oscillograms presented above.

With electric strengths on a point above several hundred kilovolts per centimeter, leader development is practically independent of the hydrostatic pressure up to the maximum value reached experimentally, equal to 1000 atm. This indicates, evidently, a high density of the matter in the leader channels while they are growing. The leader channel expansion seen in the photograph against a background of illumination produced with a certain lag relative to the discharge indicates that the matter in the leader channels is heated and under high pressure. However, the electrostatic efficiency of discharges where no channel is formed is small: the ratio of the energy of the compression wave to the energy stored in

the condenser does not exceed a few tenths of a percent [3]. This is connected with the fact that because of the great ballast resistance of water the energy liberated in the leader channels is small.

In conclusion we note that the initiation of discharges in tap water by breakdown under the influence of high voltage takes place over the course of very short intervals of time, on the order of several microseconds, requires a small consumption of energy, approximately several joules, and takes place with high stability, if a voltage of several tens of kilovolts is applied to a positive electrode having a sufficiently small, on the order of 10 mm^2, exposed surface, and the electrode gap does not exceed approximately two thirds of the maximum leader length for the voltage used.

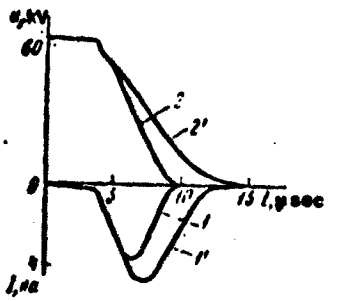

Figure 2.10. Electrical characteristics of a discharge with breakdown. Length of electrode gap 5 cm, voltage 30 k V. 1, 2 and 1', 2' - current and voltage with discharge of condensers 0.4 and 0.9 μf, respectively.

Figure 2.11. Time dependence of resistance with the breakdown of a 5 cm electrode gap with a voltage of 30 k V. Curves 1 and 1' correspond to discharges of condensers of 0.4 and 0.9 μf.

3. Initiation of discharges by high voltage breakdown in highly conducting water.

With an increase in the conductance of water from values on the order of 10^{-4} (ohm x cm)$^{-1}$, corresponding to tap water, to values on the order of 10^{-2} (ohm x cm)$^{-1}$, corresponding to the conductance of sea water, the structure of the brush corona changes substantially. These changes basically come down to the following [3]. The leaders arising on the positive point begin to branch intensively, and their maximum length with a given condenser capacitance is shortened significantly. The corona on the negative point turns into a thick brush of straight short leaders. Figs. 2.12 and 2.13 show photographs of the corona on positive and negative electrodes made in the form of the end of a type RK-2 cable with the outer insulation and braiding removed. The diameter of the high voltage insulation is 7 mm and the diameter of the inner wire 0.6 mm. The capacitance of the condenser - energy storage device is 0.9 μf, and the initial voltage is 30 kV. The water contained around 5% NaCl by weight and had a conductance of 0.069 (ohm x cm)$^{-1}$. According to these photographs it is possible to find that the maximum length of the leaders on the positive point is around 1 cm, while in tap water with a conductance of around 2.8×10^{-4} (ohm x cm)$^{-1}$ and all other conditions being equal, the maximum length of the leaders reached 6 cm.

The increase in branching of the corona together with the increase in conductance of the water causes a significant shortening of the duration of a discharge not completed by a breakdown. Figs. 2.14 and 2.15 show oscillograms of the discharge current and voltage on a positive and, correspondingly, negative electrode-point relative to a grounded electrode. The grounded electrode was made of a brass grid with a 5×5 mm^2 mesh, and in the form of a sphere and surrounded the electrode point. The radius of the sphere was several centimeters. Its size has practically no influence on the electrical characteristics of the discharge. Curves 1 and 1' correspond to the discharge of a 0.9 μf capacitance [illegible] curves 2 and 2' - to the discharge of a

0.1 μf capacitance condenser at 30 and 10 kV, and the inductance of the discharge circuit amounted to several microhenries. Fig. 2.16 shows the dependences of the interelectrode resistance at the moment of maximum current for different values of the capacitance and initial voltage.

The changes observed in the structure of the corona, evidently, are connected with the fact that by increasing the electrolyte concentration in the water the number of Townsend ionization nuclei with a low ionization potential increases. This entails an increase in the branching of the corona on the positive point and an increase in the number of leaders on the negative one. On the other hand, the condenser discharge takes place more rapidly with an increase in the corona surface and water conductance. As a result, the field strength on the head of the leaders decreases rapidly up to the threshold value and the development of the leaders stops earlier than in poorly conducting water. Thus, the length of the electrode gaps which can be broken down is shortened with an increase in conductance, and the energy expended in the pre-breakdown stage increases.

If in the case of the high voltage breakdown of poorly conducting water an insignificantly small fraction of the condonser energy is liberated in the leader channels, with an increase in conductance this fraction significantly increases. This may be judged by the energy characteristics of the hydroacoustic effects, accompanying discharges not completed by a breakdown, in water of high conductance.

Figs. 2.17 and 2.18 show oscillograms of pressure pulses recieved by a broad-band hydrophone at a distance of 50 cm from the pulse corona on positive and, correspondingly, negative points. The construction of the electrodes corresponds to the description pertaining to Figs. 2.14 and 2.15. Curves 1 and 1' refer to discharges of a capacitance of 0.9 μf at 30 and 10 kV; curves 2 and 2' - to discharges of a capacitance of 0.1 μf at 30 and 10 kV. The

acoustic field created by the discharges is sperically symmetrical.

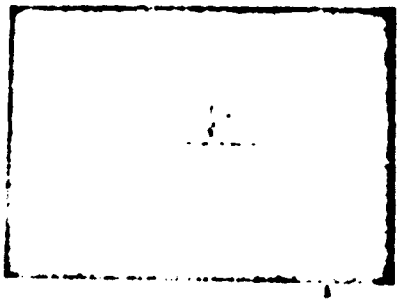

Figure 2.12. Corona on a positive point in salt water.

The duration of the compression pulses is close to the duration of the discharge current. The compression pulses emitted by the corona are reproduced well from discharge to discharge.

Table 2.2 shows experimental values of η of the ratio of the compression pulse energy to the condenser energy for different values of the condenser energy E and initial voltages u on a positive (+) and negative (-) point. The discharge durations τ, found according to oscillograms of the current are indicated in this table. The compression pulse energy is calculated according to the formula

$$W_{ак} = \frac{4\pi r^2}{\rho c}\int_0^{\tau} p^2 dt, \qquad (2.5)$$

where r is the distance from the corona to the hydrophone; ρc is the wave resistance of the water; p is the pressure in the compression wave at the distance r at the moment t.

Another hydrodynamic characteristic of a discharge is the energy of the pulsating bubble. Table 2.2 shows the bubble pulsation periods τ_b and the percentage ratio η_b of the energy of a pulsating bubble to the energy of the condenser. The energy of the bubble is calculated according to the formula [7]

$$W_б = \tau_б^3 p_0^2 / \rho \cdot 1{,}135\eta\%, \qquad (2.6)$$

where p_0 is the hydrostatic pressure; ρ is the water density.

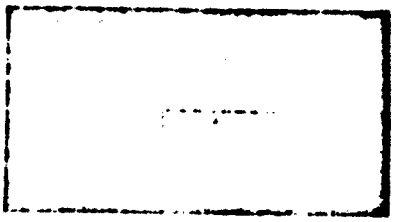

Figure 2.13. Corona on a negative point in salt water.

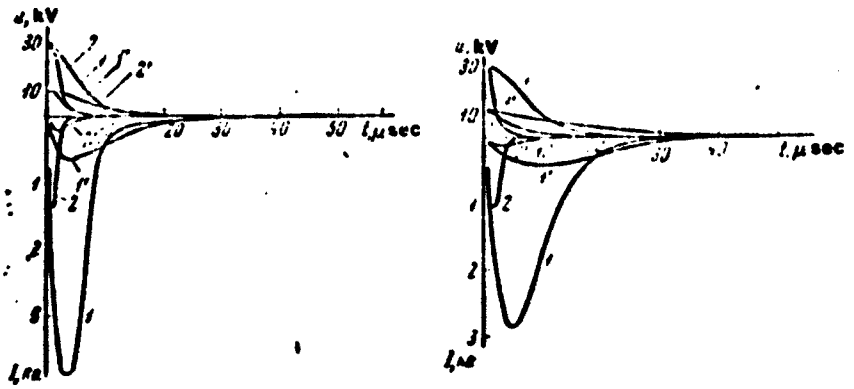

Figure 2.14. Oscillogram of discharge current and voltage in the case of coronal discharge on a positive point 1, 1' correspond to a 0.9 μf condenser at 30 and 10 kV; 2, 2' to the discharge of a 0.1 μf condenser at 30 and 10 kV.

Figure 2.15. Oscillograms of discharge current and voltage in the case of coronal discharge on a negative point.

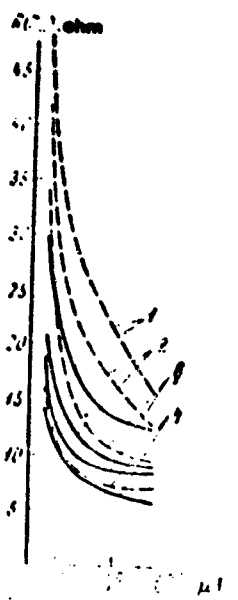

Figure 2.16. Dependence of interelectrode resistance at the moment of maximum current on the condenser capacitance in the case of different initial voltages

Curves 1, 2, 3, 4 correspond to voltages of 10, 15, 21, and 23 kV. Solid lines correspond to a corona on a positive point, and dotted lines - on a negative point.

TABLE 2.2

u, kV	polarity	E, J	τ, μsec	η_p, %	τ_p, msec	η, exp, %
			For 0.1 μf			
10	+	5	8	3,2	1,28	0,8
	−		12,5	4,4	1,43	0,4
15	+	11,3	4,5	2,4	1,53	1
	−		8,6	4,3	1,85	0,6
21,2	+	22,5	4,1	2,4	1,91	1
	−		6,5	5,4	2,33	0,8
30	+	45	3,7	2,3	2,11	1
	−		4,7	6,2	3,33	1,3
			For 0.2 μf			
10	+	10	7	3,8	1,71	0,8
	−		15	5,2	1,9	0,4
15	+	22,5	6,2	3,2	2,11	1
	−		11	5	2,15	0,7
21,2	+	45	5,2	2,5	2,16	0,9
	−		8,8	6	3,3	0,7
30	+	90	4,5	2,6	3,15	0,9
	−		6	7,2	1,4	1
			For 0.4 μf			
10	+	20	11	4,5	2,23	1,1
	−		20	5,8	2,48	0,8
15	+	45	9	3,4	2,73	1,2
	−		16,5	5,9	3,27	0,4
21,2	+	90	7	3,1	3,33	1,4
	−		13	6,7	4,3	0,7
30	+	180	6	3,1	4,21	1,3
	−		92	6,3	5,33	1
			For 0.9 μf			
10	+	45	20	5	3,1	0,9
	−		32	7,2	3,5	0,3
15	+	101	15	3,8	3,7	1
	−		27	6,8	4,5	0,5
21,2	+	202	12,5	3,5	4,55	1,1
	−		21	7	5,7	0,7
30	+	405	10,5	3,1	5,5	1
	−		18	6,4	7,2	1

According to the data in the table it is possible to conclude that the work performed by a discharge, not completed by a breakdown, reaches 7-8% of the condenser energy in the case of highly conducting water.

Such discharges are used for generating pressure impulses used in hydrogeological research [8].

The results presented above refer to comparatively small concentrations of electrolytes. The authors of [5, 9, 10-12], conducted investigations of the breakdown of electrolytes with conductances and concentrations of dissolved substances varying within a wide range of values. The authors of [5, 9-11] came to the conclusion that the "high-voltage behavior" of electrolytes does not depend on the dissolved matter and is determined only by its low voltage electric conductance. Figs. 2.19 and 2.20 show the dependences of the breakdown distance on electrolyte conductance in the case of positive and negative points (the end of an RK-3 cable). The voltage on a condenser of 0.2 and 0.4 μf capacitance was 10, 14 and 16 kV. While in the area of low concentrations there is a clear connection between the breakdown voltage and the length of the electrode gap, in an area of medium and high concentrations the condenser discharges before the breakdown of even a greatly reduced gap takes place.

In [12] the investigation of electrolyte breakdown is extended to an area of electrolyte concentration so high that a drop in electric conductance is observed. For this area it is found that a longer breakdown delay corresponds to the same electric conductance values as in the case of low concentrations.

In conclusion we note that from the point of view of initiating discharges the most significant effect of increasing the electric conductance of the liquid are the reduction in the length of the leaders and the increase in pre-breakdown currents. As a result, even in the case of small electrode gaps it is necessary to deal

with energy losses in the pre-breakdown stage, in particular, in the case of low condenser energies. The use of small electrode gaps

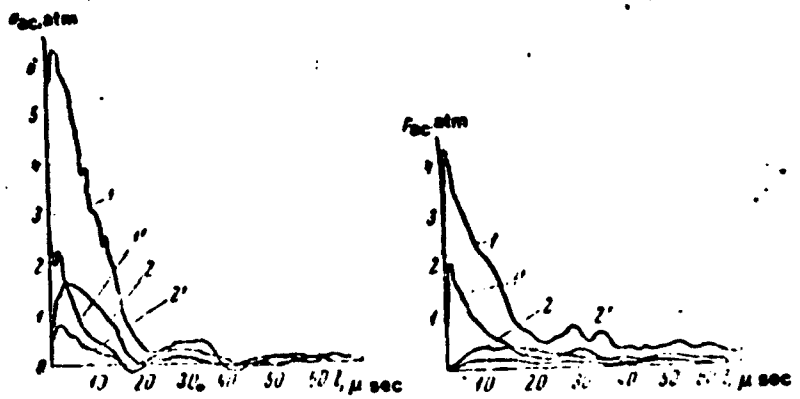

Figure 2.17. Oscillograms of pressure pulses emitted by the corona on a positive point.

Figure 2.18. Oscillograms of pressure pulses emitted by the corona on a negative point.

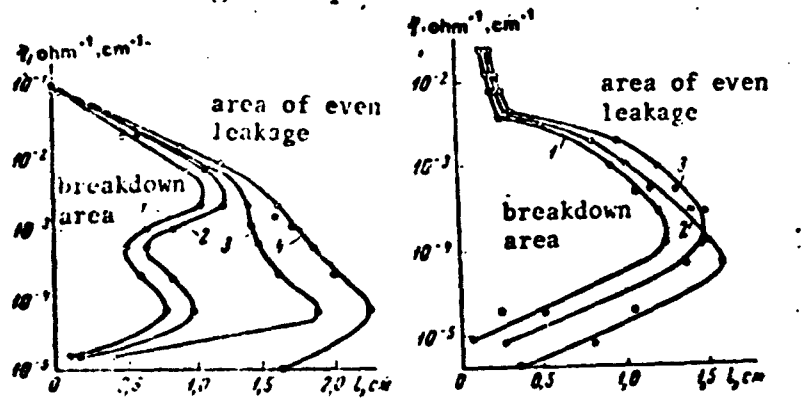

Figure 2.19. Dependence of breakdown distance on the specific electric conductance of a solution (positive point) 1-10 kV, 0.2 μf; 1-10 kV, 0.4 μf; 3-14 kV, 0.2 μf; 4-16 kV, 0.2 μf.

Figure 2.20. Dependence of breakdown distance on the specific electric conductance of the solution (negative point) Symbols as on Fig. 2.19.

requires a reduction in the effective resistance and inductance of the conducting circuit in order to provide a sufficiently complete release of the condenser energy in a discharge channel with low resistance in near-critical conditions.

4. Initiation of discharges by low voltage breakdown of a liquid.

Up until now we have considered the initiation of discharges by the high voltage breakdown of a liquid, in which the processes of the formation and development of leaders played the principle role. With a decrease in voltage the field strength near the electrode may prove to be insufficient for the formation of leaders. For tap water with a conductance on the order of 10^{-4} $(\text{ohm} \times \text{cm})^{-1}$ the critical field strength, according to Kuzhekin's data [1], is approximately 36 kV/cm. In the case of lower strengths the breakdown of the electrode gap takes place along a gas bridge formed as a result of the heating and evaporation of the water by the conduction current. Electrolysis also contributes somewhat to the formation of gas bubbles near the electrodes.

The formation of a gas bridge is an energy consuming process which takes place over the course of very great intervals of time in comparison with the time required for leader growth in the case of high voltage breakdown. For tap water these times are measured in hundreds and thousands of microseconds in relation to the configuration of the electrodes, the amount of voltage, and the length of the electrode gap. The duration of the process of forming a gas bridge is shortened with an increase in the conductance of the water.

Since for the breakdown of the electrode gap it is necessary that the gas bubble reach a certain volume, it proves to be the case that the energy consumption and duration of the breakdown stage depend on the hydrostatic pressure. These circumstances lead to the fact that the use of low voltage breakdown is very ineffective for initiating discharges. However, there is a way out of this situation, which is achieved by using a special electrode configuration: a configuration so that the channel formed after the breakdown of a comparatively small electrode gap, may be lengthened during the discharge process. In particular, the

discharger, schematically shown in Fig. 2.21 satisfies this requirement. Its coaxial electrodes, mounted one inside the other, are separated electrically by an insulating sleeve. Breakdown may take place only between the edges of the ends of the electrodes. The interelectrode clearance equal to the thickness of the insulation, may be on the order of 1 mm if the working voltage on the condenser is on the order of 1 kV. In this case the lag in the breakdown of the electrode gap amounts to several tens of microseconds. It is reduced by increasing the conductance of the water and is little dependent on the hydrostatic pressure, if it does not exceed 10-20 atm.

After the breakdown of the electrode gap a hemispherical bubble filled with plasma is formed. The current flowing along it is forced out by its free magnetic field onto the surface of the bubble. As a result, the axis of the channel acquires the form of an arc, and the effective length of the channel increases during the process of the discharge in proportion to the expansion of the bubble in the liquid.

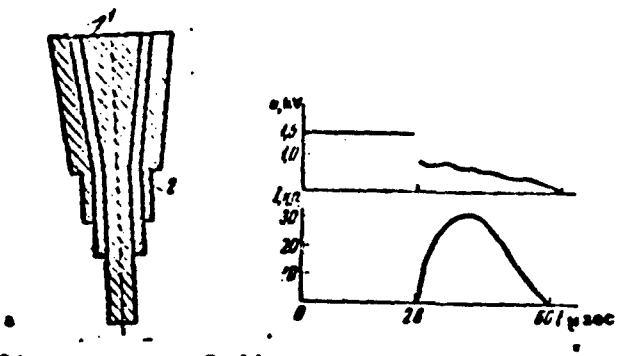

Figure 2.21. Sketch of discharger.
1 - electrodes, 2 - insulating sleeves

Figure 2.22. Oscillograms of current and voltage for the discharge of a condenser.

Thanks to the lengthening of the channel in the process of the discharge its electric resistance proves to be sufficiently high to be able, technically simply without significant losses and at the same time sufficiently rapidly, to transmit the energy of the con-

As an example, Fig. 2.22 shows oscillograms of discharge current and voltage on the electrode of a discharger, corresponding to the method of initiating a discharge described above. The parameters of the discharge circuit are as follows: condenser capacitance 320 μf, initial voltage 1.6 kV, inductance of discharge circuit 0.1 μH, interelectrode clearance - 0.1 cm. The discharge was performed in a 1.5% (by weight) solution of table salt in water. The breakdown lag is, as is seen by the oscillogram of the voltage, around 30 μsec. Around 85% of the energy stored in the condenser is released in the channel.

5. Initiation of discharges by auxilliary means.

The effective initiation of discharges in low conducting water, as follows from the preceeding sections , does not present difficulties only in the case of using high voltages. However, the use of high voltages is connected with certain difficulties. The principal difficulty is the necessity of providing reliable insulation of the high voltage circuits, which is unavoidably connected with increasing the overall dimensions of the units. The use of low voltage discharges with the same energies makes it possible to make significantly more compact units, which in many cases is the deciding factor. Therefore, there is a real purpose in seeking means of efficient initiation of low voltage discharges.

In this section we shall consider three methods of initiating low voltage discharges by auxilliary means: initiation by wire bridges - this method is practically independent of the conductance of the liquid; discharge initiation by a preliminary high voltage breakdown - this method is suitable only for low-conducting liquids, and discharge initiation by a breakdown of the working voltage in a gas bubble, preliminarily formed in the electrode gap by an auxilliary coronal discharge. This method is suitable for initiating discharges in liquids of quite high conductance. The initiation of discharges with wire bridges is based on the use of the electrical explosion of thin wires. This physical phenomenon has

attracted the attention of many researchers over the course of a number of years [13, 14]. In particular, the electrical explosion of wires in a gaseous medium has been subjected to intensive study. The basic features of this type of explosion may be characterized in the following way. Three stages of the process may be observed after the discharge circuit is closed. In the first stage, four situations may arise as a result of the flow of discharge current.

1. Melting - the energy conducted is insufficient for vaporizing the wire.

2. Slow explosion - the time required for the evaporation of the wire is much greater than the time necessary for the development of instabilities in the melted wire.

3. Rapid explosion - the time required for evaporation of the wire is small in comparison with the time required for the development of instability.

4. Explosive ablation - the time required for evaporation is small in comparison with the time required for the penetration of a temperature, equal to the boiling point, to a depth amounting to 1/e of the radius of the wire. The development of an explosion in this situation is determined by the vaporization of the wire from the surface.

The first stage ends with the conversion of the wire into a non-conducting state. After this the second stage begins - a pause in current. The pause in current lasts until the density of the gas in the channel which has expanded after the explosion drops so much that it is possible for the gas to break down under the influence of the voltage remaining on the condenser. The last or third stage begins - discharge along the gas channel.

It is possible that conditions may exist in which either the second or the third, or both of these stages either are absent

or are poorly pronounced. For example, if the condenser energies are sufficient only for vaporization of the wire, the current disappears after the end of the first stage and does not appear again. In the case of tungsten wires there is a poorly pronounced pause in current - current only somewhat decreases after the explosion of the wire and then increases - and the third stage of the process begins.

The explosion of wires in water is qualitatively similar to the explosion of wires in air. The only difference is in the quantitative characteristics of the stages. In the case of explosion of wires in water all stages, in particular, the pause in current stage, are significantly extended in time. This phenomenon is due to the great inertia of water, hindering the expansion of the wire in the first stage, and, in particular, the expansion of the gas channel in the second and third stages.

Fig. 2.23 shows oscillograms of the current and voltage on electrodes in the case of a discharge initiated by a copper wire 0.05 mm in diameter and 4 cm in length, in water (a) and in air (b). The condenser capacitance is 2 μf, the voltage is 6.7 kv. In the figure it is obvious that the pause between the current pulse, vaporizing the wire (1) and the pulse arising during the breakdown of the vapor (2), is significantly greater in the case of a discharge in water, than in the case of discharge in air. The duration of the pause in current increases with an increase in the diameter and length of wire. The duration of the pause in current

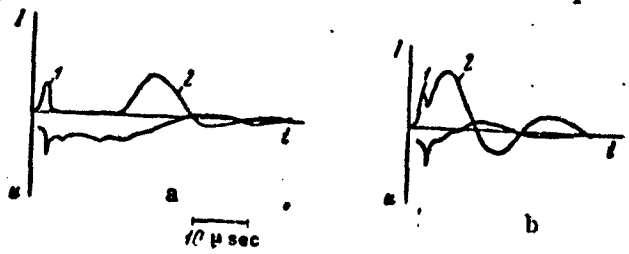

Figure 2.23. Oscillograms of current and voltage in the case of a discharge initiated with a copper wire.

depends on the material of the wire. In the case of tungsten wires the pause in current either is absent entirely or poorly pronounced. Therefore, thin tungsten wires are most suited for initiating discharges in water. With the aid of tungsten wires it is possible to initiate discharges with a working voltage of several kilovolts having a great channel length and a small lag in its formation relative to the moment of switching on the voltage.

The possibility of initiating discharges with wires of a material, the reaction of which with the oxygen, formed as a result of the dissociation of water, has a great thermal effect, is of interest. Such materials are aluminum, zirconium and beryllium. The thermal effect of exothermal reactions is capable of increasing the mechanical work performed by the channel significantly.

As an illustration we shall cite experimental data obtained in the case of initiating a discharge in water with an aluminum wire 0.4 mm in diameter and 10 cm in length. The condenser capacitance is 12 μf, the voltage 10 kV, and the inductance of the discharge circuit around 3 μH. The dimensions of the wire were chosen so that almost all the energy of the condenser was expended in vaporizing the metal. According to oscillograms of the current and voltage on the electrodes, shown in Fig. 2.24, it is possible to find that the vaporization of the wire takes place approximately after 18 μsec, and around 420 J is consumed in this process, which amounts to 70% of the energy of the condenser.

It is possible to estimate the acoustic energy, emitted by the discharge, according to the amplitudes of the compression pulse, emitted in the direction perpendicular to the axis of the channel. (An oscillogram of this pulse for a distance of 100 cm from the channel is shown in Fig. 2.25). For this we shall make use of formula 5.64, using a Gaussian curve with $\tau_0 = 0.7\tau$, where τ is the duration of the compression pulse, approximately equal to 18 μsec, [illegible] for the pulse on Fig. 2.25. Then for

p_1 = 16 atm, ℓ = 10 cm, r = 100 cm, we find $W_{ac} \approx 100$ J, which amounts to around 25% of the electrical energy released in the channel. Measurements of the pulsation period of the bubble formed by this discharge gave a value of around 16 msec. If we use formula (2.6) for determining the pulsation energy, in spite of the fact that the length of the channel in the given case is great in comparison with the radius, it so happens that this energy is approximately equal to 300 J, or 70% of the electrical energy released in the channel. At the same time, in the case of discharges initiated by high voltage breakdown, the acoustic energy amounts to 15 - 20%, and the pulsation energy 25-30% of the energy released in the channel.

Let us examine the characteristics of the method of initiating low voltage discharges in poorly conducting water, based on the use of a preliminary high voltage breakdown of the electrode gap. This method is known in high voltage engineering as the combination of voltage and current pulse generators. The difficulty of using this method for initiating a discharge in water comes down to the fact that switching on a voltage pulse generator should cause the breakdown of two parallel electrode gaps - one in water, the other in air. The breakdown of the air gap should cause the current pulse generator to be connected to the electrode gap in the water. However, the lag in the breakdown of the electrode gap in water significantly exceeds the lag in the breakdown in the air gap. Therefore, it is necessary to use switching schemes which are not sensitive to this difference in breakdown lags.

Fig. 2.26 shows a scheme which makes it possible to obtain the high voltage breakdown of an electrode gap in water with the subsequent connection of a low voltage condenser. This scheme operates in the following way. At the moment of the breakdown of electrode gap 1 under the influence of the voltage of the voltage pulse generator (C_1) their appears a sharp rise in the discharge current, which causes the appearance of a voltage surge at the output of the pulse transformer 2, the primary winding of which is

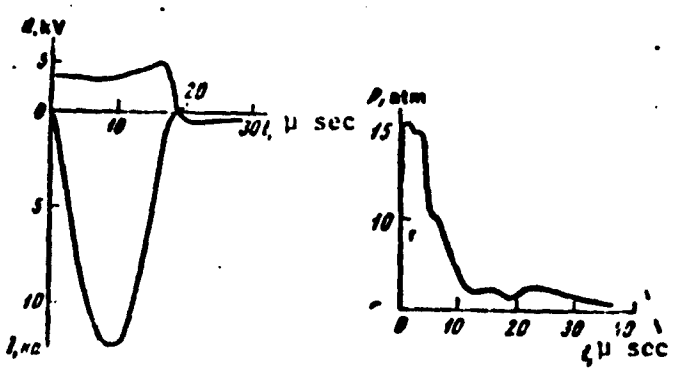

Figure 2.24. Oscillograms of current and voltage in the case of a discharge in water initiated with an aluminum wire.

Figure 2.25. Oscillograms of the compression pulse emitted by a discharge with the electrical characteristics shown in Fig. 2.24. Perpendicular direction, distance 100 cm.

connected to the voltage pulse generator circuit. The voltage surge is used for igniting the discharger 4, connecting the low voltage condenser C_2 to the discharge circuit. The choke 3 with a saturable core hinders the appearance of a voltage surge at the moment when the voltage pulse generator is switched on, when corona discharge current appears in the discharge circuit.

We shall now turn to an examination of the principle of the initiation of low voltage discharges in highly conducting liquids. As was mentioned, this principle is based on the use of the breakdown of an electrode gap along the gas bubble formed between the electrodes by a preliminary corona discharge on a third electrode inserted into the electrode gap [5].

Let us find the amount of energy of the condenser feeding the corona discharge. If the length of the electrode gap is equal to ℓ, then the radius R of the bubble, formed by the corona discharge, must reach a value of $\ell/2$ at the moment t_1 when the "power" condenser is switched on. Since it is convenient to mount

dischargers in a solid holder, we shall consider the motion of the initiating bubble along a hard wall. In this case it has the form of a hemisphere, and its potential energy at the moment of reaching its maximum radius R_b is connected with the energy of the condenser E, feeding the corona, by the relationship

$$\frac{2}{3}\pi R_b^3 p_0 = \eta_b E, \tag{2.7}$$

where p_0 is the hydrostatic pressure; η_b is the ratio of the energy of the bubble to the energy of the condenser. As was mentioned in Section 3, this value reaches 6% if the water has a salinity of several percent.

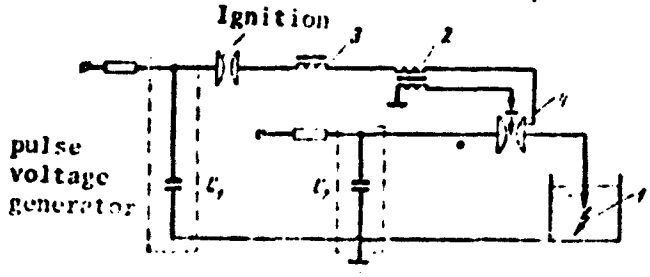

Figure 2.26. Diagram of a discharge circuit with the use of preliminary high voltage breakdown of the electrode gap.

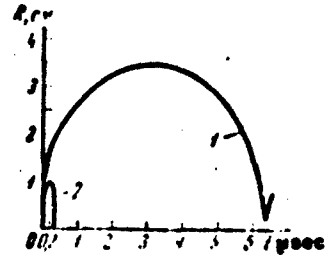

Figure 2.27. Dependence of bubble radius on time.

The pulsation period of a gas bubble τ_b for the case of a discharge in free space is determined by the relationship (see Chapter 4)

$$\tau_b = 1{,}135\rho^{1/2}p_0^{-5/6}(m\eta_b E)^{1/3}, \quad m = 1. \tag{2.8}$$

If the discharge takes place along a solid wall, then $m = 2$ must be used in the formula.

Here ρ is the density of the liquid.

For a rough estimate the law of the expansion of a bubble in water may be approximated with the formula

$$R = R_b \sqrt[3]{2t/\tau_b} \qquad (2.9)$$

where t is within the limits from 0 to $\tau_b/2$.

By using this formula we find the amount of condenser energy E, necessary for feeding a corona discharge capable of creating bubbles of radius R at the moment of time t_1

$$E = \sqrt[2.5]{\text{[illegible]}}\, R^3. \qquad (2.10)$$

The method of initiating discharges under consideration is little sensitive to hydrostatic pressure, since the bubble radius at the initial stage of growth is very slightly dependent on the amount of hydrostatic pressure if the pressure in the discharge channel, creating the bubble, is great in comparison with the hydrostatic pressure (see Chapter 4).

In order to compensate for the reduction bubble radius with hydrostatic pressure it is necessary to increase insignificantly the energy of the condenser feeding the corona discharge.

As an example, Fig. 2.27 shows how the relationship R(t) changes for a bubble, formed by an explosion, in the case of increasing p_0 from 1 - 40 atm (curves 1 and 2).

In the figure it is obvious that if $t_1 < \tau_b/2$, where τ_b is the pulsation period where $p_0 = 40$ atm, then $R(t_1)$ actually decreases little in the case of an increase in pressure from 1 - 40 atm.

REFERENCES

1. *Кужекин И. П.* Импульсный пробой и канал разряда в жидкости. Дисс. Моск. ордена Ленина энерг. ин-т, 1967.
2. *Трофимова Н. Б.* Экспериментальное исследование пробоя проводящих недегазированных жидкостей. Дисс. ЦНИЭлектром., 1965.
3. *Шуплецов К. А., Рой Н. А.*— Акуст. ж., 1967, 8, вып. 3, 417—426.
4. *Стекольников И. С., Усыскин В. И.* ЖТФ, 1965, 35, № 9, 1692—1700.
5. *Мельников Н. П., Островская Г. А., Сталь М. Ю.*— ЖТФ, 1961, 31, № 5, 919.
6. *Roy N. A., Tyelor D. P.* Generation of sound by spark discharge in water.— Proc. 3 Internat. Congr. Acoustics, Elsevier Publ. Co. 1961.
7. *Коул Р.* Подводные взрывы. М., ИЛ, 1950.
8. *Earl Van Reenen.* Low-voltage deep penetration marine seismic profiling system.— Marine Sciences Instrument. 3. Proc. 3 Nat. Marine Sci. Symp., Plenum Press, N. Y. 1965.
9. *Мельников Н. П., Островская Г. А., Штейнберг А. А.*— Вестник ЛГУ, 1962, 10.
10. *Мельников Н. П., Островская Г. А., Штейнберг А. А.*— Докл. АН СССР, 1962, 147, № 4.
11. *Мельников Н. П., Островская Г. А., Штейнберг А. А.*— Докл. АН СССР, 1963, 148, 5.
12. *Куцько Л. Г., Кортнев А. В.*— Укр. физ. ж. 1967, 12, № 9.
13. Взрывающиеся проволочки. Сборник статей. М., ИЛ, 1963.
14. Электрический взрыв проводников. М., изд-во «Мир», 1965.
15. *И. А. Роб.* Изобретение. Авт. свид. № 32032 с приоритетом от 28.XI 1961.

CHAPTER 3

PROPERTIES OF THE MATTER IN A DISCHARGE CHANNEL

1. Introduction

The processes in a discharge channel and the properties of the matter in it are examined in this chapter. Experimental data on the electrical characteristics of a discharge - the currents and voltages in the discharge depth and its resistance - represented for typical cases, making it possible to determine the conditions of energy release in the channel, that is, the characteristic time and energy scales of the phenomenon. Basically, this monograph deals with discharges in which energies of several kilojoules are released for times of tens of microseconds, which corresponds to a power of hundreds of megawatts, and only fragmentary experimental data on discharges, corresponding to other energy conditions are presented, although the theoretical information given, within the framework of certain limitations, is applicable to a wider class of cases.

Experimental data on the expansion of the discharge channel, obtained with the aid of high speed photography are described. These data make it possible to determine the rate of expansion of the channel, usually corresponding to 10^4 - 10^5 cm/sec, and, by using the hydrodynamic relationships in Chapter 4, to find the pressure in the discharge channel. In order of magnitude the pressure in the channel lies within the range from several hundreds to a thousand atmospheres.

Knowing the amount of resistance of the discharge gap and the radius of the channel, it is possible to estimate, considering the channel to be uniform and ignoring the influence of the areas near the electrodes, the conductance of the gas in the discharge

We note that given certain assumptions, it is possible to estimate the temperature of the gas, according to its conductance at a certain pressure; the values thus obtained agree, as is shown below, with the result of other experimental studies and theoretical estimates of temperature. These estimates show that the temperature of the channel is on the order of 20,000 ^{o}K.

Information on the properties of the matter, occurring as a low temperature dense plasma at the pressures and temperatures found in the channel of an underwater electrical discharge, is presented.

We present estimates of the relaxation times in the plasma, which prove to be small in comparison with the typical time scales of the phenomenon, which signifies that the plasma may be considered to be in equilibrium. This makes it possible to calculate the composition of the plasma and its thermodynamic characteristics, in particular, the proper energy of a unit volume.

Also, we present formulas for the kinetic coefficients of the plasma - the coefficient of electric conductance and thermal diffusivity, also considering and comparing different mechanisms of thermal conductivity - gas kinetic, electron, and radiant. Convective heat transfer is not considered, although it, possibly, plays a substantial role. The coefficients of thermal conductivities in the colder layers of vapor and water surrounding the plasma of the channel are estimated, which makes it possible to estimate the energy going to heat these layers.

The information and estimates presented are used for drawing up an equation for the energy balance in the discharge process.

2. Electrical characteristics of a discharge.

In this section we shall consider the electrical characteristics of the channel, understanding this term to mean the

time dependences of the discharge current and voltage in the channel, the time dependences of the resistance of the channel, and the power and energy released in the channel, that is, those characteristics which may be found by electrical measurements. We shall examine the electrical properties of the plasma in the channel - its conductance - after presenting information on the expansion of the channel.

According to the results of oscillography of the discharge current and voltage in an electrode gap it is found that the resistance of the electrode gap as a rule, is quite great at the moment of formation of a channel, if, of course, the appropriate method of initiation is used. In the case of high voltage discharges with a working voltage of several tens of kilovolts this resistance is on the order of 10^2 ohm for electrode gaps 5 - 10 cm in length. For low voltage discharges with a working voltage of several kilovolts and an electrode gap several centimeters long, the resistance of the gap at the moment of formation of a channel amounts to around 10 ohm. After the formation of a channel its resistance drops sharply, reaching a minimum approximately at the moment of maximum current, and then increases when the current approaches 0. The resistance of the channel drops, in the first place, due to the increase in the temperature of the plasma, heated by the discharge current, and in the second place due to the increase in the cross sectional area of the channel, expanding under the action of the excess pressure in the channel. At the end of the discharge, or at the end of each half period, if the discharge is oscillatory, the resistance of the channel increases as a consequence of the cooling of the plasma, although the cross section of the channel continues to increase.

The behavior of the resistance of the channel during the course of a discharge is determined by many factors: the inductance of the discharge circuit, the capacitance of the condenser, the amount of initial voltage, the length of the electrode gap, and the conditions of the initial ionization of the channel. The connection

between the resistance and the above-mentioned factors is complex. We shall illustrate it with specific examples.

First of all we note that according to the nature of the current flow, discharges may be aperiodic, if the direction of current does not change in the process of the discharge, and periodic, if current oscillation is observed. This brings up the concept of critical discharge, which is understood as meaning the limiting aperiodic discharge, which turns into a periodic discharge with a further reduction in circuit resistance. The effective resistance for a critical discharge is equal to the wave resistance: $R_{ef} = \sqrt{L/C}$.

We shall begin our examination with relatively low power high voltage discharges. Table 3.1 presents the values of the working voltage u, condenser capacitance C, discharge circuit inductance and length of the gap ℓ between a positive high voltage electrode in the form of the end of a type RK-3 cable with the outer insulation and braiding removed, and a grounded rod placed parallel to the cable.

TABLE 3.1

Number of Discharge	u, kV	C, μf	L, μH	ℓ, cm
1	30	0.4	3	4.5
2	30	0.9	3	5
3	30	0.4	55	4.5
4	30	0.9	3	2

Figure 2.10 shows oscillograms of current and voltage for discharges Nos. 1 and 2 (Table 3.1). The oscillograms show that the voltage on the electrodes after they are switched on drop slowly during the breakdown lag, corresponding to the growth of the leaders. At the moment when the electrode gap is closed by one of the leaders the voltage in the gap decreases sharply. This sudden change is due to the voltage drop on the inductance of the circuit

arising due to the sharp increase in discharge current. Later the voltage drops to 0 aperiodically. The behavior of the channel resistance, found as the ratio of the voltage of the channel to the discharge current at the corresponding moments of time, is shown in Fig. 2.11. At the stage of leader growth, the resistance of the electrode gap is approximately equal to 10^2 ohm. After breakdown the resistance drops to several ohms, and at the end of the discharge a rise in resistance is observed. In the case of such high channel resistances it is possible to ignore correction for the inductance of the channel.

With an increase in condenser capacitance, the resistance of the channel drops to lower values. However, this does not change the nature of the discharge - it remains close to critical. This means that reduction of the mean channel resistance with respect to time takes place approximately inversely proportional to the square root of the capacitance. The duration of the current pulse, if other parameters of the circuit remain invariant, increases proportional to the square root of the capacitance and approximately equals a value of $\pi\sqrt{LC}$, if the discharge remains in a close to critical mode.

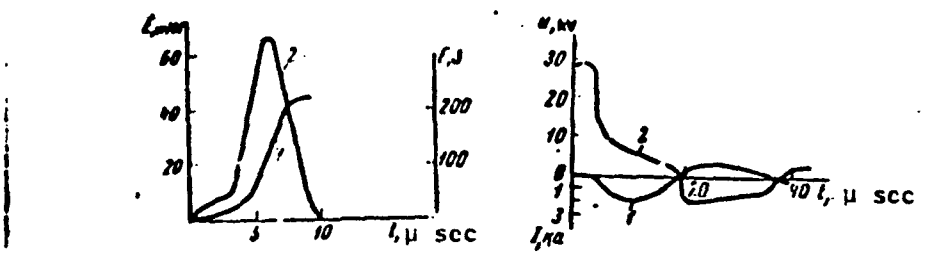

Figure 3.1. Time dependence of the energy (1) and power (2) for discharge No. 1, Table 3.1.

Figure 3.2. Oscillograms of discharge current (1) and voltage (2) for a discharge No. 3, Table 3.1.

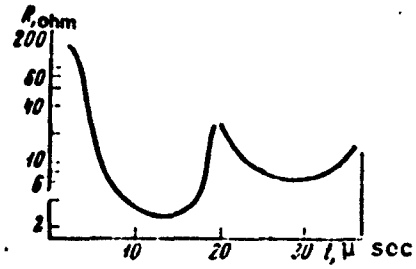

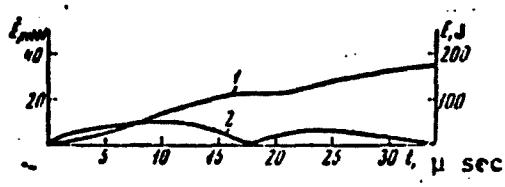

Figure 3.3. Dependence of channel resistance on time. Discharge No. 3, Table 3.1.

Figure 3.4. Time dependence of energy (1) and power (2) for discharge No. 3, Table 3.1.

Curves of the power and energy, released in the channel for discharge No. 1 (Table 3.1), are depicted in Fig. 3.1.

The influence of inductance on the behavior of a discharge may be determined according to the oscillograms in Fig. 3.2, taken for discharge No. 3 (Table 3.1). An increase in L does not cause a change in the breakdown lag, since the drop in inductance voltage in the process of discharge initiation is small. The time dependance of the channel resistance for this case is shown in Fig. 3.2. Two factors stand out: the channel resistance drops in the discharge process less in the case of low inductances, and passes through a maximum at moments of 0 values of the discharge current. As is seen in Fig. 3.4, the introduction of energy into the channel is slowed with an increase in inductance and the electrical power drops.

There is a practically complete transfer of energy from the condenser into the channel in all cases considered, since the resistance of the channel significantly exceeds the resistance of the rest of the discharge circuit.

A discharge may be converted into a damped oscillation curve not only by increasing the inductance of the discharge circuit, but

also by shortening the length of the electrode gap, as occurs in the case of discharge No. 4 (Table 3.1). The oscillograms in Fig. 3.5 show that the duration of discharge No. 4 significantly increases in comparison with discharge No. 2; as a result, the rate at which energy is introduced into the channel on the whole slows down. According to the behavior of the resistance of the channel (Fig. 3.2), it is possible to assume that in stages corresponding to minimum power, it is possible that cooling of the plasma takes place. Sometimes this effect leads to cessation of the discharge [1].

Let us now consider the role of the amount of initial voltage using the example of several discharges with a constant condenser energy, approximately equal to 45 J. Their parameters are given in Table 3.2.

Fig. 3.7 shows oscillograms of the discharge current in voltage for these discharges.

TABLE 3.2

Number of Discharge	u, kV	C, μf	L, μH	ℓ, cm
1	52	0.033	3	5
2	30	0.099	3	5
3	21.2	0.2	3	3.5
4	15	0.4	3	1.2
5	10	0.9	3	0.5

With a rise in the initial condenser voltage, the number of leaders increases. As a result, the leader current increases and the drop in condenser voltage during the breakdown lag become more noticeable. The energy left for feeding the channel decreases, and the shunting of the channel by streamer currents in the discharge process also acts in this direction.

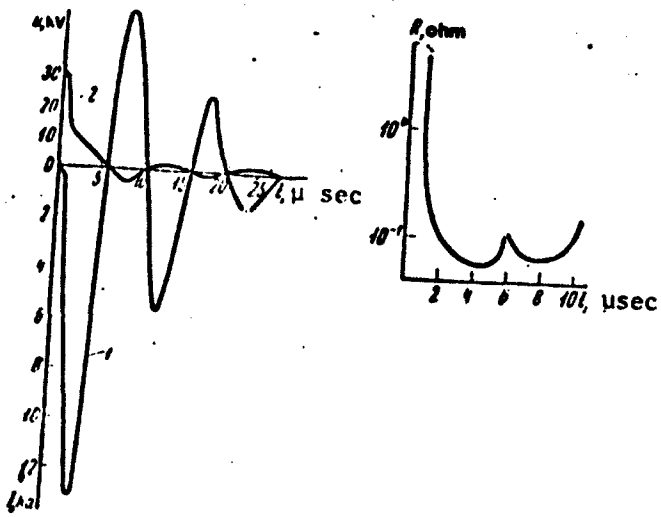

Figure 3.5. Oscillograms of discharge current (1) and voltage (2) for discharge No. 4, Table 3.1.

Figure 3.6. Dependence of channel resistance on time for discharge No. 4, Table 3.1.

With a decrease in voltage the breakdown lag increases and becomes unstable. Oscillograms showing how greatly the breakdown lag may vary from discharge to discharge in the case of low voltages are given in Fig. 3.7, e and 3.7, f for discharge No. 5 (Table 3.2). In order to provide for the breakdown of the electrode gap it is necessary to decrease its length. The channel resistance thus is reduced, and the discharge is transformed into an oscillatory mode.

We shall now consider the electrical characteristics of more powerful discharges, the parameters of which are given in Table 3.3.

TABLE 3.3

Number of Discharge	u, kV	C, μf	L, μH	ℓ, cm	E, J
1	6	158	1.5	6	2840
2	6	165	0.1	3	2970

These discharges were initiated with the explosion of tungsten wires 0.04 mm in diameter. Figs. 3.8 and 3.9 show the electrical characteristics of discharges No. 1 and 2 (Table 3.3), respectively. In the figures it is seen that the resistance of the channel drops at the moment of maximum current to approximately 0.08 and 0.05 ohm, respectively. A certain rise in resistance is observed toward the end of the discharge.

The duration of the first discharge is close to the value $\pi\sqrt{LC}$, and in the second discharge it significantly exceeds this value. Evidently, the duration of the second discharge could be shortened without conversion into an oscillatory mode by decreasing the length of the channel. In fact, the critical resistance $R_c = \sqrt{L/C}$, corresponding to the maximum rate of introduction of energy, for the first discharge is 0.1 ohm, which is close to the minimum resistance of the channel 0.08 ohm, while for the second discharge it is 0.02 ohm, which is significantly below the minimum resistance of the channel 0.05 ohm. Thus, the second discharge is controlled by the effective resistance of the channel to a significant degree.

The most powerful discharges were investigated by Komel'kov et. al., [2]. These discharges proceeded in a damped oscillation mode with several half-periods. The length of the electrode gap was 12 - 15 mm. The electrodes were made in the form of opposed coaxial brass rods, pointed at an angle of 25 - 30°. The parameters of the discharges investigated, and also the values of the maximum current I_m, maximum rate of current rise $\dot{I}_m$, voltage at the moment of maximum current and duration of the first half period $\tau/2$ are given in Table 3.4.

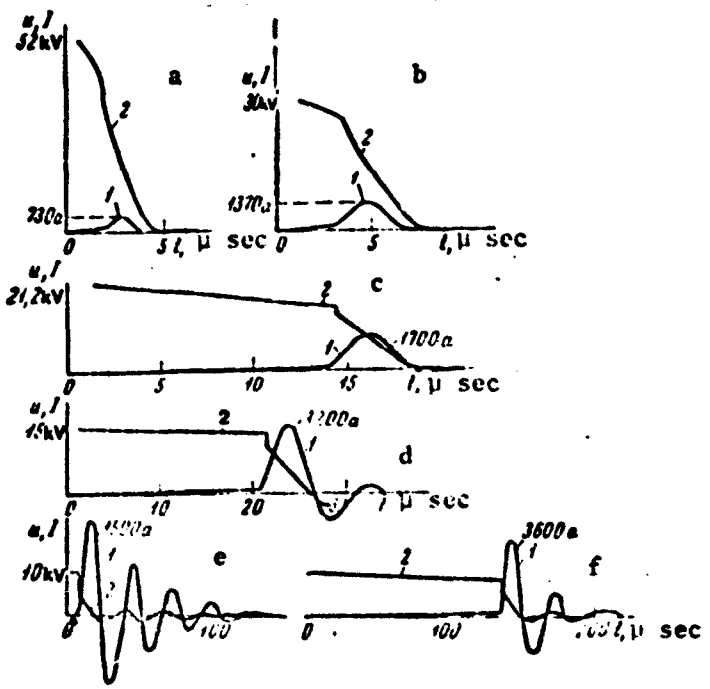

Figure 3.7. Oscillograms of discharge currents (curves 1) and voltages (curves 2) for discharger No. 1-5, Table 3.2.

TABLE 3.4

Number of Discharge	u, kv	C, μf	I_m, ka	$\dot{I}_m$, a/sec	u_{I_m}, kV	τ/2, μ sec
1	40	2.7	12	$3.6 \cdot 10^{10}$	1.3	15
2	40	5.4	61	$2.4 \cdot 10^{10}$	3.2	8.5
3	20	5.4	330	$0.5 \cdot 10^{10}$	5.5	11
4	40	130	520	$1.75 \cdot 10^{11}$	6.8	11
5	40	130	650	$2.1 \cdot 10^{11}$	7.3	11.5
6	30	240	720	$1.75 \cdot 10^{11}$		15.5

Figs. 3.10 and 3.11 show oscillograms of the discharge current and voltage in the electrode gap for discharges No. 1 and 4 (Table 3.4). For powerful discharges the correction for the inductive voltage component ($\dot{i} \geq 10^{11}$ a/sec) is significant. Evidently, due the great electrode surface the discharges investigated by Komel'kov, et. al., [7] had a significant scattering of values of the breakdown

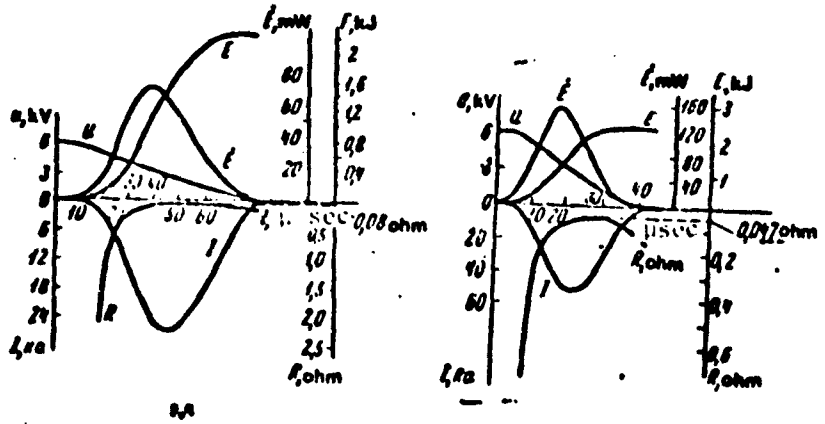

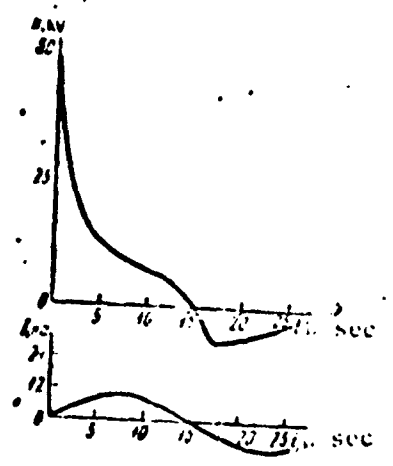

Figure 3.8. Electrical characteristics of discharge No. 1, Table 3.3.

Figure 3.9. Electrical characteristics of discharge No. 2, Table 3.3.

Figure 3.10. Oscillograms of discharge current and voltage for discharge No. 1, Table 3.4.

lag of from several tenths to several tens of microseconds, and due to the short length of the electrode gap several channels were formed at once, which then merged into one common channel. The resistance of the channel at the moment of maximum current was around 0.01 ohm.

At the beginning of this section we mentioned the complex dependence of the electrical characteristics of a discharge on the parameters of the discharge circuit. However, for estimates it is possible to use simple relationships, giving the true order of magnitude of the basic electrical values, characterizing the discharge. Actually, if the discharge proceeds in a close to critical mode (this mode, as mentioned above, is most important in practical

respects), then the duration of the discharge τ proves to be close to the value $\pi\sqrt{LC}$, and the minimum resistance of the channel R_m, is close to the critical resistance of the circuit $2\sqrt{L/C}$. Measurements show that the minimum resistance also may be estimated in the following way: it is approximately equal to the ratio of half the initial voltage to the maximum current, which in turn may be found from the relationship $Cu \sim I_m \tau/2$. From these relationships the value R_m proves to be approximately equal to the value $\tau/4C$. It is easy to become convinced that all the experimental values are in good agreement with the values found according to this formula. The maximum power developed during a discharge is determined by the value Cu^2/τ, and the maximum transconductance is $\dot{I} \sim 4Cu/\tau^2$. The values calculated according to these relationships also are in good agreement with experimental values, and the discharge mode, as stipulated, is close to critical. If the length of the channel is too great, then all relationships presented above give correct values, if τ is known from experiment. If the discharge proceeds in a mode with indications of oscillation, then the value of τ also is close to $\pi\sqrt{LC}$.

Oscillography of the discharge current and voltage in discharge channels with different parameters of the discharge circuit shows that electrical discharges in water may take place only in a damped oscillation mode if the mean channel resistance with respect to time is less than $\sqrt{L/C}$, or in a mode, similar to a critical mode, characterized by approximately symmetrical curves of current and power relative to the maximum value. There is no close to aperiodic discharge mode with a characteristic exponential drop in current and voltage in the case of discharges completed by the formation of a channel. Such a mode may occur only in the case of discharges uncompleted by the formation of a channel, which can be controlled by the ballast resistance of the water to a significant degree. The absence of a discharge mode close to aperiodic is connected with the unique behavior of the resistance of the discharge channel in the discharge process - by the passage through a minimum. [illegible], the dependence of

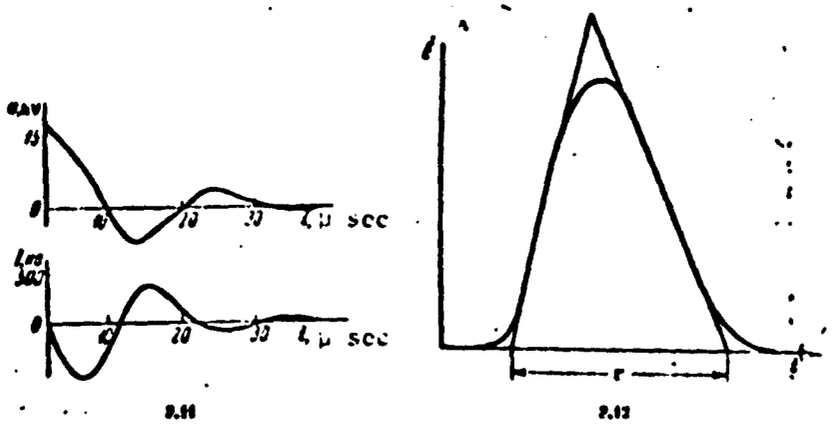

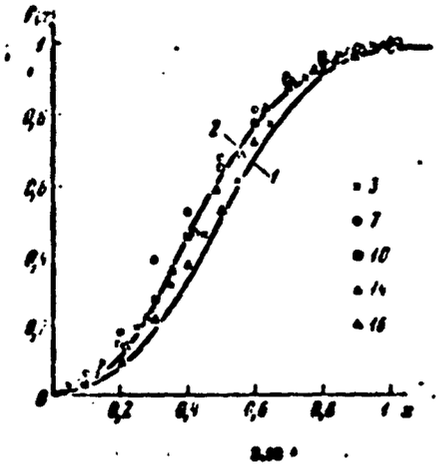

Figure 3.11. Oscillograms of discharge current and voltage for discharge No. 4, Table 3.4.

Figure 3.12. Diagram of an approximation of the power curve.

Figure 3.13. Dependence of rated energy on time. Curve 1 corresponds to formula 3.1; Curve 2 - to formula 3.2. The parameters of the discharges are given in Table 3.5. The numbers on the figure designate the order numbers of the discharges in the table.

power on time is represented by a curve of nearly triangular shape (Fig. 3.12), as is seen in Figs. 3.8 and 3.9. This leads to the idea that in the case of rough calculations the law of energy release for all discharges in a mode close to critical may be approximated with one relationship. In fact, if we introduce the dimensionless variable $x = t/\tau$ and $f(x) = E(x)/E$, where τ is the discharge duration determined according to Fig. 3.12 and E is the total energy released in the channel, it proves to be the case that the thus normalized function $f(x)$, characterizing the mode of energy release, is of quite universal nature; it varies little from

TABLE 3.5

	u,kV	C,uf	ℓ,cm	L,μH	t,μsec	$r\sqrt{LC}$ /sec	E,J	$Cu^2/2$, J	R_0,cm	According to data in reference
1	1,2	816	0,3	—	50	—	510	590	1,09	
2	1,6	321	0,1	0,2	30	25	376	412	0,84	
3	1,6	321	0,1	0,1	20	18	400	412	0,85	
4	15	1500	7,5	--	400	--	—	160000	6,80	[20]
5	4	100	5	1,5	100	47	1070	1200	1,15	
6	6	150	5	1,5	80	47	2240	3000	1,21	
7	6	158	6	1,5	83	47	2290	2511	0,90	
8	6	150	7	1,5	85	47	2290	3000	1,21	
9	6	150	12	1,5	100	47	2350	3000	1,43	
10	6	105	3	0,1	30	11	2300	2070	0,89	
11	40	2,7	1,5	--	—	15	1980	2160	0,66	[4]
12	40	5,4	1,5	—	—	9	1200	4320	0,47	[2]
13	25	5,8	1,5	0,25	--	4	450	2025	0,29	[13]
14	20	1,3	2,0	2,0	5,3	5	--	250	0,405	
15	30	0,3	3,0	3,0	-	3	171	180	0,211	
16	30	0,3	1,5	2,0	5	4	162	180	0,166	

discharges to discharges with a significant variation of the discharge parameters. In confirmation of what has been stated, Fig. 3.13 shows the time dependences of the rated energy for five different discharges. The parameters of these discharges are given in Table 3.5. The numbers used below to refer to each discharge are given in the first column, and in the second, third, and fourth columns--the initial pressure of the condensor, its capacitance and the length of the discharge gap, respectively.

The rough value of the inductance, estimated according to the parameters of the discharge circuit, is given in the fifth column. Discharge durations and the total energy released in a discharge, calculated according to electrical oscillograms, are shown in the sixth and eighth columns. The characteristic radius of the discharge channel determined subsequently is given in the tenth column, and bibliographical references for those discharges, the information on which was obtained from the literature, are cited in the eleventh column.

Graphs of simple functions, approximating the actual dependence of the rated energy on time, are represented in Fig. 3.13 by the solid curves.

Curve 1 is a graph of the function

$$f(x)=\begin{cases}2x^3 & 0\leqslant x\leqslant\frac{1}{2}\\ 4x-2x^3-1 & \frac{1}{2}\leqslant x\leqslant 1\\ 1 & 1\leqslant x\end{cases} \qquad (3.1)$$

Curve 2 is a graph of the function

$$f_1(x)=\begin{cases}3x^3 & 0\leqslant x\leqslant\frac{1}{3}\\ 3x-\frac{3}{2}x^3-\frac{1}{2} & \frac{1}{3}\leqslant x\leqslant 1\\ 1 & 1\leqslant x\end{cases} \qquad (3.2)$$

The function $f_1(x)$ corresponds to an approximation of the power of an isosceles triangle of unit area, a projection of the vertex of which onto the base divides it according to the ratio 1 : 3.

As is seen in Fig. 3.13, the difference in the experimental curves corresponds approximately to the difference of the curves of $f(x)$ and $f_1(x)$. Comparing the results of a numerical calculation of the hydrodynamic characteristics, obtained with the use of $f(x)$ and $f_1(x)$, it is possible to determine the degree to which the theoretical curve accurately approximates the real law of energy release. Such a comparison will be made in Chapter VI.

Section 3. Expansion of the Channel

After the completion of the process of initiating a discharge in a liquid there appears a channel filled with partially ionized gas. The initial form of the channel is determined by the process of initiation. In the case of the initiation of discharges by the high voltage breakdown of a liquid, the initial form of the channel is determined

by the form of the leader closing the electrode gap. In this case, geometrically regular channels practically never appear. A channel usually has small scale and large scale distortions. Fig. 2.2 shows photographs of channels, taken by the self-exposure method. The initial channel diameter is on the order of 10^{-2} cm.

In the case of low voltage discharges, the initial form of the channel is determined by the gas bubbles formed on both electrodes, if they are symmetrical, or by one gas bubble on the high voltage electrode, if the construction of the discharger is asymetrical. In this case, in contrast to high voltage breakdown, the initial diameter and length of the channel are close in value. Only in the case of initiating discharges with wire bridges, by breakdown along a gas bubble formed by a preliminary corona discharge in the conducting liquid, and by breakdown by parallel electrodes, a description of which is given in Section 4, may geometrically regular channels be obtained: in the first case--in the form of a right cylinder with spherical sides, in the second and third cases--in the form of a hemisphere, since in these cases discharges usually are produced on a rigid reflector in which the discharger is mounted. The initial diameter of the channel in the case of initiation with wires is determined by the diameter of the wire, in the second case, by the diameter of the initiating bubble, and in the third--by the width of the interelectrode clearance.

The pressure in the channel rises and the channel expands because of the intensive heating of the plasma by the discharge current. In the process of expansion the channel boundary may be considered to be impenetrable for the liquid. This does not mean that it is possible to ignore evaporation of the liquid in examining the processes inside the channel.

However, against the background of rapid hydrodynamic expansion the displacement of the boundary due to evaporation is insignificant. In fact, we shall compare the volumes of the evaporating liquid and the channel. The energy released in the channel basically is spent

in dissociating water molecules and heating gas (see Section 5, Chapter 3). Then, if D is the dissociation energy for one molecule, the energy described by the following formula is required for the dissociation of the molecules in a mass m of water and for heating the monatomic gas formed:

$$\frac{m}{\mu} N_0 \left(D + \frac{9}{2} kT\right), \qquad (3.3)$$

where μ is the molecular weight of water and N_0 is the Avogadro number.

Assuming that all the energy released in the channel goes to form heated gas, we find

$$m = E\mu / N_0 \left(D + \frac{9}{2} kT\right). \qquad (3.4)$$

Having taken $E = 10^3$ J, $T = 10^4$ K, we find $m = 10^{-1}$ g. Consequently, the volume of water evaporated in this case equals 10^{-1} cm^3, while the volume of the channel of such a discharge amounts to several cubic centimeters.

Judging by the glow of the discharge, the plasma fills the channel quite uniformly in the process of expansion. Photographing the channel through a slit perpendicular to the axis of the channel with a high speed photographic recorder against a background of intensive illumination shows that the plasma separates from the channel walls only at the end of the discharge. Figs. 3.14 and 3.15 show photographs of channels taken against a background of a flash bulb and against a background of a second discharge identical to the one investigated. The interlayering of cold gas between the luminescent plasma and the water during the entire discharge is not seen in the photographs. It becomes noticeable after the end of the discharge, when the plasma beginning with the periphery of the channel cools down. At this stage areas of lower luminosity and, consequently, of lower temperature also inside the channel [illegible] uniformity of

overall greater luminosity.

Flows of cold gas from the channel walls may be the cause of the appearance of nonuniformity. Such flows may arise due to the instability of the transition layer between hot plasma and water. It is difficult to take account of this factor in calculations. Therefore, in choosing a discharge model below we shall consider the plasma to be uniform.

The shape of the channel at the end of the discharge and its diameter with a given length of the electrode gap are determined by the duration of the discharge and the amount of energy introduced into the channel. The longer the discharge and the more energy introduced, the greater is the radius of the channel and the closer the ultimate form of the channel is to a sphere, even if the initial form of the channel was close to cylindrical. If the initial form of the channel had spherical symmetry, the ultimate form, naturally, retains this symmetry. The dependence of the characteristic channel radius R_0 on the discharge duration τ and on the amount of energy introduced into the channel E may be found approximately from the following considerations.

If R_0 is the characteristic radius of the channel, reached over time τ, then the rate of expansion of the channel $R = U$ in order of magnitude is $U = R_0/\tau$. Then, in agreement with the results of Chapter 4, the pressure of the liquid on the walls of the expanding channel at subsonic and near-sonic speeds of its expansion is estimated by the formula $P \sim \rho_0 R_0^2/\tau^2$.

Further, the intrinsic energy of a unit volume of plasma in a discharge channel, as is shown in Section 4 of this chapter, is determined by the formula $P/(\gamma - 1)$, where the effective adiabatic exponent $\gamma = 1.26$ for discharges in water.

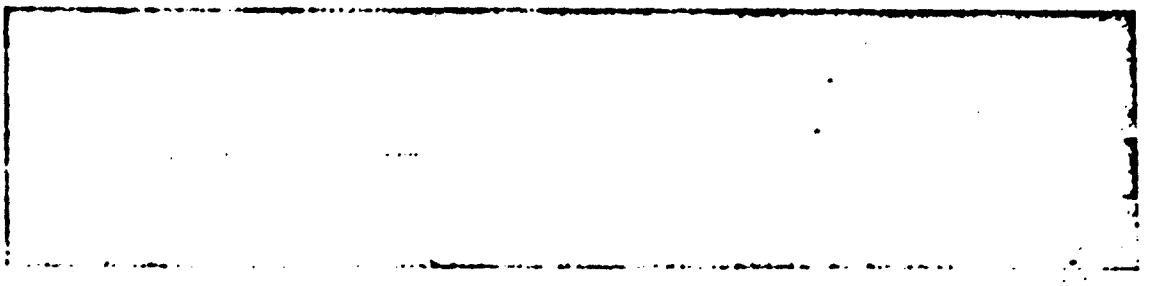

Fig. 3.14. Photogram of the expansion of a discharge channel.

Fig. 3.15. Photogram of the expansion of a discharge channel.

Then for discharges, the shape of whose channel is close to spherical, the intrinsic energy of the plasma in the discharge channel is determined by the formula $PV/(\gamma-1)=\frac{4}{3}\pi R_0^2\rho_0(R_0^2/\tau^2)/(\gamma-1)$. In order of magnitude this energy is equal to the total energy E released in the channel at the end of the discharge. Hence, the radius of the channel at the end of the discharge

$$R_0\approx\left[(3/4\pi\rho_0)(\gamma-1)\tau^2E\right]^{\frac{1}{5}}. \qquad (3.5)$$

For a cylindrical channel the intrinsic energy of the plasma is

$$\pi R_0^2 l\rho_0(R_0'\tau)^2/(\gamma-1)\approx E.$$

[illegible] the radius of the

[illegible]:

$$R_0 \approx \left[\frac{(\gamma-1)}{\pi p_0}\tau^2 \frac{E}{l}\right]^{\frac{1}{4}}. \qquad (3.6)$$

We note that formulas (3.5) and (3.6) will be obtained more rigorously in Chapter 5 in a calculation of hydrodynamic models of discharges.

By using formulas (3.5) and (3.6) it is possible to estimate the characteristic rate of expansion of a channel and the order of magnitude of the pressure in a discharge channel if the energy E released in the discharge channel and the time of its release τ are known. For example, for the discharges, the parameters of which are given in Table 3.5, the characteristic rates of expansion of the channel prove to be in agreement with the experimental data on the order of 10^4 cm/sec., and the pressure in the channel--on the order of from several hundreds to a thousand atmospheres.

An experimental investigation of the expansion of the channels of high voltage discharges with a channel length of 5-10 cm shows that the ratio of the radius of the channel to its length at the end of the discharge remains less than unity if the duration of the discharge does not exceed several tens of microseconds, and the energy released in a unit length of the channel is several kilojoules. This is in good agreement with the estimates obtained according to formula (3.6). The rate of expansion of the channels of such discharges is practically invariable along the channel. However, if the length of the channel is short, then substantial changes in the rate of expansion of the channel along its axis are observed. Fig. 3.16 shows a photograph of a channel at the end of a discharge of 150 μf capacitance with a voltage of 6kV. The length of the initiating wire (material--tungsten, diameter 0.04 mm) is around 3 cm. The inductance of the discharge circuit is approximately equal to 0.1 μH. In the photograph it is obvious that the sections of the channel near the electrodes expanded more intensely, imparting a dumbbell shape to the channel. A possible cause of this phenomenon may be the preferential release of energy in the

Fig. 3.16. Photograph of a discharge channel.

As a result the picture is the same as if there were two closely situated point discharges.

The time dependence of the radius of the channel in the discharge process to a first approximation is linear, as is seen, for example, in the photograms Nos. 7 and 10, shown in Figs. 3.17 and 3.18.

Section 4. Conditions of Gas Equilibrium In the Discharge Channel

The rapid release of energy in the channel of an electrical discharge in a liquid leads to intense heating of the matter in the channel and to evaporation of the liquid from the channel walls.

The number of particles in the channel during the discharge increases noticeably. The newly evaporating molecules of liquid are heated, dissociate, and are ionized. As a result there is formed in the discharge channel a dense low temperature plasma, the temperature of which as the experimental and theoretical results presented below (see Section 7) show, corresponds to the region of the first ionization of atoms (15,000 -- 50,000° K), and the particle concentration reaches 10^{19} cm^{-3}. Bearing in mind the brevity of a discharge

(the flow of current usually lasts $10^{-6}-10^{-4}$ sec.), it is necessary to consider the question of the gas equilibrium in the channel, in other words, to determine whether an equilibrium expansion of energy according to degrees of freedom succeeds in being established. A detailed examination of the relaxation processes in gases is given in reference [3]. We shall make, following reference [3]

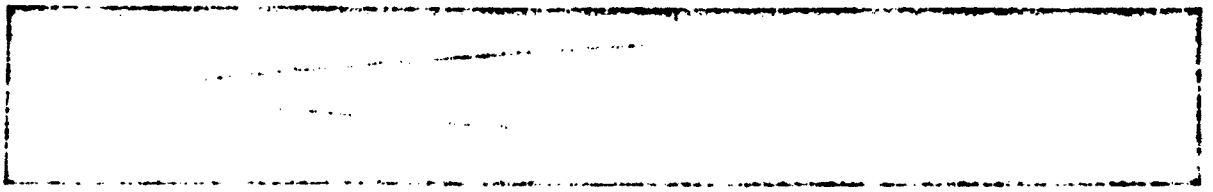

Fig. 3.17. Photogram of the expansion of discharge channel No. 7.

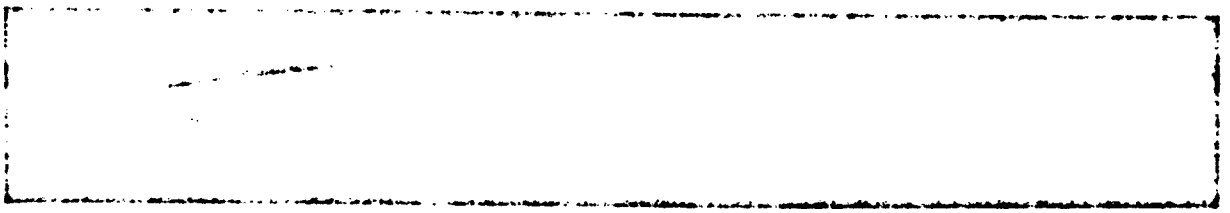

Fig. 3.18. Photogram of the expansion of discharge channel No. 10.

an estimate of the times required for the establishment of a Maxwellian distribution in an electron gas, in a gas of atoms and of ions, and also of the relaxation times of the processes of dissociation and ionization. All numerical estimates will be made relative to discharges in the water.

The time required for the establishment of a Maxwell distribution of electrons according to the speeds characterizing the establishment of temperature in an electron gas is determined by the time in the course of which the kinetic energy of an electron, as the result of Coulomb interaction with other electrons is changed by a value of the order of the very kinetic energy of the electron.

[illegible], [illegible] to reference [3], this time τ_{ee} is de[illegible]

$$\frac{1}{\tau_{ee}} = \frac{3{,}8 n_e \ln \Lambda}{(T_e)^{3/2}} \ [\text{sec}^{-1}], \tag{3.7}$$

where n_e is the number of electrons in one cubic centimeter, and the so-called "Coulomb logarithm" is expressed by the formula

$$\ln \Lambda = \ln \frac{3(kT_e)^{3/2}}{2(\pi)^{1/2} e^3 n_e^{1/2}} \approx \ln 0{,}62 \cdot 10^4 \left(\frac{T_e^2}{n_e}\right)^{1/2}. \tag{3.8}$$

For the case $T \approx 15{,}000°$ K, characteristic of electrical discharges, $n_e \approx 4 \cdot 10^{18}$ cm^{-3} and $\tau_{ee} \sim 10^{-12}$ sec., that is, a Maxwell distribution of electrons in the channel of an electrical discharge is established very rapidly in comparison with the duration of the discharge. It is necessary to note that formula (3.7) used below has also the expressions describing collisions between charged particles, is suitable only for estimating the orders of magnitude of the characteristics of a dense low temperature plasma formed in the channel of an electrical discharge in a liquid.

The time required for the establishment of an equilibrium distribution in a gas of atoms (or ions) may be estimated according to the formula (3)

$$\frac{1}{\tau} \sim n \bar{v} \sigma_{aa}, \tag{3.9}$$

where n is the number of particles in a unit volume,

$$\bar{v} = (8kT/\pi m)^{1/2} \approx 1{,}45 \cdot 10^4 \sqrt{T} \ [\text{cm/sec}] \tag{3.10}$$

is the mean thermal rate of their motion, σ_{aa} is the gas kinetic effective cross section, in order of magnitude amounting to 10^{-15} cm^2.

If $n = 10^{20}$ cm^{-3}, $T = 20{,}000°$K, A = 16 (oxygen), $\bar{v} \approx 4 \cdot 10^5$ cm/sec., $\tau \sim 10^{-10}$ sec., that is, an equilibrium Maxwell distribution is established within times which are short in comparison with the duration of the discharge.

The equalization of the electron and ion (or gas kinetic) temperatures takes places much more slowly. As a consequence of the sharp difference in the masses of the electrons and atoms (or ions) in the case of elastic interaction they are replaced by an energy amounting to a small proportional ratio of their masses or fraction of the kinetic energy. Therefore, for a significant exchange of energies between particles of different mass they must undergo still more, on the order of m_a/m_e, collisions (m_a is the mass of an atom, m_e is the mass of an electron.

Consideration of this factor, as is shown in [3], leads to the following formula for the time required for establishing equilibrium between an electron gas and a gas of heavy particles--atoms or ions.

$$\frac{1}{\tau_{ea}} = \frac{1}{\tau_{ei}} + \frac{1}{\tau_{en}}, \tag{3.11}$$

$$\frac{1}{\tau_{ei}} = \frac{n_i Z^2 \ln \Lambda}{2\cdot 0.11 T_e^{3/2}}, \tag{3.12}$$

where n_i is the number of ions in 1 cm^3; A is the atomic weight; Z is the ionic charge; the Coulomb logarithm is determined by formula (3.8)

$$\frac{1}{\tau_{en}} = n_a \bar{v}_e \sigma_{en} 2 \frac{m_e}{m_a} = 6.8\cdot 10^3 \frac{n_a \sigma_{en}}{A} \sqrt{T_e}, \tag{3.13}$$

where n_a is the number of atoms in 1 cm^3,

$$\bar{v}_e = (8kT_e/\pi m_e)^{1/2} = 6.21\cdot 10^7 \sqrt{T_e} \ [cm/sec] \tag{3.14}$$

is the mean thermal velocity of an electron; σ_{en} is the nuclear cross section of the elastic collisions of an electron with atoms, [illegible].

Where T_e = 15,000° K, $n_a = 10^{20}$ cm^{-3}, $n_e = 4 \cdot 10^{18}$ cm^{-3}, the relaxation times calculated according to formulas (3.12) and (3.13) prove to be equal: for hydrogen $\tau_{ei} \approx \tau_{ea} \sim 10^{-10}$ sec., for oxygen $\tau_{ei} \sim 10^{-9}$ sec., $\tau_{ea} \sim 10^{-8}$ sec.. Here the nuclear electron-ion scattering cross section proves to be equal to

$$\sigma_{ei}^{*} = 1{,}2 \cdot 10^{-6} \frac{Z^2 \ln \Lambda}{T_e^2} \approx 10^{-13}\ \text{cm}^2,$$

and for the nuclear scattering cross sections of an electon on atoms of hydrogen and oxygen the following were assumed with the same values I, n_a, n_e, according to the data in [4]

$$\sigma_{ea} \approx 2 \cdot 10^{-15}\ \text{cm}^2 \quad \text{(hydrogen)},$$
$$\sigma_{ea} \approx 0{,}4 \cdot 10^{-15}\ \text{cm}^2 \quad \text{(oxygen)}.$$

Let us now consider the slower processes of establishing equilibrium ionization and dissociation. As is indicated in [3], with electron concentrations of more than 10^{-17} cm^{-3}, the ionization of atoms from the ground state takes place basically because of inelastic collisions with electrons. The speed of this process is characterized by the relaxation time

$$\tau_0 = \frac{1}{\alpha_e n_a},$$

where α_e is the ionization rate constant; n_a is the number of atoms in cm^3.

Simple considerations lead to the following formula for the rate [3].

$$\alpha_e = \sigma_e \bar{v}_e \left(\frac{I}{kT_e} + 2 \right) e^{-\frac{I}{kT_e}},$$

where $\sigma_e = \sigma kT_e$ is some mean value of the effective cross section; the constant $\sigma = 10^{-17} e^2/eV$; v_e is the mean thermal speed of an electron, determined by formula (3.14), and I is the ionization [illegible].

We [illegible] cm^{-3}, I = 13.6 eV (hydrogen) and T_e = 15,000° K,

we obtain: $\sigma_e \approx 1.3 \cdot 10^{-17} cm^2$, $\bar{v}_e \approx 7.7 \cdot 10^7$ cm/sec., $\alpha_e \approx 3.3 \cdot 10^{-14}$ cm^3/sec., $\tau_e \sim 5 \cdot 10^{-7}$ sec.

We shall now examine how rapidly the dissociation of molecules evaporating from the channel walls takes place. As will be shown below, at temperatures of 10^{4}° K water molecules are practically completely dissociated (see also [5,6]).

As is shown in [3], the time required for the establishment of equilibrium dissociation (where $1-\alpha \ll 1$) in order of magnitude, may be estimated according to the formula

$$\frac{1}{\tau_d} \approx \frac{8}{1-\alpha} n^2 k_r, \tag{3.15}$$

where $\alpha = \frac{n_a}{n_a + n_m}$ is the degree of ionization: $n = n_a + n_m$ is the total number of particles in a unit volume; k_r is the recombination rate constant.

Simple considerations [3] lead to the following formula for an approximate estimate of this constant:

$$k_r \sim \bar{v} \sigma \frac{4\pi r^3}{3},$$

where $\bar{v}$ is the mean thermal speed of an atom, determined by formula (3.10); σ is the gas kinetic scattering cross section; r is a distance on the order of the molecular dimensions.

For water $\bar{v} \approx 3.4 \cdot 10^3$ cm/sec., $\sigma \sim 10^{-15}$ cm^2, $r \sim 2.6 \cdot 10^{-8}$ cm. Then $k_r \approx 2.4 \cdot 10^{-38}$ cm^6/sec.

Bearing in mind that the preliminary decomposition of a water molecule into molecules of hydrogen and oxygen, which then dissociate, may take place in the dissociation process, we estimate the reaction

rate constants for these molecules.

For hydrogen

$$\bar{v} = 1{,}45 \cdot 10^4 \sqrt{T}\ \text{cm/sec}, \quad \sigma \sim 10^{-15}\text{cm}^2, \quad r = 2{,}5 \cdot 10^{-8}\ \text{cm},$$
$$k_r = 9{,}1 \cdot 10^{-21} \sqrt{T}\ \text{cm}^6/\text{sec}.$$

For oxygen

$$v \approx 0{,}36 \cdot 10^4 \sqrt{T}\ \text{cm/sec}, \quad \sigma \sim 10^{-15}\text{cm}^2, \quad r \approx 3 \cdot 10^{-8}\ \text{cm},$$
$$k_r \approx 3{,}7 \cdot 10^{-21} \sqrt{T}\ \text{cm}^6/\text{sec}.$$

Using formula (3.15) and bearing in mind that close to complete, for example 90% (see following section), dissociation is reached at temperatures at least of several thousand degrees, we find, that there $n \approx 10^{20}$ cm^{-3}, $\tau_d \lesssim 10^{-8}$ sec.

Thus it is obtained that the rates of the processes of dissociation and ionization, the establishment of a Maxwell distribution of particles according to velocities and the equalization of the electron and ion temperatures, are close in comparison with the rates at which the matter in the channel of an electrical discharge changes state, which makes it possible to consider the plasma in the channel to be equilibrial.

Section 5. Composition of the Gas in a Discharge Channel

The equilibrium nature of the plasma makes it possible to calculate its composition easily. First we shall consider the process of dissociation. The dissociation of water molecules may take place according to different schemes. For example, a water molecule first may break down into hydrogen and oxygen molecules which dissociate at higher temperatures, or the decomposition of the molecule into atoms at once may take place, etc.

In what is coming one of the possible processes in order to

evaluate the conditions for complete ionization of water molecules. Namely, we shall consider the decomposition of water molecules into hydrogen and oxygen molecules. The dissociation energy in this process D = 2.48 eV/molecule* ≈ 57 kcal/mole, the characteristic temperature D/k ≈ 28,800° K. The hydrogen and oxygen molecules formed possess great binding energies. For H_2D ≈ 4.48 eV/molecule = 103 kcal/mole, D/k = 52,000°K; for O_2D = 5.11 eV/molecule = 118 kcal/mole, D/K = 59,400°K.

We note also, that the energy required for the dissociation of a molecule of H_2O into three atoms is D ≈ 10 eV/molecule ≈ 230.5 kcal/mole; D/k = 116,000°K.

In the case of the decomposition of a water molecule according to the scheme under consideration, its dissociation is determined by the dissociation of the hydrogen and oxygen molecules. Therefore, we shall examine these processes.

The degree of dissociation of a gas of diatomic molecules may be found from the condition of minimality of free energy [1]. It is convenient to write the formula obtained from this condition in the form [5]

$$\frac{a_m^2}{1-a_m} = \frac{\rho_d}{\rho} e^{-\frac{D}{kT}}, \tag{3.16}$$

where $a_m = \frac{n_a}{n_a+2n_2}$ is the mass concentration of the atomic component; n_a, n_2 are the number of atoms and molecules in 1 cm^3; for hydrogen ρ_d = 1.50 g/cm^3, for oxygen ρ_d = 150 g/cm^3; D is the dissociation energy. As an example, Table 3.6 presents the results of a calculation of the degree of dissociation of hydrogen and oxygen at a pressure of p = 500 atm. As is seen, significant dissociation takes

* 1 eV/molecule corresponds to 23.05 kcal/mole.

place even at temperatures of T<D/k (see also the calculations of gas plasma composition, made in [6].

Table 3.6

T, °K	$\alpha = \frac{n_a}{n_a + n_m}$	
	D_{H_2} = [illegible] °K (hydrogen)	D_{O_2} = [illegible] °K (oxygen)
4000	0,074	0,077
5000	0,250	0,269
6000	0,550	0,629
9000	0,945	0,975
12000	0,985	0,995

This is connected with the great statistical weight of the dissociated state, reflecting the fact that where kT<D the molecules are "frightened" by the impacts of fast particles, belonging to the far "tail" of a Maxwell distribution according to speeds (see [3]).

For these reasons the gas proves to be significantly ionized at temperatures which are low in comparison with the characteristic ionization temperature I/k, where I is the ionization potential.

In the temperature range we are interested in, when only the first ionization of atoms is significant, the degree of ionization is determined by the Saha formula in the form (see [3])

$$\frac{n_e n_1}{n_a} = A \frac{\sum_1}{\sum_a} T^{3/2} e^{-\frac{I}{kT}}. \qquad (3.17)$$

Here n_e, n_1, n_a are the numbers of electrons, ions, and atoms in 1 cm^3;

$$A = 2\left(\frac{2\pi m_e k}{h^2}\right)^{3/2} = 4{,}83 \cdot 10^{15}\,cm^{-3} \cdot deg^{-3/2} = 6{,}06 \cdot 10^{21}\,cm^{-3} \cdot eV^{-3/2};$$

Σ_i, Σ_a are the statistical ionic and atomic sums; I is the ionization potential; T is the temperature. For oxygen and hydrogen in the temperature range under consideration, the ratio Σ_i/Σ_a is close to unity. Actually, in the case of not too high temperatures Σ_i/Σ_a is approximately equal to the ratio of the statistical weights of the ground ionic and atomic states, and these ratios are 1/2 for hydrogen and 4/9 for oxygen. The ionization potentials of hydrogen and oxygen also are close and approximately equal 13.6 eV. The results of a calculation of the composition of a hydrogen or oxygen plasma for typical values of particle concentrations and temperatures are presented in Table 3.7.

Table 3.7

T, °K	n_e, cm^{-3}	n_0, cm^{-3}	$\alpha = \frac{n_e}{n_i + n_a}$	ln Λ
10 000	10^{20}	$1,81 \cdot 10^{20}$	$0,181 \cdot 10^{-2}$	2,67
15 000	10^{20}	$3,46 \cdot 10^{19}$	0,014	1,81
20 000	10^{20}	$1,60 \cdot 10^{19}$	0,138	1,48
30 000	10^{20}	$8,11 \cdot 10^{19}$	0,117	1,27
10 000	$3 \cdot 10^{20}$	$3,18 \cdot 10^{17}$	$0,106 \cdot 10^{-2}$	2,40
15 000	$3 \cdot 10^{20}$	$5,99 \cdot 10^{19}$	0,0196	1,54
20 000	$3 \cdot 10^{20}$	$2,78 \cdot 10^{19}$	0,085	1,20
30 000	$3 \cdot 10^{20}$	$1,4 \cdot 10^{20}$	0,319	1,00

As is seen, the degree of ionization in the channel of an electrical discharge in water, when a hydrogen-oxygen discharge plasma is formed, usually is small but due to the high density, the concentration of charged particles proves to be very high, reaching 10^{18}—10^{19} cm^{-3}.

Let us clarify what the degree of deviation from an ideal ionized gas with such a particle concentration gives. An ionized gas

may be considered to be ideal if the energy of the Coulomb interaction of adjacent particles is small in comparison with their energy of heat motion, that is, it is necessary to fulfill the condition $(Ze)^2/r_0 \ll kT$, where Z is the mean particle charge; $r_0 \approx n^{-1/3}$ is the mean distance between them; and n is the number of particles in 1 cm^3 of gas. This inequality may be rewritten in the form (see [3]).

$$n \ll 2{,}2 \cdot 10^{9} \left(\frac{T^{\circ}}{Z^2}\right)^3 1/cm^3. \tag{3.18}$$

In the plasma of discharges in a liquid usually $n_e \sim n_i \sim 10^{18}$—$10^{19}$; $T \approx 2 \cdot 10^4$°K, Z = 1, so that condition (3.18) is fulfilled: $10^{19} \ll 1.76 \cdot 10^{21}$. The presence of Coulomb interaction between particles leads to the fact that on the average attracting forces act between particles, by virtue of the fact that each ion surrounds itself with a cloud of particles of the opposite sign. This attraction influences the state of the gas in two respects (see [3]). On the one hand, it somewhat reduces the pressure and energy of the gas, in the case of a van der Waals gas with mutually attractive particles. On the other hand, the presence of attraction means that an electron possesses a certain binding energy in an ionized gas, so that in order to remove it from an atom it is necessary to expend somewhat less work, which also is manifested in a reduction of the ionization potential.

The second effect is more perceptible since even a small correction for the ionization potential, entering the exponent, leads to a significant shift in ionization equilibrium. With the Debye-Hueckel method it is possible to calculate the corrections for the thermodynamic functions of the ionized gas, stipulated by the Coulomb interaction.

As is shown in [3], for a singly ionized gas the correction for pressure

$$p_e = -\frac{2e^3}{3}\sqrt{\frac{\pi}{kT}}(n_e)^{\frac{3}{2}},$$

and the correction for the ionization potential is expressed by the formula

$$\Delta I = 2e^2\left(\frac{2\pi n_e}{kT}\right)^{1/2}.$$

However, we shall use this calculation only in the case of very slight nonideality of a gas, when the Debye radius is large in comparison with the mean distance between particles, which is expressed by the condition [3]

$$n \ll \left(\frac{kT}{4\pi e^2 \bar{Z}^2}\right)^3 = 1{,}10\cdot 10^{\circ}\left(\frac{T}{\bar{Z}^2}\right)^3 \text{cm}^{-3}, \qquad (3.19)$$

where $\bar{Z}$ is the mean particle charge.

Hence, it follows where T - 20,000° K for the applicability of the Debye-Hueckel theory it is necessary that the particle concentration be much less than 10^{18} cm^{-3}, while in a plasma discharge the charged particle concentration reaches 10^{18}—10^{19} cm^{-3}, which makes this approach unacceptable. It is possible only to say that the values of the degree of ionization of a hydrogen (or oxygen) plasma, given in Table 3.7, are somewhat understated due to the fact that the reduction in the ionization potential was not considered. This factor, however, is not significant for the hydrodynamic theory of a discharge, developed later, in view of the fact that the contribution of ionization energy to the energy of a unit volume of plasma is negligibly small, as we shall now see, and therefore errors in calculating the degree of ionization do not influence a calculation of the internal energy.

Part of the atoms and ions are in an excited state, and their number n_a^* is determined by the Boltzman n formula

$$n_a^*/n_a = g^*/g_a \exp(-I_{exc}/kT), \tag{3.20}$$

where g_a^* and g_a are the statistical weights of the ground and excited atomic levels.

The total number of particles in a unit volume of plasma $n = n_a + n_i + n_e = n_a + 2n_e$, since in the case of single ionization $n_i = n_e$. The intrinsic energy of a unit volume of a plasma formed in the case of a discharge in water is composed of the kinetic energy of the translational motion of particles $w_k = 3/2\ (n_a + 2n_e)kT$, the evaporation energy $w_{evap} = \frac{n}{3} D_{evap}$, where $D_{evap} = 0.045$ eV/molec = 1.05 kcal/mole is the evaporation energy of a water molecule; the dissociation energy $w_d = \frac{D_d}{3} n_a$; D_d is the dissociation energy equal to 10eV/molecule; the ionization energy $w_i = n_e I$, where I is the ionization potential equal to 13.6 eV for hydrogen and oxygen; the atomic excitation energy $w_{exc} = n_a^* I_{exc}$; the ionic excitation energy $w'_{exc} = n_i^* I'_{exc}$

$$w = w_k + w_e + w_d + w_{exc} + w'_{exc}. \tag{3.21}$$

The magnitude of the different terms of this sum in relation to temperature is shown in Fig. 3.19 for a pressure of p = 500 atm. Negligibly small, excitation energy values are not shown on the graph. As is seen, the energy of a unit volume of plasma basically is composed of the translational particle motion energy and the dissociation energy. The ionization energy provides an insignificant correction. The contribution of the remaining terms is negligibly small.

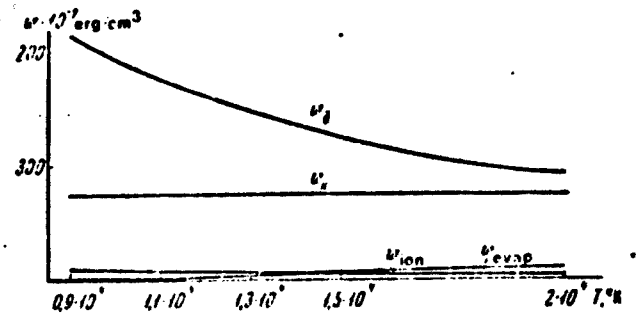

Fig. 3.19. Dependence of the energy density of a plasma on temperature.

Therefore, in practice the intrinsic energy of a unit volume of water plasma in the area of temperatures corresponding to the first ionization of atoms may be calculated according to the formula

$$w = \frac{3}{2} nkT + n\frac{D_d}{3} + n_e I, \tag{3.22}$$

where $n = n_a + 2n_e$ is the total number of particles in a unit volume; D_d is the molecule dissociation energy; I is the ionization energy.

For an ideal gas the intrinsic energy of a unit volume is expressed by the formula

$$w = \frac{p}{\gamma - 1}, \tag{3.23}$$

where $\gamma = c_p/c_v = 1.66$ for a monatomic gas.

In the case of a plasma this ratio proves to be variable, though its variations in the pressure and temperature ranges of interest to us are small, which makes it possible, as usually is done [3], to introduce a certain effective constant γ, approximating the real value of this quantity. The mean value of γ in the range of pressure from 500 to 1500 atm. and temperatures from 15,000 to 25,000° K, was taken as this effective γ. These values are given in Table 3.8. The value of γ, as is seen in Table 3.8, prove to be approximately equal to 1.26. This value also will be used below.

It is interesting to note that where $\gamma = 1.26$ the energy of a unit volume of plasma exceeds the energy of a unit volume of a monatomic ideal gas, at the same pressure, by more than three times.

Section 6. Kinetic Coefficients of the Gas in the Discharge Channel

Now we shall estimate the kinetic coefficients: the coefficient of electric conductivity and thermal conductivity of the plasma in the discharge channel, and also the coefficients of thermal conductivity in the transition layer between plasma and water. The resistance of the plasma is due to the collision of electrons with ions and neutral atoms. The times between these collisions may be estimated according to the formulas [3]:

$$\frac{1}{\tau_{ei}} \approx 3{,}6 \frac{n_i Z^2 \ln \Lambda}{T_e^{3/2}}, \tag{3.24}$$

$$\frac{1}{\tau_{ea}} \approx n_a \bar{v}_e \sigma_{ea}, \tag{3.25}$$

where n_i, n_a are the numbers of ions and atoms in cm^3, Z is the ionic charge; $\bar{v}_e = (8kT/\pi m_e)^{1/2}$ is the mean thermal velocity of an electron; σ_{ea} is the electron-atom scattering cross section. We note that formulas (3.24) and (3.25) differ from formulas (3.12) and (3.13) only by the absence of a factor equal to the ratio of the masses of the electron and the atom, considering the fact that a great number of collisions is necessary for a significant exchange of energies between these particles.

Table 3.9 presents the times between particle collisions, calculated according to these formulas, for typical temperatures and concentrations of plasma in a discharge channel in a liquid. This same

Table 3.8

$p \cdot 10^{-7}$, dyne cm^{-3}	$T \cdot 10^{-4}$ °K											
	1.5·10^{4}	1.6	1.7	1.8	1.9	2.0	2.1	2.2	2.3	2.4	2.5	γ_{av}
5	1.236	1.246	1.251	1.256	1.258	1.260	1.261	1.261	1.261	1.261	1.261	1.255
7	1.238	1.246	1.253	1.258	1.262	1.264	1.265	1.266	1.267	1.267	1.266	1.259
9	1.238	1.246	1.254	1.259	1.266	1.268	1.269	1.271	1.271	1.271	1.271	1.262
11	1.239	1.248	1.254	1.260	1.265	1.268	1.271	1.273	1.274	1.274	1.275	1.263
13	1.240	1.249	1.256	1.262	1.266	1.273	1.274	1.274	1.274	1.276	1.277	1.265
15	1.240	1.249	1.257	1.262	1.268	1.273	1.274	1.274	1.277	1.279	1.280	1.266

Table 3.9

$T \cdot 10^{-4}$ °K	n_a, cm^{-3}	n_e, cm^{-3}	σ_{ei}^{*}, cm^{2}	τ_{ei}^{*}, sec	H		O	
					τ_{en}^{*}, sec	σ_{en}, cm^{2}	τ_{en}^{*}, sec	σ_{en}, cm^{2}
1,5	10^{20}	$3,46 \cdot 10^{18}$	$0,9 \cdot 10^{-13}$	$7 \cdot 10^{-14}$	$5 \cdot 10^{-14}$	$2,2 \cdot 10^{-15}$	$4 \cdot 10^{-13}$	$0,35 \cdot 10^{-15}$
2,0	10^{20}	$1,60 \cdot 10^{19}$	$0,4 \cdot 10^{-13}$	$3 \cdot 10^{-14}$	$5 \cdot 10^{-14}$	$1,9 \cdot 10^{-15}$	$3 \cdot 10^{-13}$	$0,44 \cdot 10^{-15}$
3,0	10^{20}	$0,814 \cdot 10^{20}$	$0,2 \cdot 10^{-13}$	$1 \cdot 10^{-14}$	$5 \cdot 10^{-14}$	$1,6 \cdot 10^{-15}$	$2 \cdot 10^{-13}$	$0,53 \cdot 10^{-15}$

table contains the values of the effective cross sections of Coulomb collisions which, with the aid of formula (3.24) and the usual relationship

$$\frac{1}{\tau_{ei}} \sim n_i \bar{v}_e \sigma_{ei}$$

may be expressed by the formula [3]

$$\sigma_{ei} \approx 1.2 \cdot 10^{-5} \frac{\ln \Lambda}{T_e^2}. \qquad (3.26)$$

Nuclear electron-atom scattering cross sections, taken from [4], also are given in this table. It is necessary to emphasize once that the data cited in the table are of the nature of rough estimates, giving only the order of magnitude of the values calculated. Nevertheless, the data presented in the table give some idea of the cross sections. Moreover, it is possible to conclude that if the frequency of the collisions of electrons with hydrogen atoms and ions are on the same order of magnitude, in the ranges of concentrations and temperatures of interest to us, in argon electron collisions with ions will take place more frequently than with atoms.

By knowing the frequency of collisions, it is easy to determine the electric conductivity of the plasma. The general formula for conductivity has the form [8]

$$\eta = \frac{n_e e^2 \tau'}{m_e}, \qquad (3.27)$$

where n_e is the number of electrons in 1 cm^3; e is the electron charge; m_e is the mass of an electron; τ' is the time between collisions of an electron with ions and neutral atoms,

$$\frac{1}{\tau'} = \frac{1}{\tau_{ei}} + \frac{1}{\tau_{en}}. \qquad (3.28)$$

collision of electrons with ions, then the formula for conductivity is somewhat more precise than that obtained in the case of the direct substitution of (3.24) into (3.27) (taking account of electron-electron collisions), obtained by Spitzer [9] (see also [3]), and has the form*

$$\eta_{ei} = 2{,}63\cdot 10^{4}\gamma(Z)\,\frac{T_e^{\frac{3}{2}}}{Z\ln\Lambda}\,\frac{1}{\text{ohm}\cdot\text{cm}} = 2{,}38\cdot 10^{6}\gamma(Z)\,\frac{T_e^{\frac{3}{2}}}{Z\ln\Lambda}\,\text{sec}^{-1}, \tag{3.29}$$

where Z is the particle charge;

$$\Lambda = \frac{3(kT)^{\frac{3}{2}}}{2(4\pi)^{\frac{1}{2}}Z^{3}e^{3}n_e^{\frac{1}{2}}};$$

But if $\tau_{ea} \ll \tau_{ei}$, that is, the resistance of the plasma is due to collisions with neutral atoms, then the formula for conductivity has the form [10]

$$\eta_{ea} = 0{,}51\,\frac{e^{2}n_e}{(m_e kT)^{\frac{1}{2}}}\,\frac{1}{n\sigma_{ea}}. \tag{3.30}$$

In the general case, as is seen from (3.27) and (3.28), inverse conductivities are added.

The dependence of η on temperature in the case of pressure of 500 and 700 atm. is shown in Fig. 3.20.

A magnetic field influences the kinetics of the electrons if the frequency of electron rotation in a magnetic field $\omega = eH/mc$ equals the frequency of collisions $1/\tau$, that is, if $\omega\tau$ is approximately 1, in other words, when an electron succeeds in performing a significant part of its orbit during the time between collisions. But if $\omega\tau \ll 1$, i.e., the collisions disturb motion along the orbit,

the influence of a magnetic field is insignificant. It is precisely this case that takes place usually in the plasma of electrical discharges in a liquid. In fact, $\omega = eH/mc$, $H = 2I/rc$. Where $I \approx 3 \cdot 10^4$ a, $r \approx 1$ cm, $H \approx 6 \cdot 10^3$ e, $\omega \approx 10^{11}$ sec.$^{-1}$. According to the data in Table 3.9, $\tau \approx 10^{-14}$ sec., consequently, $\omega\tau \approx 10^{-3}$.

The influence of a magnetic field also is manifested in the formation of a skin layer. The depth of penetration of a magnetic field is

$$\delta_H \approx \frac{c}{2\pi\eta}, \tag{3.31}$$

where η is the speed of light.

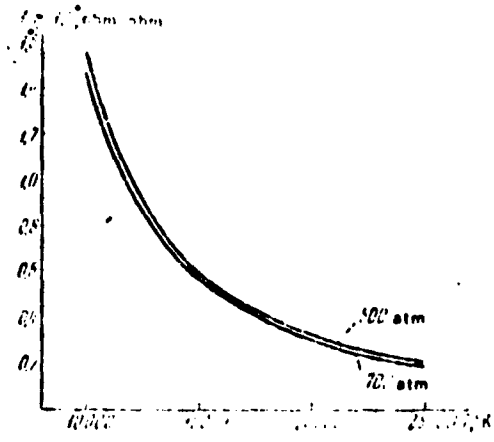

Fig. 3.20. Dependence of plasma conductivity on temperature.

The conductivity of the plasma in a discharge channel usually amounts to 10^{14} sec^{-1}. Then the ratio of the thickness of the skin layer to a channel radius, equal in order of magnitude to 1 cm, is

$$\delta^2/R_0^2 \sim \frac{c^2}{2\pi\eta R_0^2} \sim 10^2 \gg 1.$$

We note that the possibility of ignoring the skin effect at the same time signifies, as was mentioned in [11], that the magnetic pressure is small in comparison with the gas dynamic pressure in the channel.

In fact, since a significant part of the energy released in the channel in the form of Joule heat goes to increase the internal energy of the gas, and the density of the intrinsic energy in order of magnitude is equal to the gas dynamic pressure,

$$p \sim \frac{I^2}{\eta} t \sim \frac{I^2}{(\pi R_0^2)^2 \eta} \sim \frac{H^2}{8\pi} \frac{\delta^2}{R_0^2},$$

hence,

$$\frac{p}{\frac{H^2}{8\pi}} \sim \frac{\delta^2}{R_0^2} \qquad (3.32)$$

and therefore it is possible to ignore the influence of magnetic pressure when the influence of the skin effect is not significant.

Actually, a direct estimate of the amount of magnetic pressure gives the following:

$$p_M \sim \frac{H^2}{8\pi}, \quad H \sim \frac{2I}{cR_0},$$

where $I \sim 4 \cdot 10^4$ a, $R_0 \sim 1$ cm, $H \sim 8 \cdot 10^3$ e, and $p_M \sim 2.0$ atm., which actually is small in comparison with the gas dynamic pressure,

equal to 10^3 atm.

The energy transfer in electrical discharge channels is performed by atoms (or ions), electrons, and photons. These processes are characterized respectively by the coefficients of gas kinetic, electron, and radiant thermal conductivities [3, 10]

$$\varkappa_{gk} = \frac{1}{3} l_a \bar{v} \rho c_v, \tag{3.33}$$

where $l_a = (n\sigma_a)^{-1}$ is the free path length; $\bar{v} = (8kT/\pi m)^{1/2}$ is the mean thermal velocity of an atom; ρ is the gas density; c_v is the specific heat given at constant volume, so that ρc_v is equal to the heat capacity of a unit volume; n is the number of molecules in 1 cm^3; σ_a is the nuclear scattering cross section of the atom;

$$\varkappa_{el} = \xi \cdot 1{,}03 \cdot 10^{-8} \frac{T^{5/2}}{Z \ln \Lambda} \text{ erg/sec} \cdot \text{cm} \cdot \text{deg}, \tag{3.34}$$

where Z is the ion charge; $\ln \Lambda$ is the Coulomb logarithm; $\xi(Z)$ is a function weakly dependent on Z; $\xi(1) = 0.95$; $\xi(2) = 1.5$; $\xi(4) = 2.1$;

$$\varkappa_l = \frac{1}{3} l_e 16 \sigma T^3, \tag{3.35}$$

where l_e is the Rosseland light path; $\sigma = 5.67 \cdot 10^{-5}$ erg/cm^2·sec·deg^4 is the Stephan Boltzmann constant.

It is necessary to emphasize that the radiation transfer is of the nature of thermal conductivity in the case where the radiation energy density at each point is close to equilibrium. For this it is necessary that the length of the radiation path l_e be

small in comparison with the dimensions of the heated area. The path length is expressed by the formula [3]

$$l_c = 0{,}9 \cdot 10^7 \frac{T^2}{nZ^2} e^{\frac{I}{kT}}, \qquad (3.36)$$

where n is the number of atoms in 1 cm^3; I is the ionization potential of the atoms; Z = 1.

If the path length l_c equals or is greater than the dimensions of the heated area, the radiation is nonequilibrium and freely passes from the entire volume of the heated area.

As is seen the path length l_c strongly depends on temperature. Where $T = 1.5 \cdot 10^{4}$° K, $n = 10^{20}$ cm^3 in hydrogen or oxygen (I = 13.6 eV) $l_c = 1$ cm, and where $T = 2 \cdot 10^{4}$, $n = 10^{20}$, $l_c \sim 10^{-1}$ cm.

The characteristic channel diameter is usually around 1 cm, since the mechanism of radiant thermal conductivity may act in a discharge channel.

Let us compare the coefficients of thermal conductivity resulting from these three mechanisms. Where $T \approx 20 \cdot 10^{3}$° K, $n = 10^{20}$ cm^{-3} in hydrogen, $\varkappa_{Bk} \approx 1.5 \cdot 10^5$ erg/cm·sec·deg, $\varkappa_{el} \approx 5 \cdot 10^5$ erg/cm·sec·deg, $\varkappa_l \approx 2.4 \cdot 10^8$ erg/cm·sec·deg. Thermal conductivity leads to equalization of the temperature inside the channel. This process, as is known, (see [3]), is characterized by the spatial scale $\delta \sim 2\sqrt{\chi t}$, indicating the diameter of the area heated after the time t; χ is the coefficient of thermal diffusivity.

In gas the coefficient of thermal diffusivity is approximately equal to the coefficient of diffusion of the atoms

$$\chi_{at} \sim \frac{1}{3} l_c \bar{v}, \qquad (3.37)$$

where l_a is the length of the free path of an atom; $\bar{v}$ is its mean thermal velocity.

Similarly, the coefficient of electron thermal diffusivity may be estimated according to the formula

$$\chi_{e1} \approx \frac{1}{3} l_e \bar{v}_e. \qquad (3.38)$$

where $\bar{v}_e$ is the mean thermal velocity of an electron; l_e is the length of its free path.

The coefficient of radiant thermal diffusivity χ_c is [8]

$$\chi_1 = \frac{1}{3} l_c c \frac{c_{rad}}{c_v}. \qquad (3.39)$$

As is seen, in contrast to the coefficient of thermal diffusivity in gases, where molecules are the energy carrier, the coefficient of radiant thermal diffusivity is not simply equal to the coefficient of radiation diffusion $l_c \frac{c}{3}$, but contains another factor equal to the ratio of the heat capacities of a unit volume of radiation and matter. The cause of the appearance of this factor is the fact that in the given case radiation plays the role of the carrier of energy from such sections of the gas to the others, thus causing heating (or cooling) of the matter [3].

We shall now present the values of the coefficients of thermal diffusivity and the scales of the heated area for typical conditions in a discharge channel: $T = 20{,}000°$ K, $n = 10^{20}$ cm^{-3}, assuming that the discharge duration is 10^{-4} sec.

[illegible] formulas (3.37)—(3.39) for hydrogen we have:

$$\chi_{0h} \approx 6\,\text{cm}^2/\text{sec}, \qquad \delta_{0h} \approx 5\cdot 10^{-3}\,\text{cm},$$
$$\chi_{0l} \approx 2{,}5\cdot 10\,\text{cm}^2/\text{sec}, \qquad \delta_{0l} \approx 10^{-1}\,\text{cm},$$
$$\chi_1 \approx 10^4\,\text{cm}^2/\text{sec}, \qquad \delta_1 \approx 2\,\text{cm}. \tag{3.40}$$

As is seen, radiant thermal conductivity provides for rapid equalization of the temperature inside the channel, which makes it possible to consider the plasma of the channel to be uniform in an approximate examination of the discharge.

The intensely heated gas in the channel is separated from the surrounding water by a transition layer, the temperature in which drops from several tens of thousands to several hundred degrees. Dissociation of newly evaporated molecules takes place in the transition layer. The gas in the transition layer is relatively cold and therefore is transparent for radiation, and the release of heat in it takes place due to thermal conductivity from the more heated central area of the channel. In addition, together with the usual gas kinetic mechanism of heat conductivity, a unique mechanism, connected with the transfer of dissociation energy by molecules, acts in the transition layer. Atoms which come into the cold layers recombine, releasing dissociation energy, and the molecules which strike layers of higher temperature dissociate, thus absorbing energy.

The coefficient of thermal conductivity of a diatomic gas, resulting from such a mechanism, is calculated in [5, 12] and approximately is expressed by the formula

$$\varkappa_d \approx \frac{3}{16}\left(\frac{1}{\pi m_a}\right)^{\frac{1}{2}} \frac{D^2(\alpha-\alpha^2)}{d_{12}^2 k^{\frac{1}{2}} T^{\frac{1}{2}}},$$
$$d_{12} = \frac{d_1+d_2}{2}, \quad \alpha = \frac{n_a}{n_a+n_M}. \tag{3.41}$$

Here m_a is the atomic mass; D is the dissociation energy; α is the degree of dissociation; d_1, d_2 are the atomic and molecular diameters.

The coefficient of dissociative thermal conductivity has a maximum at the temperature where half of the molecules are dissociated. Its value in the area of the maximum exceeds the value of the coefficient of gas kinetic heat conductivity by several times.

For example, in hydrogen $T \approx 7{,}000°$ K, $p = 500$ atm., $n = 5 \cdot 10^{20}$ cm^{-3}, where n is the total number of particles in 1 cm^3, $\varkappa_d = 7 \cdot 10^4$ erg/cm·sec·deg, $\varkappa_{gk} \approx 10^4$ erg/cm·sec·deg. In oxygen $T = 6{,}000°$ K, $p = 500$ atm, $n = 6 \cdot 10^{20}$ cm^{-3}, $\varkappa_d = 1.6 \cdot 10^5$ erg/cm·sec·deg, $\varkappa_{gk} = 3 \cdot 10^4$ erg/cm·sec·deg. In water vapor, according to the data in [6], the maximum value of $\varkappa_d \approx 3.5 \cdot 10^5$ erg/cm·sec·deg.

The relationship of the coefficients of dissociative and gas kinetic thermal conductivity becomes clearer if we bear in mind that the value of the coefficient of dissociative thermal conductivity may be estimated according to the standard formula $\varkappa = (1/3) l \bar{v} c_{vd}$, if c_{vd} is understood as the heat capacity of a unit volume taking account of the losses of energy in dissociation. Consequently, the ratio $\varkappa_d / \varkappa_g \sim c_{vd}/c_v$, where c_{vd} and c_v are the dissociative and gas kinetic heat capacity of a unit volume.

Bearing in mind that $c_v = \left(\frac{\partial w}{\partial T}\right)_v$, and $w \sim \frac{D}{3} n_a$, where the dependence of n_a on temperature is determined by formula (3.16), it is possible to obtain that $\varkappa_d / \varkappa_g \sim 10^{-1}(D/kT_D,)$ where T_D is the temperature at which the degree of dissociation is close to half. This temperature, as already was mentioned above (see Table 3.6), is small in comparison with D/k which also causes the coefficient of dissociative thermal conductivity to exceed the

coefficient of gas kinetic thermal conductivity.

The value of the coefficient of thermal diffusivity both in the case of gas kinetic, and in the case of dissociative thermal conductivity, is determined by the coefficient of molecular diffusion (see formula (3.7)) and equals 0.4 cm^2/sec where $T = 6{,}000°$ K, $p = 500$ atm, $n = 6 \cdot 10^{20}$ cm^{-3}.

In conclusion let us consider even colder layers of the channel where the water vapor is not dissociated. The coefficient of thermal diffusivity in these layers is less than in the more heated ones. Thus, for example, according to the data in [13], the thermal diffusivity of water vapor $\chi = 0.7 \cdot 10^{-1}$ cm^2/sec where $T = 2500°$ K, $p = 300$ atm, $\rho = 0.175$ g/cm^3, $c_p = 3 \cdot 10^7$ erg/g·deg; where $T = 700°$ K, $p = 300$ atm, $\rho = 0.33$ g/cm^3 $\chi = 0.7 \cdot 10^{-3}$ cm^2/sec. Finally, in water, in the temperature range from 623 to 293° K (room temperature) $\chi = 1.4 \cdot 10^{-3}$ cm^2/sec and $c_p = 4.18 \cdot 10^{-7}$ erg/g·deg.

Section 7. Temperature of the Plasma in a Channel. Energy Balance Equation

The temperature of the plasma in a channel usually is determined experimentally by the optical method. Assuming that a channel radiates as a black body it is possible to determine the temperature of the matter in it according to the relative intensity of several sections of the luminous radiation spectrum. In practice such measurements are performed in the visible part of the section, corresponding to the region of water transparency.

The measurements performed in [14-16] showed that in the case of discharges in a liquid, in which several kilojoules of energy

are released during tens of microseconds, the temperature in the channel is in the area of the first ionization of atoms and is approximately 15,000-25,000° K. The radiation spectrum proves to be Planckian, that is, corresponding to the emission of an absolutely black body.

The plasma temperature also may be estimated according to measurements of the electrical resistance of the channel if the radius of the channel and the pressure in it are known. Actually, by knowing the resistance of a channel and its radius, it is possible to determine the conductivity, and this value, according to formula (3.29), basically is determined by the temperature of the channel and only slightly--logarithmically--depends on the electron concentration.

A graph of the dependence of conductivity on temperature is shown in Fig. 3.20 for several values of the pressure in the channel. By using this graph it is easy to solve the inverse problem--to determine the temperature of the channel according to its conductivity at a given pressure. Estimates of this type were performed in [17] and led to results which agree with the above-mentioned results of optical measurements. Thus, for example, for a discharge no. 8 (see Table 3.5), in which $3 \cdot 10^3$ J was released in a channel $l = 7$ cm in length for $\tau = 10^{-4}$ sec the temperature proved to be approximately equal to 15,000° K.

Thanks to the high particle density, the heated plasma of the discharge channel is an intensive light source, radiating as an absolutely black body. This circumstance opens the possibility of using electrical discharges as high intensity light sources [18, 19].

The amount of energy removed by luminous radiation greatly depends on the temperature of the plasma [illegible]. It is small in the case of temperatures of 15,000° K, but becomes significant even [illegible]

discharge No. 8 (see Table 3.5) experimental data and theoretical estimates (see Section 2, Chapter III) show that the characteristic radius R_0 of a channel, the form of which is close to cylindrical, is equal in order of magnitude to 1 cm. Assuming that the plasma temperature of a channel $T_{ef} \approx 15{,}000°$ K and that the mean radius of the channel is $R_0/2$, we obtain that the energy of luminous radiation is

$$\Delta E_{rad} \approx 2\pi \left(\frac{R_0}{2}\right)^2 l \sigma T_{ef}^4 \sim 600 \text{ J} .$$

Where $T_{ef} = 20{,}000°$ K the energy of radiation is already around 1800 J. However, not all luminous radiation escapes the channel. In the case of temperatures on the order of 15,000° K and higher the wave length, corresponding to the maximum of a Planck distribution, according to the Wien Law is $\lambda_m = A/T \approx 2000$ Å, i.e. lies in the ultraviolet region of the spectrum, and water strongly absorbs luminous radiation in this region. Thus, for example, at 1500 Å the coefficient of light absorption in water is approximately 10^4 cm^{-1}. Therefore, only the visible part of the radiation escapes the channel, and a significant part of the luminous radiation is "trapped."

This gives some basis for ignoring the energy removed from the channel by luminous radiation when calculating the energy balance of a discharge. On the other hand, the assumption of the trapped nature of the radiation makes it possible to perform a very rough estimate of the temperature in the discharge channel, which is, however, of a tentative nature and which leads, rather, to a clarification of the qualitative picture of the phenomenon.

Actually, if we assume that radiation is absorbed in the envelope of the channel and goes for the evaporation and dissociation of water particles, then the number of the particles evaporated

from a unit of channel surface for a unit of time is $\sigma T_{ef}^4/D = \sigma T^4 l_c/DR_0$, where $T_{ef}^4 = \frac{l_c}{R_0} T^4$ [3]; D is the dissociation energy of a water molecule relative to one atom; R_0 is the characteristic channel radius. In a discharge plasma $(l_c/R_0)^{1/4} \approx 1$, and therefore $T_{ef} \approx T$. The total number of particles transferred from the water into the channel is

$$N = \sigma T^4 \tau S l_c / D R_0,$$

where S is the surface area of the channel; R_0 is its radius; τ is the discharge duration. With the aid of this relationship it is possible to express the intrinsic energy of plasma in a discharge channel as a function of temperature

$$W = \frac{pV}{\gamma - 1} = \frac{NkT}{\gamma - 1} = \frac{kTl_c}{\gamma - 1} \frac{\sigma T^4}{DR_0} \tau S. \qquad (3.42)$$

In order of magnitude the intrinsic energy of plasma is equal to the total energy E released in the channel after the time

$$\frac{l_c k \sigma T^5}{R_0 (\gamma - 1) D} \tau S \sim E,$$

Hence

$$T \sim \left[\frac{E(\gamma - 1) D R_0}{\sigma k \tau S l_c} \right]^{\frac{1}{5}}. \qquad (3.43)$$

The surface area S of a discharge channel may be determined on the basis of theoretical estimates or experimental data; for cylindrical $S = 2\pi R_0 l$, where $R_0 \approx \left(\frac{(\gamma - 1)}{\pi p} \chi_c^2 \frac{E}{l} \right)^{1/4}$; for spherical discharge $S = 4\pi r_0^2$, $r_0 = \left(\frac{3}{\pi} \frac{(\gamma - 1)}{p} \tau^2 E \right)^{1/5}$ (see Section 3, Chapter III).

We shall now give an example of an estimate of channel temperature according to formula (3.43). For the above mentioned discharge No. 8 (see Table 3.5) with l = 7 cm, E ≈ $3 \cdot 10^3$ joules, $\tau = 10^{-4}$ sec, $R_0 \approx 1$ cm, $S = 2\pi l R_0$ formula (3.43) gives $T \sim 1.5 \cdot 10^4$° K. It is interesting to note that, as is seen from (3.43) the temperature slightly depends on the amount of energy and the time of its release. This circumstance is in qualitative agreement with test results.

On the basis of that which has been said it is possible to consider approximately that the energy, released in the channel, basically goes to heat the matter in the discharge channel and to expand the channel over the surrounding liquid.

In addition it proves to be the case that the energy going to heat the matter is concentrated in the basically comparatively uniformly heated part of the channel, while the energy stored in the thin surface layer is comparatively small. The amount of this energy ΔE may be estimated according to the formula $\Delta E \sim wS\delta$, where w is the energy of a unit volume; S is the surface area of the channel; $\delta \sim 2\sqrt{\chi t}$ is the thickness of the transition layer. The value of the coefficient of thermal diffusivity varies over the length of the surface layer.

First let us examine the temperature range corresponding to molecular dissociation, that is, T ~ 6,000° K. When p = 500 atm, $n = 6 \cdot 10^{20}$ the coefficient of thermal diffusivity in this area is 0.4 cm^2/sec (see the end of the preceding section), and the energy of a unit volume is approximately equal to $w \sim \frac{D}{3} \approx 3 \cdot 10^9$ erg/cm^3. Then for discharge No. 8 (see Table 3.5) with the parameters l = 7 cm, E = $3 \cdot 10^3$ J, $\tau = 10^{-4}$ sec we obtain: $\delta \approx 10^{-2}$ cm and ΔE ≈ [illegible] J.

The amount of energy stored in the colder regions of the surface layer also is small. The corresponding estimates, made for the above-mentioned discharge with the use of the results of the preceding section and information on the thermodynamic properties of water vapor [13] show that in the temperature range $T \approx 2500°$ K, $\delta \approx 5 \cdot 10^{-3}$ cm, $\Delta E \approx 10$ J; with temperatures of $T \approx 700°$ K, $\delta \approx 5 \cdot 10^{-4}$ cm, $\Delta E \approx 5$ J. Finally, in the heated layer of water with temperatures of $T \approx 350°$ K, $\delta \approx 7 \cdot 10^{-4}$ cm, $\Delta E \approx 10$ J.

Thus, it is possible to consider that the intrinsic energy of the matter in the channel, taking account of the increased number of particles in it, is determined by the energy of the plasma filling it, the energy density of which, according to formula (3.23), is $w = p/(\gamma - 1)$ where $\gamma = 1.26$.

The work of expansion A is determined by the expression $\int p dv$, since the expansion of the channel as a result of heating is negligibly small in comparison with the purely hydrodynamic process of expansion, and in this sense it is possible to consider the channel wall to be impenetrable.

The equation of the balance of energy in the discharge process therefore acquires the form

$$\frac{d}{dt}\frac{pv}{\gamma - 1} + p\frac{dv}{dt} = N(t), \tag{3.44}$$

where $N(t)$ is the rate of energy released in the channel. This equation will be examined in detail in the following chapters.

LITERATURE

1. *Кужекин И. П.* — ЖТФ, 1966, 36, вып. 2.
2. *Кожельков В. С., Кузнецов Н. А., Скворцов Ю. В.* — ЖТФ, 1960, 30, вып. 10.
3. *Зельдович Я. Б., Райзер Ю. П.* Физика ударных волн и высокотемпературных гидродинамических явлений. М., изд-во «Наука», 1966.
4. *Мак-Даниэль И.* Процессы столкновений в ионизированных газах. М., изд-во «Мир», 1967.
5. *Lighthill M. J.* — J. Fluid Mech., 1957, 2, 1.
6. *Греков Л. И., Москвин Ю. В., Романычев В. С., Фаворский О. Н.* Основные свойства некоторых газов при высоких температурах. М., 1964.
7. *Аллен К. У.* Астрофизические величины. М., ИЛ, 1960.
8. *Арцимович Л. А.* Управляемые термоядерные реакции. М., Физматгиз, 1961.
9. *Спитцер Л.* Физика полностью ионизированного газа. М., изд-во «Мир», 1965.
10. *Жданов В. М.* — ПМТФ, 1965, № 4.
11. *Брагинский С. И.* — ЖЭТФ, 1958, 34, вып. 6, 1548.
12. *Батлер Д., Брокау Р.* Теплопроводность газовых смесей при химическом равновесии. Сб. «Проблемы движения головной части ракет дальнего действия». М., ИЛ, 1959.
13. Теплотехнический справочник. Учеб. пособие для энергет. и политех. вузов. М., Госэнергоиздат, 1957.
14. *Бонн Г. А.* — Оптика и спектроскопия. 1965, 18, 529.
15. *Martin E. A.* — J. Appl. Phys., 1960, 31, 255.
16. *Куценко А. Н., Корнеев А. В.* — Изв. вузов. Физика, 1963, 1, 112.
17. *Иоффе А. И., Наугольных К. А., Рой Н. А.* — ПМТФ, 1964, № 4.
18. *Early H. C., Martin E. A.* — Comm. and Electronics, 1956, 1, 783.
19. *Н. Н. Огурцова, И. В. Подмошенский, В. М. Шелемина.* — Оптика и спектроскопия, 1964, 16, вып. 6.
20. Электрический взрыв проводников. М., Изд-во «Мир», 1965.

CHAPTER IV

HYDRODYNAMIC PROBLEMS OF THE EXPANSION OF A CAVITY IN A LIQUID

Section 1. Introduction

From the hydrodynamic point of view an electrical discharge may be considered as a process of the expansion of a cavity in a fluid. The hydrodynamic characteristics of this process depend on the relationship between three spatial scales of the phenomena; the length of the discharge gap l, the characteristic channel radius R_0, and the characteristic wave length $\lambda = c_0\tau$, where τ is the discharge duration. In connection with this it is possible to distinguish two classes of cases.

The first of them refers to the situations where $R_0 \ll \lambda$, which means that the rate of expansion of the channel R_0/τ is small in comparison with the speed of sound c_0, and the disturbances in the density of the fluid, caused by the expansion of the channel, are insignificant. Among these, in turn, it is possible to isolate three cases, allowing for a simple approximation of the shape of the channel and distinguished by the relationship of the length of the discharge gap l with the remaining spatial scales R_0 and λ.

If $l \ll R_0 \ll \lambda$ (Fig. 4.1, a), the shape of the channel, evidently, is close to spherical, which makes it possible to use the simplest spherical model in calculation.

If $R_0 \ll l \ll \lambda$ (Fig. 4.1, b), it is necessary to consider the extent of the channel in calculating the hydrodynamic values near the discharge, while from the acoustic point of view, as before,

In this case a model of a cylinder, short in comparison with the wave length, is acceptable.

Where $R_0 \ll \lambda \ll l$ (Fig. 4.1, c) it is possible to use a model of a cylinder long as compared with the wave length.

The second class includes modes in which $R_0 \gtrsim \lambda$, which corresponds to expansion of the channel at speeds close to or exceeding the speed of sound. In this case disturbances in the density of the fluid caused by the expansion of the channel become intense and it is necessary to consider the compressibility of the fluid. Here also it is possible to isolate the two simplest cases, when a spherical model ($l \ll \lambda \lesssim R_0$), and a cylindrical model ($\lambda \lesssim R_0 \ll l$) are acceptable (Fig. 4.1, d and 4.1, e).

In this chapter we shall examine some aspects of the hydrodynamic problem of the expansion of cavities--spherical and cylindrical--in a fluid, with the intention of using the results obtained here later in studying the hydrodynamic phenomena caused by discharges.

We shall be interested, in particular, in the pressure produced by a fluid on a cavity expanding in it in relation to the mode of expansion of the cavity, and also the characteristics of the compression wave radiated by the expanding cavity. In addition, the problem of the pulsations of a gas filled cavity in a liquid will be solved.

The motion of the liquid here is assumed to be isentropic, described by the system of hydrodynamic equations [1, 2],

$$\frac{\partial \mathbf{v}}{\partial t} + \mathbf{v}\nabla\mathbf{v} = -\frac{\nabla p}{\rho}, \qquad (4.1)$$

$$\frac{\partial \rho}{\partial t} + \operatorname{div} \rho \mathbf{v} = 0, \qquad (4.2)$$

and the equation of state

$$p = A\left(\frac{\rho}{\rho_0}\right)^n - B, \qquad (4.3)$$

where A = 3001 atm, B = 3000 atm, n = 7 for water.

In calculating the pressure in a moving liquid it is convenient to use a relationship representing a generalization of

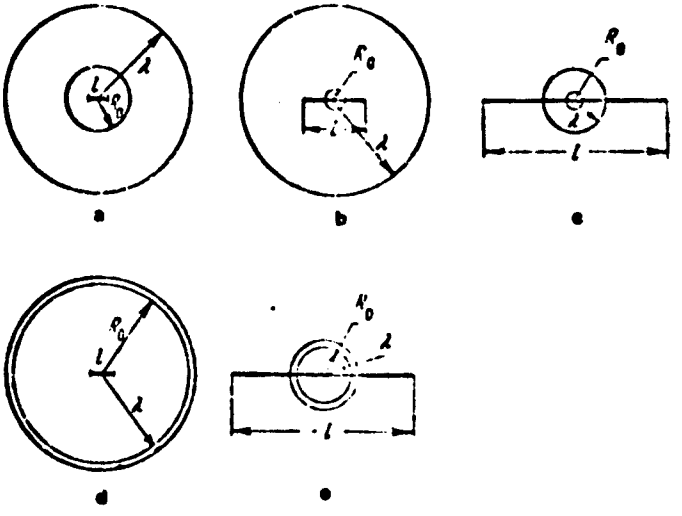

Fig. 4.1. Dimensional scale of the cavity expansion problem.

the Bernoulli equation to the nonsteady-state case and being the first integral of the Euler equation (4.1) [1],

$$h + \frac{1}{2}v^2 + \frac{\partial\varphi}{\partial t} = f(t) = \text{const}, \qquad (4.4)$$

where h is the specific enthalpy; v is the hydrodynamic velocity; φ is the velocity potential ($v = \text{grad}\ \varphi$).

If the excess pressures in the liquid caused by the expansion of the cavity are comparatively small and insignificantly change its density, then h is approximately p/ρ_0 and instead of (4.4) we obtain

$$\frac{p}{\rho_0} + \frac{1}{2}v^2 + \frac{\partial\varphi}{\partial t} = \text{const}. \qquad (4.5)$$

This relationship makes is possible to determine the pressure at a given point under the condition that the flow of the liquid is known, that is, that the velocity distribution and its variation with time are given.

We shall ignore the influence of the viscosity of the liquid, which is not significant for the problems examined here.

Section 2. The Problem of the Expansion of a Sphere in the Case of Low Rates of Expansion.

Let there be a spherical cavity of radius R_1 in a liquid at rest. The pressure in the surrounding liquid is p_0. At the initial moment t = 0 the sphere begins to expand according to a given law R(t). Let us find the pressure on the surface of the sphere, assuming that the rate of expansion of the sphere is small, so that the liquid may be considered to be incompressible.

From the continuity equation where $\rho = \rho_0 = \text{const}$ we obtain the following formula for the velocity, satisfying the boundary condition of equality of velocities on the surface of the sphere

$$v = \frac{R^2}{r^2}\dot{R}, \tag{4.6}$$

where r is the radial coordinate.

It is easy to obtain the velocity potential distribution of the liquid along the radius from the formula (4.6)

$$\varphi = -\frac{R^2\dot{R}}{r}. \tag{4.7}$$

Now substituting the formula for the velocity (4.6) and the velocity potential (4.7) into formula (4.5) and determining the

constant entering this formula from the boundary condition at infinity, we find the pressure distribution in the liquid

$$p - p_0 = \rho_0 \frac{R^2\ddot{R} + 2R\dot{R}^2}{r} - \rho_0 \frac{R^4}{2} \frac{\dot{R}^2}{r^4}. \tag{4.8}$$

This relationship also may be rewritten in the form

$$p - p_0 = \rho_0 \frac{\ddot{V}}{4\pi r} - \frac{1}{2} \rho_0 \frac{\dot{V}^2}{(4\pi r^2)^2},$$
$$V = \frac{4}{3} \pi R^3. \tag{4.9}$$

Assuming r = R in formula (4.8), we obtain a formula for the pressure P on the surface of a sphere expanding according to the given law

$$P = p_0 + \rho_0 \left(\frac{3}{2} \dot{R}^2 + R\ddot{R} \right). \tag{4.10}$$

We note that near the sphere at distances of r ≈ R the last term in the right member of formula (4.8), resulting from the presence of the nonlinear Bernoulli term in formula (4.5), proves to be a value on the same order of magnitude as the remaining terms of this formula with any rates of expansion of the sphere, however small.

Let us now deal with the compressibility of the liquid. The expansion of the sphere causes a density disturbance, propagating in the form of a spherical diverging wave. If the rate of expansion of the sphere is small in comparison with the speed of sound in the disturbed medium, and the density disturbances are small and consequently, the propagation of the diverging wave, may be described by a solution of the linear acoustics, approximately satisfying the boundary condition of continuity of velocity on the surface of the sphere [1],

$$\varphi = -\frac{\dot{V}\left(t - \frac{r}{a}\right)}{4\pi r}, \tag{4.11}$$

where $V = (4/3)\pi R^3$ is the volume of the sphere; c_0 is the speed of sound.

Substituting the formula for the velocity potential in formula (4.5) we find the pressure in the radiated wave

$$p - p_0 = \rho_0 \frac{\dot{V}\left(t - \frac{r}{c_0}\right)}{4\pi r} + \frac{1}{2}\rho_0 \frac{\dot{V}\left(t - \frac{r}{c_0}\right)}{(4\pi)^2 r^4}. \qquad (4.12)$$

In the wave zone the second term in the right member of this formula is negligibly small, so that relationship (4.12) turns into formula

$$p - p_0 = \rho_0 \frac{\dot{V}\left(t - \frac{r}{c_0}\right)}{4\pi r}. \qquad (4.13)$$

Near the sphere at distances of $r \ll c_0 t$ formula (4.12) turns into formula (4.9) obtained in approximation of an incompressible liquid.

The radiated energy may be found by integration of the energy flow through the surface, encompassing the sphere

$$W_{ac} = 4\pi r^2 \int_0^\infty \frac{(p - p_0)^2}{\rho c_0}\, dt.$$

We shall use the results obtained for examining the problem of the expansion of a sphere under the influence of a compressed gas filling it.

Let a sphere of radius R_1 be at rest at an initial moment, and the pressure P_1 of the gas in it be greater than the pressure p_0 of the surrounding medium. Under the action of this pressure difference the sphere begins to expand. Assuming that in the expansion of the sphere the change in the state of the gas takes place adiabatically, we obtain the following connection between

the gas pressure in the cavity and its radius:

$$P = P_1\left(\frac{R_1}{R}\right)^{3\gamma}. \tag{4.14}$$

where γ is the adiabatic gas exponent, equal to the ratio of heat capacities with constant pressure and volume.

Substituting formula (4.14) for the pressure into formula (4.10), we obtain an equation describing the process of the expansion of the cavity

$$R\ddot{R} + \frac{3}{2}\dot{R}^2 = \frac{1}{\rho_0}\left[P_1\left(\frac{R_1}{R}\right)^{3\gamma} - P_0\right]. \tag{4.15}$$

This differential equation often is called the Rayleigh equation, first used in approximation of an incompressible liquid to examine the problem of the expansion and slamming of a cavity in a liquid [3]. It may be integrated one time if R is taken as an independent variable instead of t.

Thus, it is possible to obtain the first integral of equation (4.15) [4]

$$\dot{R}^2 = \frac{2P_1}{3\rho_0}\left\{\frac{1}{\gamma-1}\left(1-\frac{R_1^{3\gamma-3}}{R^{3\gamma-3}}\right)\frac{R_1^3}{R^3} - \frac{P_0}{P_1}\left(1-\frac{R_1^3}{R^3}\right)\right\}. \tag{4.16}$$

This formula also may be obtained indirectly from energy considerations.

The intrinsic energy of an ideal gas filling a volume V,

$$W = \frac{PV}{\gamma-1} \tag{4.17}$$

may be expressed as a function of the radius of the cavity R with the aid of formula (4.14)

$$W = \frac{p_1}{\gamma - 1} \frac{4}{3} \pi R^3 \left(\frac{R_1}{R}\right)^{3\gamma}. \qquad (4.18)$$

We shall take the energy of a liquid without a bubble as zero. Then the potential energy of a cavity of radius R in a liquid, equal to the work against the forces of external pressure, performed in forming such a cavity, is

$$A = p_0 \frac{4}{3} \pi R^3. \qquad (4.19)$$

The kinetic energy of the spreading flow of liquid may be expressed by the following formula with the aid of formula (4.7)

$$W_k = \int_R^\infty 4\pi r^2 \frac{\rho u^2}{2} dr = 2\pi \rho_0 R^3 \dot{R}^2. \qquad (4.20)$$

Then it is possible to write the law of the conservation of energy in the process of bubble expansion in the following way:

$$2\pi \rho_0 R^3 \dot{R}^2 + \frac{4}{3} \pi p_0 R^3 + W(R) = \frac{4}{3} \pi p_0 R_1^3 + W(R_1) = E, \qquad (4.21)$$

where E is the initial energy of the bubble.

This equation which, with the substitution of formula (4.18) into it, coincides with equation (4.16), describes the motion of a gas filled cavity in a liquid. It may be integrated numerically under given initial conditions.

In the case under consideration, when the initial gas pressure in the sphere is greater than equilibrium, integration of equation (4.16) shows that initially the cavity expands, reaching dimensions greater than equilibrium, and then slams shut, returning to the initial state, after which the process is repeated in the form of successive pulsations.

[illegible]

The amplitude of the pulsations within the framework of the approximation used here, not considering energy dissipation, does not decrease.

By analyzing equation (4.21) it is possible to obtain a number of approximate relationships, describing the process of the cavity pulsation [4].

During the greater part of the pulsation period, as a consequence of the record reduction in pressure in the cavity with an increase in its radius, a relative part of the intrinsic energy in the energy balance equation (4.21) is small and may be ignored.

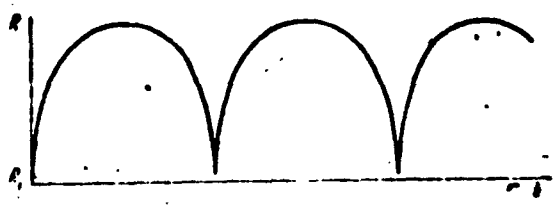

Fig. 4.2. Dependence of the radius of a pulsating sphere on time.

Then from (4.21) we obtain the approximation equation

$$2\pi\rho_0 R^3\dot{R}^2 + \frac{4}{3}\pi p_0 R^3 = E. \qquad (4.22)$$

At the moment of the maximum expansion of the bubble the rate of motion of its surface becomes zero, and thus from formula (4.22) it is possible to express the maximum radius through the total pulsation energy

$$\frac{4}{3}\pi p_0 R_{max}^3 = E. \qquad (4.23)$$

Now excluding E from formula (4.22) with the aid of relationship (4.23), we obtain the equation

$$R^3 = \frac{2p_0}{3\rho}\left(\frac{R_{max}^3}{R^3} - 1\right), \tag{4.24}$$

examined by Rayleigh (see [3]) in studying the slamming of a hollow cavity in a liquid under the action of hydrostatic pressure.

This equation may be integrated, which leads to the relationship

$$t = \sqrt{\frac{3\rho}{2p_0}} \int \frac{dR}{\sqrt{\frac{R_{max}^3}{R^3} - 1}} + \text{const.} \tag{4.25}$$

The integral entering in this equation is not expressed in elementary functions, although it may be reduced to the sum of incomplete beta functions.

Choosing R = 0 and R = R_{max} in the integral of formula (4.25) as the limits of integration, we find the time required for the expansion of a cavity from zero to maximum radii. By virtue of the fact that in the cases of interest to us $R_1 \ll R_{max}$, this time is approximately equal to half the pulsation period of the cavity [4]

$$\frac{\tau_0}{2} = \sqrt{\frac{3\rho}{2p_0}} \int_0^{R_{max}} \frac{dR}{\sqrt{\frac{R_{max}^3}{R^3} - 1}}, \tag{4.26}$$

hence

$$\tau_0 \approx 1{,}83 R_{max}\left(\frac{\rho}{p_0}\right)^{\frac{1}{2}}, \tag{4.27}$$

By using relationship (4.23) it is possible to express the pulsation period by the amount of total energy of the pulsating bubble [5]

$$\tau_0 = 1{,}14\rho_0^{\frac{1}{2}} \frac{E^{\frac{1}{3}}}{p_0^{\frac{5}{6}}}. \qquad (4.28)$$

Sometimes this equation is called the Willis formula.

As is seen, the pulsation period increases in proportion to the cube root of the amount of total pulsation energy and decreases in proportion to the amount of hydrostatic pressure to the exponent 5/6. It is necessary, however, to note that the formula is not applicable if the pulsating bubble is located near the boundary of the liquid as a consequence of a change in the nature of the expanding flows.

Ignoring the pressure of the gas inside the cavity, correct for the greater part of the pulsation period, proves to be unacceptable in the initial stage of the process of bubble expansion. This is connected with the fact that at the initial moment the pulsation energy is concentrated in the form of the intrinsic energy of the compressed gas, the pressure of which is the factor determining the motion. At this stage it is possible, on the other hand, to ignore the influence of the external pressure and to omit, correspondingly, the second term in the braces of relations (4.16).

The equation thus obtained

$$\dot{R}^2 = \frac{p_1}{\rho_0} - \frac{2}{3(\gamma-1)} \left[\left(\frac{R_1}{R} \right)^{3\gamma} \left(1 - \frac{R_1^{3\gamma-3}}{R^{3\gamma-3}} \right) \right] \qquad (4.29)$$

together with equation (4.15), in which p_0 is assumed to be omitted, forms a system which makes it possible to determine the maximum rate of bubble expansion $\dot{R}_{max}$ and the bubble radius at the moment

of reaching the maximum rate from the condition of $\ddot{R}$ vanishing

$$\dot{R}^2_{max} = \frac{2}{3}\frac{P_1}{\rho_0}\gamma^{-\frac{\gamma}{\gamma-1}} \quad \text{where} \quad \left(-\frac{R_1}{R}\right)^{3-3\gamma} = \gamma. \tag{4.30}$$

Further, in the particular case, when $\gamma = 4/3$, equation (4.29) may be integrated, which gives the approximate dependence of the radius of the sphere on time, valid for the initial stage of expansion when $P \gg p_0$ [4].

$$t = \sqrt{2}\frac{R_1}{\sqrt{\frac{P_1}{\rho_0}}}\sqrt{Y}\left(1 + \frac{2}{3}Y + \frac{1}{5}Y^2\right), \tag{4.31}$$

where

$$Y = \frac{R}{R_1} - 1.$$

As is seen from relationships (4.30) and (4.31), in the initial stage of expansion, when the internal pressure is the decisive factor in the process, the rate of expansion, in order of magnitude, is equal to

$$\dot{R} \sim \sqrt{P_1/\rho_0}, \tag{4.32}$$

and the time τ_1, during which the radius of the sphere increases by the order of magnitude of its initial value, is $\tau_1 \sim R_1/\sqrt{P_1/\rho_0}$.

During this time the pressure in the bubble decreases by an amount equal to its initial value (Fig. 4.3).

We shall now give a numerical example for illustration.

Let $P_1 = 10^3$ atm, $R_1 = 1$ cm, $\gamma = 1.4$.

Then, the maximum rate of bubble expansion which can be reached where $R = 1.3\ R_1$, is approximately $1.4 \cdot 10^4$ cm/sec; corresponding to this the bubble radius reaches a value of $2R_1$ during the time $\tau \sim 10^{-4}$ sec.

The velocity distribution in the liquid surrounding the sphere is described by relationship (4.7), and the pressure distribution by formula (4.8), which may be converted into the following form with the aid of formulas (4.10) and (4.14):

$$p - p_0 = \frac{R}{r}\left[p_1\left(\frac{R_1}{R}\right)^{3\gamma} - p_0 + \frac{1}{2}\rho_0 \dot{R}^2\left(1 - \frac{R^4}{r^4}\right)\right], \tag{4.33}$$

which is convenient for explaining the connection between the pressure in the bubble and the pressure at a fixed point in the liquid r.

From this formula it is obvious that the pressure at a point sufficiently distant from the bubble ($r \gg R$) differs from the pressure in the bubble at a given moment of time not only by the factor $1/r$, but also by an additive term proportional to $\rho_0 \dot{R}^2$.

This term, lowering the pressure near the bubble, where the speeds of the liquid are great is sometimes arbitrarily called the Bernoulli term.

A velocity profile is schematically represented in Fig. 4.4 and a profile of the pressure in the vicinity of an expanding sphere is represented in Fig. 4.5.

Curve 1 in Fig. 4.5 corresponds to the moment of time when the pressure inside the bubble still exceeds the hydrostatic pressure, while curves 2 and 3 depict the pressure distribution at later moments of time, when $p < p_0$. The sharp change in pressure near the bubble, at distances of several R, is due to

the influence of the Bernoulli term; at greater distances the basic cause of the decrease in pressure is its reduction according to the spherical law 1/r.

Let us now clarify the limits of applicability of the solution obtained, based on the assumption of the incompressibility of the liquid.

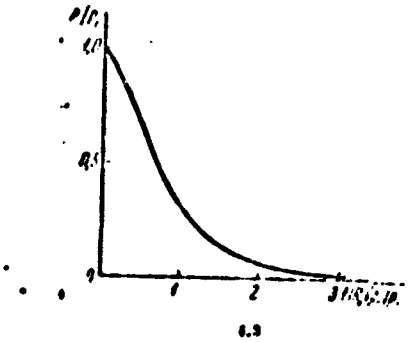

Fig. 4.3. Reduction of the pressure in a cavity during its expansion.

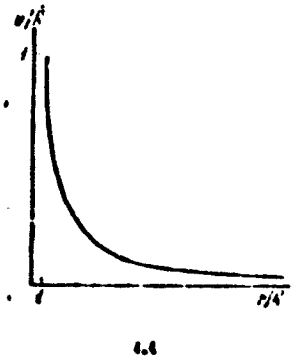

Fig. 4.4. Velocity distribution in the vicinity of an expanding sphere.

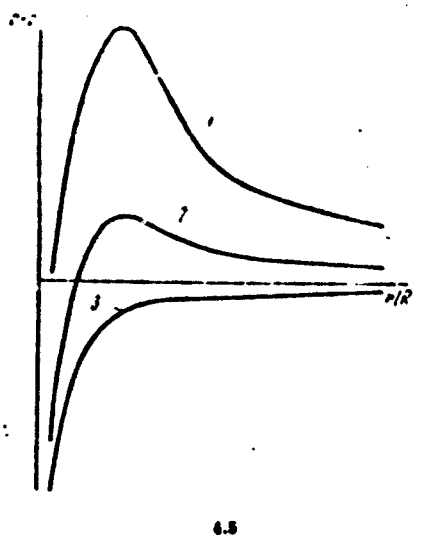

Fig. 4.5. Pressure distribution in the vicinity of an expanding sphere.

Namely, we shall now define the condition that the changes in the density of the liquid are small.

From the equation of state of a liquid (1.3) we have

$$\frac{\Delta\rho}{\rho} = \frac{p}{AA}, \qquad (4.3)$$

For water, for example, we therefore obtain that compressibility may be ignored in the case where

$$\frac{\Delta p}{p_\infty} \sim \frac{p}{21000} \ll 1. \qquad (4.35)$$

Rewriting formula (4.35) with regard to relationship (4.32), determining the order of magnitude of the rate of expansion of the sphere,

$$\frac{\Delta p}{p_\infty} \sim \frac{\rho U_0^2}{n^2 p_\infty} \sim \frac{U_0^2}{c^2} \ll 1, \qquad (4.36)$$

we note that the compressibility of a liquid in the problem of the expansion of a cavity may be ignored if the rate of expansion of the sphere is small in comparison with the speed of sound in the liquid.

Calculation of the compressibility, however, is necessary in examining the compression wave radiated by the sphere, to which we shall now turn. In the case of low rates of expansion of the sphere this calculation may be performed in approximation of linear acoustics.

We note that ignoring the compressibility of the liquid in calculating the expansion of the sphere and taking account of it in calculating the radiation are not inconsistent in the given case.

In the case of low rates of expansion under consideration the influence of compressibility has an insignificant effect on the rate of expansion of the sphere.

It may be said that the energy of radiation is small in comparison with the kinetic energy of the spreading flow of liquid and therefore it is not necessary to consider it in the energy balance

equation (4.21).

Consequently, in the given case the problem of radiation is subdivided into a calculation of the sphere expansion, which may be performed in an approximation of an incompressible liquid, and a subsequent calculation of the radiation of a sphere, expanding according to a known law in a compressible medium.

The solution of the first problem is described by formula (4.16). Substituting the results of integration of equation (4.16) into formula (4.12) it is possible to find the pressure profile of the wave radiated by the sphere.

In practical calculations it is convenient to rewrite formula (4.12) with the aid of formulas (4.10) and (4.14) in the form

$$p - p_0 \approx \frac{R}{r}\left[p_1\left(\frac{R_1}{R(\tilde{t})}\right)^{3\gamma} - p_0 + \frac{1}{2}\rho_0 \dot{R}(\tilde{t})^2\left(1 - \frac{R^3(\tilde{t})}{r^3}\right)\right],$$

$$\tilde{t} = t - \frac{r}{c_0}. \qquad (4.37)$$

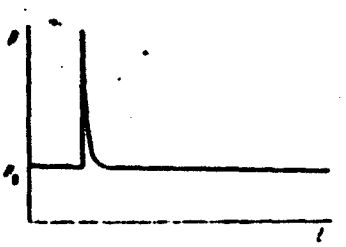

Fig. 4.6. Schematic profile of the compression wave radiated by an expanding sphere.

Calculation shows that a gas cavity, containing a gas under elevated pressure at the initial moment, in the process of expansion radiates a wave consisting of a comparatively short pressure pulse and a longer rarefaction pulse. The shape of the wave is depicted schematically in Fig. 4.6. The pressure pulse is emitted at the initial stage of the expansion process, when the pressure in the cavity is still high. Then, during the course of that part of the pulsation period

when the pressure in the cavity is lower than the hydrostatic pressure, the rarefaction pulse is emitted. When the cavity slams shut a compression pulse is emitted again, and the picture is repeated.

It is possible to make a simple estimate of the parameters of the compression pulse. In the initial stage of the expansion process $R \sim R_1$ and $\dot{R}^2 \sim P_1/\rho_0$, according to (4.32). Then $\ddot{V}/4\pi \sim R_1\dot{R}^2 \sim R_1 P_1/\rho_0$ and therefore the pressure in the compression pulse, in accordance with (4.13), in order of magnitude is equal to $p \sim P_1 R_1/r$, and the duration of the compression pulse

$$\tau_1 \sim R_1/\sqrt{P_1/\rho_0}.$$

The radiated energy is concentrated, basically, in the compression pulse; its value is determined by the formula

$$W_{ac} \approx 4\pi r^2 \frac{p^2}{\rho c} \tau_1,$$

which makes it possible to determine what part of the energy, initially stored in the form of the potential energy of the gas in the cavity

$$W = \frac{P_1}{\gamma - 1} \cdot \frac{4}{3}\pi R_1^3,$$

is removed by the compression wave

$$\frac{W_{ac}}{W} \sim 3(\gamma - 1)\frac{R_1}{ct}. \qquad (4.38)$$

As is seen, in the case of low rates of expansion R/t, as compared with the speed of sound, the amount of energy removed by the wave is small.

Section 3. Expansion of a Cylindrical Cavity in a Liquid.

We shall now consider a cylindrical cavity expanding in an ideal liquid according to the given law R(t). The pressure in the surrounding liquid is p_0. We shall assume that the rate of expansion is small in comparison with the speed of sound, and, correspondingly, the radius of the cylinder is small in comparison with the characteristic wave length. The liquid is assumed to be at rest up to the beginning of the expansion of the cylinder. The velocity potential of the medium which is put into motion as a result of the expansion of the cylinder in the case of low rates of expansion may be obtained by summing the potentials of the elementary sources, each of which, for example, located at a point z', creates at a point of observation with the coordinates r, z the potential

$$d\varphi = -\frac{S\left(t-\frac{\sqrt{r^2+(z-z')^2}}{c_0}\right)dz'}{4\pi\sqrt{r^2+(z-z')^2}}, \qquad (4.39)$$

where $S = \pi R^2$ is the cross sectional area of the cylinder. The meaning of the remaining terms is clear from Fig. 4.7.

The potential created by a cylinder of length l is expressed by the integral

$$\varphi = -\frac{1}{4\pi}\int_{-\frac{l}{2}}^{\frac{l}{2}} \frac{S\left(t-\frac{\sqrt{r^2+(z-z')^2}}{c_0}\right)}{\sqrt{r^2+(z-z')^2}}dz'. \qquad (4.40)$$

Formula (4.40) also may be used for calculating the potential of a cylinder of infinite length. For this we set $z = 0$ and introduce the new variable $t' = t-\sqrt{r^2+z'^2}/c_0$ in place of z'. Then

$$c_0^2(t-t')^2 = r^2 + z'^2$$

$$dz' = -\left[c_0^2(\bar{t}-t)/\sqrt{c_0^2(\bar{t}-t)^2-r^2}\right]d\bar{t}.$$

Passing to the limits of integration from 0 to $l/2$, we rewrite formula (4.40) in the following form:

$$\varphi = \frac{c_0}{2\pi}\int_{\alpha}^{\beta}\frac{\dot{S}(\bar{t})\,d\bar{t}}{\sqrt{c_0^2(\bar{t}-t)^2-r^2}}, \qquad (4.41)$$

where

$$\alpha = t-\frac{r}{c_0}; \quad \beta = t-\frac{\sqrt{r^2+(l/2)^2}}{c_0}.$$

Letting l tend to infinity, we obtain

$$\varphi = -\frac{c_0}{2\pi}\int_{-\infty}^{t-\frac{r}{c_0}}\frac{\dot{S}(\bar{t})\,d\bar{t}}{\sqrt{c_0^2(\bar{t}-t)^2-r^2}}, \qquad (4.42)$$

which exactly coincides with the well-known formula for the potential of an infinite cylinder.

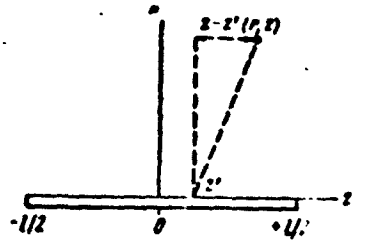

Fig. 4.7. For calculating the potential in a cylindrical problem.

If we limit ourselves to an examination of the hydrodynamic values in the vicinity of the cylinder, in an area of low values of the ratio r/c_0t, then instead of the relationships written above it is possible to use simpler approximation formulas, obtained by expansion of exact formulas with respect to the small parameter r/c_0t.

[illegible] cylinder, the length of which is small

as compared to the characteristic wave length

Then in the case of the low rates of expansion under consideration here the formula for the potential (4.40) may be simplified in the following way. Expanding the integrand into a Taylor series with respect to a small phase "advance" $\sqrt{r^2+(z-z')^2}/c_0$ for sufficiently late moments of time when $t>\sqrt{l^2/4+r^2}$, we obtain

$$\dot{S}\left(t-\frac{\sqrt{r^2+(z-z')^2}}{c_0}\right)\approx\dot{S}(t)-\ddot{S}(t)\frac{\sqrt{r^2+(z-z')^2}}{c_0}. \tag{4.43}$$

Performing term by term integration, we find

$$\varphi=-\frac{1}{2}\frac{\dot{S}(t)}{2\pi}\ln\frac{z+\frac{l}{2}+\sqrt{\left(z+\frac{l}{2}\right)^2+r^2}}{z-\frac{l}{2}+\sqrt{\left(z-\frac{l}{2}\right)^2+r^2}}+\frac{\ddot{S}(t)\,l}{4\pi c_0}. \tag{4.44}$$

In a plane perpendicular to the cylinder and passing through its center ($z = 0$)

$$\varphi=-\frac{\dot{S}(t)}{4\pi}\ln\frac{\frac{l}{2}+\sqrt{\frac{l^2}{4}+r^2}}{-\frac{l}{2}+\sqrt{\frac{l^2}{4}+r^2}}+\frac{\ddot{S}(t)\,l}{4\pi c_0}. \tag{4.45}$$

We shall now examine the two limiting cases of this formula. Let $l\ll r$, so that

$$\varphi=-\frac{\dot{S}(t)\,l}{4\pi r}+\frac{\ddot{S}(t)\,l}{4\pi c}+\dots \tag{4.46}$$

If, on the other hand, $r\ll l$,

$$\varphi=-\frac{\dot{S}(t)}{2\pi}\ln\frac{l}{r}+\frac{\ddot{S}(t)\,l}{4\pi c_0}+\dots \tag{4.47}$$

Substituting formula (4.47) into (4.5) and then assuming

$r = R$, we find the pressure on the surface of a short (in comparison with the wave length) cylinder

$$p - p_0 = \rho_0 \frac{\ddot{S}(t)}{2\pi} \ln \frac{l}{R} - \frac{1}{2} \rho_0 \frac{\dot{S}(t)^2}{4\pi^2 R^2}. \tag{4.48}$$

Let us now consider a cylinder of infinite length. Substituting $\cosh \zeta = \frac{c_0(t-\bar{t})}{r}$ in formula (4.42) we obtain

$$\varphi = -\frac{1}{2\pi} \int_0^{\operatorname{Arch} \frac{c_0 t}{r}} \dot{S}\left(t - \frac{r}{c_0} \cosh \zeta\right) d\zeta. \tag{4.49}$$

Bearing in mind that where $r/c_0 t \ll 1$ $\operatorname{Arch} \frac{c_0 t}{r} \approx \ln \frac{2c_0 t}{r}$ and, in the cases of interest to us, $S(t) = 0$ where $t<0$, formula (4.49) may be rewritten in the form

$$\varphi = -\frac{1}{2\pi} \int_0^{\ln \frac{2c_0 t}{r}} \dot{S}\left(t - \frac{r}{c_0} \operatorname{ch} \zeta\right) d\zeta. \tag{4.50}$$

Expanding the integrand in series and integrating term by term, we obtain

$$\varphi \approx -\frac{\dot{S}(t)}{2\pi} \ln \frac{2c_0 t}{r} + \frac{S(t)}{2\pi}. \tag{4.51}$$

In the particular case of the expansion of a cylinder at a constant rate from formula (4.51) we obtain the relationship

$$\varphi = -U^2 t \ln \frac{r}{2c_0 t} + U^2 t + \ldots \tag{4.52}$$

Whence, using the general connection between pressure and velocity potential (4.5), we find

$$p - p_0 = \rho_0 U^2 \left(\ln \frac{2c_0}{U} - \frac{1}{2}\right). \tag{4.53}$$

It is interesting to note that within the framework of the approximation under consideration (a low rate of expansion) this formula satisfies the exact similitude equation of the problem of the expansion of the cylinder at a constant rate, cited in [6].

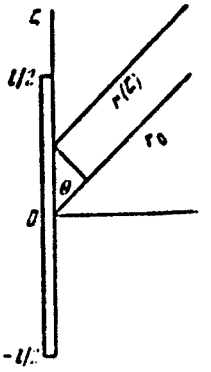

Fig. 4.8. For calculating the radiation of a cylinder.

Substituting formula (4.51) into relationship (4.5) and assuming r = R, we obtain a formula for the pressure exerted by a medium on an expanding cylinder.

$$p - p_0 = \rho_0 \frac{\dot{S}(0)}{2\pi} \ln \frac{2al}{R} - \frac{1}{2} \rho_0 \frac{\dot{S}^2}{4\pi^2 R^2}. \qquad (4.54)$$

This formula is applicable if the rate of expansion of a cylinder is not great, $R/c_0 t \ll 1$ and its length is much greater than the characteristic wave length $l \gg c_0 \tau$.

We shall now turn to a calculation of the acoustic radiation of a cylindrical cavity expanding in a liquid. We shall consider the channel to be a set of point sources. Then a general expression for the potential of the field created in the liquid by the expanding cylinder is given by formula (4.40). If we consider the field only at a sufficient distance from the discharge, in the Fraunhofer zone, this formula, as is known, may be rewritten approximately in the form

$$\varphi = -\frac{1}{4\pi r} \int_{-\frac{l}{2}}^{+\frac{l}{2}} \dot{S}\left(t - \frac{r(\zeta)}{c_0}\right) d\zeta, \qquad (4.55)$$

where $r = r_0 - \zeta \cos\theta$ is the distance to the point of observation and the meaning of θ and ζ is clear from Fig. 4.8.

Hence, it is easy also to find the pressure in the radiated wave

$$p - p_0 = \frac{\rho_0}{4\pi r} \int_{-\frac{l}{2}}^{\frac{l}{2}} \ddot{S}\left(t - \frac{r}{c_0}\right) d\zeta = \frac{\rho_0 c_0}{4\pi r \cos\theta} \int_{\alpha}^{\beta} \ddot{S}(\xi)\, d\xi. \qquad (4.56)$$

where

$$\alpha = t - \frac{r_0}{c_0} - \frac{l\cos\theta}{2c_0},$$

$$\beta = t - \frac{r_0}{c_0} + \frac{l\cos\theta}{2c_0}.$$

For the direction perpendicular to the axis of the channel $\theta = \pi/2$, $\cos\theta = 0$ and from the first half of formula (4.56) we obtain immediately

$$p - p_0 = -\frac{\rho_0 l}{4\pi r} \ddot{S}\left(t - \frac{r_0}{c_0}\right). \qquad (4.57)$$

For the case of a short cylinder the maximum phase difference l/c_0 of the signals radiated by the different ends of the cylinder is small in comparison with the pulse duration τ, $l/c_0 \ \tau \ll 1$. This makes it possible to obtain a simple approximation formula from (4.56), if we expand the integrand into the series

$$\ddot{S}\left(t - \frac{r}{c_0}\right) = \ddot{S}\left(t - \frac{r_0}{c_0}\right) + \dddot{S}\left(t - \frac{r_0}{c_0}\right)\frac{\zeta\cos\theta}{c_0} + \ldots$$

After integration, omitting the now superfluous zero index of the coordinate, we obtain

$$p - p_0 = \rho_0 \frac{l}{4\pi r} \ddot{S} + \rho_0 \frac{l^2\cos\theta}{8\pi r c_0} \dddot{S} + \ldots \qquad (4.58)$$

Using (4.58), it is easy to calculate the radiated acoustical energy, integrating the flow of energy with respect to a spherical reference surface and with respect to time

$$W_{ac} = 2\int_0^{\frac{\pi}{2}} \int_0^{t} \frac{(p - p_0)^2}{\rho_0 c_0} dt 2\pi r^2 \sin\theta d\theta. \qquad (4.59)$$

In the case of a cylinder long in comparison with the wave length, the phase difference of the signals emitted by the different ends of the cylinder is great and formula (4.58) cannot be applied; in place of it, it is necessary to use the exact formula (4.56), the transverse signal, naturally, being described by formula (4.57) as before.

The total acoustical energy radiated by a long cylinder may be calculated according to formula (4.59), in this case using the Parseval equation

$$\int_{-\infty}^{+\infty} (p - p_0)^2 dt = \frac{1}{\pi} \int_0^{\infty} |s(\omega, 0)|^2 d\omega, \tag{4.60}$$

where $s(\omega,\theta)$ is the spectrum of the signal emitted by a discharge in the direction θ with respect to the channel axis.

This spectrum may be determined according to the formula

$$s(\omega, 0) = s(\omega) \frac{\sin n\omega \frac{\Delta t}{2}}{\sin \omega \frac{\Delta t}{2}}, \tag{4.61}$$

where $\Delta t = \frac{\Delta \zeta}{c_0} \cos \theta$, $n = \frac{l}{\Delta \zeta}$, which represents the signal spectrum of a system of n point sources, arranged at a distance $\Delta\zeta$ from one another. If we let $\Delta\zeta$ tend to zero it is possible to convert to a continuous distribution of sources on the length l. The quantity $s(\omega)$ in formula (4.61) is the spectrum of an elementary signal, coinciding, correct to within a constant factor, with the spectrum of the signal, emitted by a channel in the perpendicular direction

$$s(\omega) = \frac{\Delta \zeta}{l} \int_{-\infty}^{\infty} p_{\perp}(t) \exp(-i\omega t) dt, \tag{4.62}$$

where $p_1 = p - p_0$ when $\theta = \pi/2$ and at a distance r from the channel.

If we assume, for example, that $p_\perp(t)$ has the form of a rectangle with the amplitude $p_\perp$ at a distance r and with the duration τ, then from formula (4.62) it follows that

$$s(\omega) = 2\tau \frac{\Delta\zeta}{l} p_\perp \frac{\sin \omega\tau/2}{\omega\tau/2}. \qquad (4.63)$$

Substituting (4.63) into (4.61), after integration we find

$$\int_0^\infty |s(\omega, 0)|^2 d\omega = \frac{32 p_\perp^2 \cdot \frac{3}{4}}{\omega^2 \cos^2 \theta}. \qquad (4.64)$$

Turning now to formula (4.59), we find the acoustic energy radiated by a cylinder of length $l \gg c_0\tau$ under the condition that the expansion of the cylinder is such that a rectangular pulse of duration τ and amplitude $p_\perp$ at a distance r from the channel is radiated in a direction perpendicular to the channel axis [12]

$$W_{ac} = \frac{4\pi r^2 p_\perp^2 \tau^2}{\rho_0 l} \left[\frac{1}{8} \cdot \frac{c_0 \tau}{l} + \frac{1}{2} - \ln \frac{c_0 \tau}{l} \right]. \qquad (4.65)$$

We note that in the case of a rectangular approximation of the signal, calculation of the radiation may be performed comparatively simply and by direct summation of the elementary signals emitted in a given direction.

If we approximate the shape of the emitted compression wave in the direction perpendicular to the channel axis by a Gauss curve with a constant decay τ_0, i.e., we assume, that the shape of the signal at a distance r from the discharge is described by the formula

$$p - p_0 = p_\perp e^{-\pi \left(\frac{t}{\tau_0}\right)^2}, \qquad (4.66)$$

then a calculation analogous to the preceding leads to the following formula for the energy of radiation:

$$W_{sc} = \frac{4\pi r^2 p_1^2 \tau_0^2}{\rho_0 l}\left[\frac{1}{4} - \frac{c_0\tau_0}{l} + 0{,}42 + \ln\frac{l}{c_0\tau_0}\right]. \qquad (4.67)$$

Section 4. Influence of Compressibility on the Process of the Expansion of a Cavity in a Liquid

We shall now turn to an examination of cases where the rate of expansion of a cavity in a liquid is great ($R_0 \approx \lambda$) and the density disturbances caused by the expansion of the cavity are significant. First we shall consider the case of a spherical cavity.

It is not possible to obtain an exact solution of the problem of the expansion of a spherical cavity in a liquid that reduces to the integration of the hydrodynamic equations, which forces us to use numerical or approximation methods.

The Kirkwood-Bethe method (see [5], which they developed in investigating underwater explosions, is a very effective approximation method of solving the problems of spherical (and cylindrical) flows.

If instead of the velocity potential φ we introduce $\Phi = R\varphi$, then equations (4.1), and (4.2) may be transformed into one equation of the form [5]

$$\frac{\partial^2\Phi}{\partial t^2} - c^2\frac{\partial^2\Phi}{\partial r^2} = \left[\frac{v}{2}\left(\frac{\partial v}{\partial r}\right)^2 - \left(\frac{\partial v}{\partial t}\right)^2\right], \qquad (4.68)$$

where

$$c(p) = \left(\frac{\partial p}{\partial \rho}\right)_s.$$

In the case of small disturbances where it is possible to ignore quadratic terms equation (4.68) reduces to a wave equation. This means that in this case the values of Φ are "shifted" at the speed c_0, where $c_0 = c(\rho_0)$ is the speed of sound in an undisturbed liquid.

obtain a solution of equation (4.68) in the form of a translational wave. Nevertheless, Kirkwood and Bethe assumed that the value Φ in this case propagates at the speed $\bar{c} = c + v$ similar to the way in which fixed values of pressure and velocity propagate in a plane Riemann wave.

This means that the value $-r\frac{\partial\varphi}{\partial t}$ also propagates at the speed $\bar{c}$. From equation (4.4) it follows that

$$-\frac{\partial\varphi}{\partial t} = h + \frac{v^2}{2}, \tag{4.69}$$

where h is the specific enthalpy, determined by the following formula in the case of isentropic flows

$$h = \int_{p_\infty}^{p} \frac{dp}{\rho}. \tag{4.70}$$

Thus, according to the Kirkwood-Bethe theory it is assumed that the function

$$G(t,r) = -r\frac{\partial\varphi}{\partial t} = r\left(h + \frac{v^2}{2}\right) \tag{4.71}$$

propagates at the speed $\bar{c}$, that is, the following equation is valid

$$\frac{\partial G}{\partial t} + \bar{c}\frac{\partial G}{\partial r} = 0, \tag{4.72}$$

which is the basic equation of the theory. We emphasize that equation (4.72) does not derive from the equations of hydrodynamics; it may be considered simply as a successful hypothesis, justified by the good agreement of its solutions with the results of numerical calculations. This equation may be rewritten in a different form convenient for calculating the pressure on the surface of an expanding sphere in a compressible fluid [5].

From (4.71) we have

$$\frac{\partial}{\partial t}\left(\frac{p}{\rho^{\gamma}}\right) + \frac{\partial}{\partial r}\left(\frac{p}{\rho^{\gamma}}\right) = 0. \tag{4.73}$$

Substituting formula (4.73) into (4.72) and then eliminating the partial derivatives with respect to time and the coordinate with the aid of the relationships:

$$\frac{\partial p}{\partial t} = \frac{dp}{dt} + \rho v \frac{dv}{dt},$$

$$\frac{\partial v}{\partial t} = \frac{dv}{dt} + v\left(\frac{1}{\rho c^2}\frac{dp}{dt} + \frac{2v}{r}\right),$$

$$\frac{\partial p}{\partial r} = -\rho \frac{dv}{dt}, \qquad (4.74)$$

$$\frac{\partial v}{\partial r} = -\frac{1}{\rho c^2}\frac{dp}{dt} - \frac{2v}{r},$$

obtained from equations (4.1) and (4.2) and the formula for the total derivative

$$\frac{d}{dt} = \frac{\partial}{\partial t} + v\frac{\partial}{\partial r},$$

we find after simple transformations

$$\frac{dv}{dt}\left[c - 2v\right] + \frac{3}{2}\frac{v^2}{r}\left[\bar{c} - \frac{4}{3}v\right] = -\frac{\bar{c}h}{r} + \frac{dh}{dt}\left[1 + \frac{3v^2}{c^2} - \frac{\bar{c}v}{c^2}\right]. \qquad (4.75)$$

On the surface of the sphere r = R, v = U, h = H; considering also that $\bar{c} = c + v$, we obtain finally

$$\frac{dU}{dt}\left(1 - \frac{U}{c}\right) + \frac{3}{2}\frac{U^2}{R}\left(1 - \frac{U}{3c}\right) = \left(1 + \frac{U}{c}\right)\frac{H}{R} + \left(1 - \frac{U}{c}\right)\frac{1}{c}\frac{dH}{dt}. \qquad (4.76)$$

If the law of expansion of the sphere R(t) is known, equation (4.76) makes it possible to determine the value of the enthalpy on the surface of the sphere as a function of time, and together with it also the pressure exerted by a compressible fluid on an expanding sphere.

The connection between pressure and enthalpy is expressed by a relationship deriving from the equation of state (4.3) and the definition of enthalpy (4.70),

$$p = A\left[1 + \frac{n-1}{2} H\right]^{\frac{n}{n-1}} - B. \tag{4.77}$$

Relationships (4.76) and (4.77) may be considered as a generalization of formula (4.10), applicable for an incompressible fluid.

As may be seen from (4.76) and (4.77), the influence of compressibility leads to an increase in pressure on the surface of an expanding sphere in the case where the pressure decreases with time ($dv/dt<0$), and to an increase in pressure with a growth in pressure, that is, compressibility of the fluid produces a damping effect, which is natural to expect.

We note that equation (4.76) may be simplified somewhat if we bear in mind that the hydrodynamic velocity U remains small in comparison with the local speed of sound c even in the case of rapid motion of the surface of the sphere, equal to c_0. This makes it possible to neglect terms of values U/c in comparison with unity and to write equation (4.76) in the form

$$\frac{dU}{dt} + \frac{3}{2}\frac{U^2}{R} = \frac{h}{R} + \frac{1}{c}\frac{dh}{dt}. \tag{4.78}$$

It is possible to have another simplification of equation (4.76) obtained by expansion of this equation with respect to the small parameter U_c and with the use of the approximation expression for enthalpy $h \approx \frac{p - p_0}{\rho_0}$,

$$\frac{dU}{dt}\left(1 - \frac{2U}{c}\right) + \frac{3}{2}\frac{U^2}{R}\left(1 - \frac{4}{3}\frac{U}{c}\right) = \frac{U}{\rho c}\frac{dp}{dR} + \frac{p}{\rho R}. \tag{4.79}$$

This relationship coincides with the equation obtained in [7].

We shall now examine the problem of the radiation in the case of small speeds of the expanding sphere when it is necessary to

calculating the process of sphere expansion.

The basis of the method suitable for solving this problem, in the presentation of which we follow here [8], is the assumption that the function

$$G = r\left(h + \frac{r^2}{2}\right) \tag{4.8}$$

propagates with the speed $\bar{c} = c + v$.

Therefore, if the value of this function on the boundary is known, then it may be calculated at any point in space.

Thus, the problem is divided into two stages: 1) determining the function $G(\bar{t})$ on the surface of the expanding sphere ($\bar{t}$ is used to designate the time reckoned on the surface of the sphere); 2) determining the function $G(t, r)$, and together with it the other hydrodynamic values at an arbitrary point of observation.

If the motion of the sphere is given, $R = R(\bar{t})$, then $U = \dot{R}$ is known, and the enthalpy h on the surface of the sphere may be found from relationship (4.76), which also completes determining $G(\bar{t})$ on the surface of the sphere.

In correspondence with the basic assumption of the Kirkwood-Bethe theory (see [5]) the value of the function $G(t, r)$ at an arbitrary point in space is determined by the relationship

$$G(t, r) = G(R, \bar{t}) = G(\bar{t}), \tag{4.81}$$

whereby

$$t = \bar{t} + \int_R^r dr/c. \tag{4.82}$$

Near the wave front at distances small in comparison with the [illegible] of the sphere the [illegible] relationships are valid:

$$G = rc_0 v(1 + \beta v), \tag{4.83}$$

$$\tau = c_0(1 + 2\beta v), \tag{4.84}$$

where

$$\beta = \frac{n+1}{4c_0}.$$

Expressing dr from (4.83) and bearing in mind that the function G remains constant during propagation we obtain

$$\int \frac{dr}{c} = -\frac{G}{c_0^2}\int_v^v \frac{dv}{v^2(1+\beta v)^2}, \tag{4.85}$$

where $U = V(r)$.

Expressing τ as a function of G from formula (4.81), performing integration in formula (4.85), and substituting the results into (4.82), finally we determine t as a function of G, r, and R

$$t = \tau(G) + \frac{G}{c_0^2}\beta\left[\frac{1+2\beta v}{\beta v(1+\beta v)} - \frac{1+2\beta U}{\beta U(1+\beta U)} - 2\ln\frac{(1+\beta v)\beta U}{\beta v(1+\beta U)}\right], \tag{4.86}$$

where, according to formula (4.83)

$$\beta v = \frac{1}{2}\left[\left(1 + \frac{n+1}{rc_0^2}G\right)^{\frac{1}{2}} - 1\right], \tag{4.87}$$

$$\beta U = \frac{1}{2}\left[\left(1 + \frac{n+1}{Rc_0^2}G\right)^{\frac{1}{2}} - 1\right]. \tag{4.88}$$

We shall now analyze the solution obtained.

If the disturbances are small and it is possible to ignore βv in comparison with unity in formula (4.85), then instead of formula (4.86) there follows the well-known result of linear acoustics

$$t = \tau + \frac{r-R}{c_0}. \tag{4.89}$$

the surface of a radiating sphere of radius R to the point of observation R does not depend on G.

Consideration of the following term in the expansion of the denominator of formula (4.85) in βv leads to the solution

$$t-\tau=\frac{r-R}{c_0}-\frac{G}{c_0^3}2\ln\frac{r}{R}. \tag{4.90}$$

In this approximation, the lag $t-\frac{r}{c_0}$ proves to be a linear function of G. Hence, it follows that, in contrast to formula (4.89), this solution describes a wave, the profile of which changes during propagation.

It is interesting to note that the solution of (4.90), in particular coincides with the result of the direct integration of the equations of hydrodynamics to a second approximation with respect to βv [9, 10].

In the general case for arbitrary disturbances formula (4.86) makes it possible to determine t as a function of G, R, and r and in the same way to find the fields of the hydrodynamic quantities--the velocity, according to formula (4.87), and the pressure, which may be expressed by the formula

$$p(r,t)=A\left[\frac{2}{n+1}+\frac{n-1}{n+1}\left(1+\frac{n+1}{rc_0^2}G\right)^{\frac{1}{2}}\right]^{\frac{2n}{n-1}}-B. \tag{4.91}$$

As an illustration of the method discussed we shall present the result of a calculation of the radiation of the compression wave of a sphere expanding under the influence of the pressure of the gas contained in it. The solution of this problem is obtained with the aid of the Kirkwood-Bethe theory (see [8]).

The change in the state of the gas inside the cavity was assumed to be adiabatic. Corresponding to this, the value of the

function $G(\bar{t})$ on the surface of the expanding sphere was determined by numerical integration of the system of equations (4.76) and (4.77) and the adiabatic equation

$$\frac{p}{p_1} = \left(\frac{R_1}{R}\right)^{3\gamma}. \qquad (4.92)$$

where R_1 and p_1 are the initial values of the radius of the sphere and the pressure in it.

The the profiles of the pressure at different distances from the source were calculated according to formula (4.86) with respect to the known function $G(\bar{t})$.

In the case of sufficiently high initial gas pressures the pressure profile calculated becomes ambiguous, which signifies the formation of shock waves.

Their position and the magnitude of their distortion are determined according to the solution obtained with the aid of Rankine-Hugoniot relationships, which, in the case of low intensity shock waves, reduce to the simple law of "equality of areas" [1].

A typical result of a calculation is shown in Fig. 4.9, taken from [8]. Curve 1 is plotted according to formulas (4.86) and (4.91) where $r/R = 10^{-4}$, $R = 0.1$ cm, $P_1 = 10^5$ atm, and curve 2 represents the profile of the shock wave formed.

The expansion of a cylindrical cavity in a liquid with great rates of expansion may be examined in similar fashion.

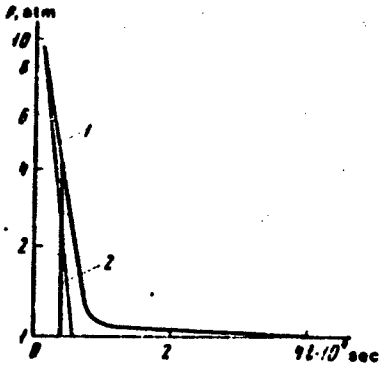

Fig. 4.9. Formation of a shock wave in the case of the propagation of the compression wave radiated by an expanding sphere.

It is assumed that the function $G = r^{\frac{1}{2}}\left(h+\frac{v^2}{2}\right)$ propagates at the speed $c = c + v$ and, correspondingly, satisfies the equation

$$\frac{\partial G}{\partial t}+\tilde{c}\frac{\partial G}{\partial r}=0. \tag{4.93}$$

This equation may be transformed and, being applicable to the surface of the expanding cylinder, is written in the form

$$\frac{dU}{dt}\left(1-\frac{U}{c}\right)+\frac{3}{4}\frac{U^2}{R}\left(1-\frac{1}{3}\frac{U}{c}\right)=\frac{1}{2}\frac{H}{R}\left(1+\frac{U}{c}\right)+ \\ +\left(1-\frac{U}{c}\right)\frac{1}{c}\frac{dH}{dt}. \tag{4.94}$$

If the law of the expansion of the cylinder R(t) is known, equation (4.93) makes is possible to calculate the enthalpy, and together with it with the aid of formula (4.77),the pressure on the surface of the cylinder as a function of time.

The distribution of hydrodynamic values in the vicinity of the cylinder at distances which are short in comparison with its length also may be found with the Kirkwood-Bethe method.

In fact, by using the condition of the constancy of the function G in the process of wave propagation and with known values of this function on the surface of an expanding cylinder, it is possible to determine its values at those points in space where the wave still may be considered to be cylindrical.

The [illegible] is proved to be more convenient to calculate the function $\varphi(r)$ in the inverse of G according to the formula

$$t = \tau(G) + 2\frac{G^2}{c_0^2}\left[G\beta^2 \ln\frac{(1+\beta r)U}{(1+\beta U)v} + \frac{4\beta^2 v}{1+\beta v} - \frac{4\beta^2 U}{1+\beta U} - \right.$$
$$- \frac{\beta^4 v^2}{2(1+\beta r)^2} + \frac{\beta^4 U^2}{2(1+\beta U)^2} + \frac{(1+\beta v)^2}{2v^2} - \frac{(1+\beta U)^2}{2U^2} -$$
$$\left. - \frac{4\beta(1+\beta r)}{v} + \frac{4\beta(1+\beta U)}{U}\right], \quad \beta = \frac{n+1}{4c_0}. \tag{4.95}$$

In this case the hydrodynamic values are connected with the auxiliary function G by the relationships

$$\beta v = \frac{1}{2}\left[\left(1 + \frac{4\beta G}{r^{1/2}c_0}\right)^{\frac{1}{2}} - 1\right], \tag{4.96}$$

$$\beta U = \frac{1}{2}\left[\left(1 + \frac{4\beta G}{R^{1/2}c_0}\right)^{\frac{1}{2}} - 1\right], \tag{4.97}$$

which also makes it possible to find the spatial distributions of these values.

In the case of moderate rates of expansion formula (4.95) is simplified

$$t - \frac{r-R}{c_0} = \tau(G) - \frac{4\beta}{c_0^2} G\left(r^{\frac{1}{2}} - R^{\frac{1}{2}}\right) \tag{4.98}$$

in agreement with the well-known result of linear acoustics [11].

In the case of low rates of expansion ($\beta v \to 0$) formula (4.95) transforms into the well-known result of linear acoustics

$$t - \frac{r-R}{c_0} = \tau(G). \tag{4.99}$$

LITERATURE

1. *Ландау Л. Д., Лифшиц Е. М.* Механика сплошных сред. М., ГИТТЛ, 1954.
2. *Зельдович Я. Б., Райзер Ю. П.* Физика ударных волн и высокотемпературных гидродинамических явлений. М., Физматгиз, 1966.
3. *Rayleigh.*— Philos. Mag., 1917, 34, 94.
4. *Ламб Г.* Гидродинамика. М., ОГИЗ, 1947.
5. *Коул Р.* Подводные взрывы. М., ИЛ, 1950.
6. *Кочина Н. Н., Мельникова Н. С.*— ПММ, 1959, 23, № 1, 93.
7. *Trilling L.*— J. Appl. Phys., 1952, 23, 14.
8. *Акуличев В. А., Богуславский Ю. Я., Иоффе А. И., Наугольных К. А.*— Акуст. ж., 1967, 13, вып. 3, 321.
9. *Whitham G. B.*— Fluid Mech., 1956, 1, 305.
10. *Наугольных К. А.*— Акуст. ж., 1965, 11, вып. 3, 351.
11. *Наугольных К. А., Султанов С. И., Хохлов Р. В.*— Вестник МГУ, 1962, вып. 4, 65.
12. *Иоффе А. И., Кожелупова Н. Г., Наугольных К. А., Рой Н. А.*—Акуст. ж., 1967, 13, вып. 2, 208.

CHAPTER V

THEORY OF THE EXPANSION OF A DISCHARGE CHANNEL

Section 1. Introduction

The release of energy in a discharge channel induces an increase in pressure in it which leads to the rapid expansion of the channel, accompanied by the radiation of a compression wave and the subsequent formation of a pulsating gas bubble.

In the process of the expansion of the channel the walls of the channel may be considered to be impermeable for the liquids surrounding it. This does not mean, of course, that in considering the processes inside the channel it is possible to ignore evaporation of material on the channel wall, but, by virtue of the significant difference between the densities of the matter in the channel and in the liquid, evaporation on the sheath of the channel, being significant for the processes inside it, leads to a displacement of the boundary of the channel in the liquid which is insignificant against the background of rapid hydrodynamic expansion.

Another important characteristic of discharges in a liquid is the fact that efficient mechanisms of heat conductivity--radiant and electron, leading to rapid equalization of temperature along the radius of the channel, act inside the discharge channel thanks to the high plasma density, while less efficient mechanisms of heat conductivity act in peripheral areas of the channel, which leads to a slow heating of the matter in this area and, correspondingly, to a rapid temperature drop on the channel boundary.

The above-mentioned characteristics of the phenomenon make it possible to propose a simple theoretical model, satisfactorily

describing the process of channel expansion.

We shall consider a discharge channel as a cavity in a liquid filled with a uniform plasma and having a sharp boundary with cold liquid. The amount of plasma increases in the process of the discharge due to evaporation from the channel walls. We shall consider the temperature, pressure, and density of the plasma to be constant along the radius of the cavity.

Limiting ourself to an examination of discharges with moderate currents, we shall ignore also the magnetic pressure in comparison with the gas kinetic pressure and the influence of the skin effect.

As a result of the release of energy, pressure in the cavity rises and it expands.

In the process of expansion the hydrodynamic and electrical characteristics of the discharge are connected by an energy balance equation, the solution of which makes it possible to determine the dependence of the radius on time, the pressure in the channel, the parameters of the emitted compression wave, and the pulsating bubble according to the given mode of energy release, determined by the electrical characteristics of the discharge [1].

Ignoring energy losses due to the radiation of light and heating of the liquid outside the channel in agreement with the results of Chapter III, it is possible to consider that the energy E released in the form of Joule heat is expended in increasing the intrinsic energy of the plasma W and in the work A over the surrounding liquid performed by the channel during expansion,

$$W + A = E. \qquad (5.1)$$

An actual calculation depends on the relationship between three dimensional scales: the length of the discharge gap l, the characteristic channel radius R_0, and the characteristic wave length λ, determining both the nature of approximations in examining the hydrodynamic

phenomena, and also the choice of one or another hydrodynamic model of the discharge. Several models of a discharge will be examined.

A spherical model of a discharge, applicable under the condition $l \ll R_0 \ll \lambda$, a model of a short cylinder ($R_0 \ll l \ll \lambda$), and a model of a long cylinder ($R_0 \ll \lambda \ll l$) will be examined in an approximation based on the smallness of the density disturbances (acoustic, or an approximation of incompressible fluid).

A spherical model ($l \ll \lambda \ll R_0$) will be examined in a nonlinear approximation considering the finite nature of the density disturbances.

Section 2. Spherical Model of a Discharge.

Let us consider an electrical discharge in a liquid, the length of the discharge gap of which is small in comparison with the characteristic channel radius, and the latter, in turn, is small in comparison with the wave length, that is, $l \ll R_0 \ll \lambda$.

The fact that the characteristic channel radius R_0 is large in comparison with the length of the discharge gap makes it possible to consider that the shape of the channel is close to spherical in the discharge process, while the smallness of the channel radius in comparison of the length of the radiated wave means that the density disturbances of the liquid produced by the discharge are small. In addition, from the acoustic point of view, such a discharge is similar to a point source of sound, which provides the basis for calling such discharges point discharges [2].

We shall examine the energy balance equation (5.1) as applied to the case of a point discharge.

As was shown earlier (see Chapter III), the intrinsic energy of a plasma in a limited range of temperatures may be expressed

approximately by the ordinary formula for the energy of an ideal gas

$$W = \frac{pV}{\gamma - 1}, \tag{5.2}$$

where p is the pressure; V is the volume occupied by the plasma, $V = 4/3\pi R^3$, R is the channel radius, if some effective value of the adiabatic index, equal, for example, to 1.26 in the case of a plasma formed from water, is used as γ.

The expansion work is equal to

$$A = \int_{V_0}^{V} p dV. \tag{5.3}$$

The energy E(t) released in the channel is determined according to the electrical characteristics of the discharge--the current I and voltage U in the discharge gap t

$$E(t) = \int_0^t IU dt. \tag{5.4}$$

The pressure inside the channel may be expressed as a function of the radius of the channel and its derivatives with respect to time may be found by solving the hydrodynamic problem of the expansion of a spherical cavity in a liquid.

In the case under consideration $R_0 \ll \lambda$, this problem may be solved in approximation of an incompressible liquid, since the density disturbances of the liquid are small.

A corresponding solution was obtained in Section 2 of Chapter IV; ignoring the pressure in the undisturbed liquid in comparison with the pressure in the channel in this formula, we obtain

$$p = \rho_0\left(\frac{3}{2}\dot{R}^2 + R\ddot{R}\right) = \rho_0\frac{\ddot{V}}{4\pi R} - \frac{1}{2}\rho_0\frac{\dot{V}^2}{16\pi^2R^4}. \qquad (5.5)$$

Substituting (5.5) into (5.3) we find the work of the expansion of the channel

$$A = \frac{\rho_0}{4\pi}\int_{V_0}^{V}\left(\frac{\ddot{V}\dot{V}}{R} - \frac{\dot{V}^2}{8\pi R^4}\right)dt = \rho_0\frac{\dot{V}^2}{8\pi R}, \qquad (5.6)$$

assuming that $\dot{V}(0) = 0$.

This result may be interpreted in the following way:

A is the work expended in increasing the kinetic energy of the virtual mass of the expanding sphere,

$$A = \rho_0 4\pi R^3\frac{\dot{R}^2}{2}. \qquad (5.7)$$

Substituting (5.2), (5.5), (5.6) into (5.1), we obtain the following equation:

$$\ddot{V}V - \frac{4\beta - \gamma}{2}\dot{V}^2 = \frac{(\gamma-1)}{\rho_0}4\pi RE(t). \qquad (5.8)$$

In this equation it is possible to ignore the second term having a small coefficient. It is possible to verify the correctness of this approximation if we compare the different terms in equation (5.8) by using the results of numerical integration of the simplified equation.

Therefore, we shall use the following equation below

$$\ddot{V}V = \frac{(\gamma-1)}{\rho_0}4\pi RE(t). \qquad (5.9)$$

We shall introduce the dimensionless variables

$$x = \frac{t}{\tau}, \quad f(x) = \frac{E(t)}{E}; \quad y = \frac{R}{R_0}, \qquad (5.10)$$

where τ is the discharge duration; $E = E(t)$ is the energy released

in the discharge channel during the time τ; R_0 is a unit of length to be determined.

In the new variables equation (5.9) acquires the form

$$y^3 \frac{d}{dx}\left(y^3 \frac{dy}{dx}\right) = \left[\frac{3}{4\pi} \frac{\gamma-1}{p_0} \tau^3 E R_0^{-5}\right] f(x). \qquad (5.11)$$

We shall choose R_0 so that the coefficient in the right member of equation (5.11) becomes unity

$$R_0^5 = \frac{3}{4\pi} \frac{\gamma-1}{p_0} \tau^3 E = 0{,}062 \tau^3 E. \qquad (5.12)$$

This relationship exactly coincides with the previously obtained expression (3.5), determining the order of magnitude of the radius of the channel at the end of the discharge.

This means that the new unit of length introduced by relationship (5.12) has the sense of the critical channel radius.

The equation obtained

$$y^3 \frac{d}{dx}\left(y^3 \frac{dy}{dx}\right) = f(x) \qquad (5.13)$$

For numerical calculation can be written in the form of the system

$$\frac{dz}{dx} = \frac{f(x)}{y^3}, \qquad \frac{dy}{dx} = \frac{z}{y^3}. \qquad (5.14)$$

From physical considerations it is natural to choose the initial conditions in the form

$$x = 0, \quad y = y_0, \quad z = 0, \qquad (5.15)$$

where $y_0 = R_{str}/R_0$ is the initial radius of the channel. In

correspondence with the data in Chapter II it is possible to consider that the streamer radius $R_{str} \sim 10^{-2}$ cm. A precise determination of the initial radius is not required since the expansion process basically is determined by the conditions of energy release in the channel, and not by the initial conditions, which the system rapidly "forgets."

Equation (5.13) together with the initial conditions (5.15) completely describes the process of channel expansion if the function f(x) characterizing the mode of energy released in the channel is known (for example, from experiment). We note that thanks to the special selection of the units of time, energy, and length the parameters of the discharge do not enter into equation (5.13) in explicit fashion; their influence is exerted on the equation only through the function f(x). It is possible to state, therefore, that all discharges characterized by identical modes of energy release (identical f(x)) are similar in the sense that they are described by one and the same equation.

In particular, as was mentioned in Chapter III, for all discharges close to critical, the appearance of the standard law of energy release--the function f(x)--is identical, which points out the similarity of these discharges in the above-mentioned sense.

We shall now express the principal quantities characterizing a uniform spherical model of a discharge through the solution of equation (5.13). Since the radius of the channel is

$$R = R_0 y, \tag{5.16}$$

then, substituting this relationship into (5.5) and using (5.14), we find the pressure in the channel

$$p = \rho_0 \frac{R_0^2}{\tau_1^2} \zeta(x), \tag{5.17}$$

where

$$\zeta(x) = \frac{f(x)}{y^3} - \frac{1}{2}\frac{x^2}{y^3}.$$

The work of expansion, according to (5.7), is expressed by the formula

$$A = 2\pi\rho_0 \frac{R_0^3}{\tau^2} y^2\dot{y}^2, \tag{5.18}$$

and the intrinsic energy of the plasma in the channel by

$$W = \rho_0 \frac{R_0^3}{\tau^2} \frac{4\pi}{3(\gamma-1)}\left[f(x) - \frac{x^2}{2y}\right]. \tag{5.19}$$

The density disturbances of the surrounding liquid arising in the discharge channel propagate in the form of a spherical compression wave. The profile of this wave may be determined by using the solution of the problem of the radiation of a sphere, expanding according to a given law in a liquid. In the case of the small rates of expansion under consideration here this problem may be solved in an approximation if linear acoustics (see Section 2 of Chapter IV) where the velocity potential of the radiated wave is determined simply by the bulk speed of the source (4.11), and the pressure in the wave radiated by the sphere is proportional to the bulk acceleration (formula 4.13).

Designating the excess pressure created by the wave as p below, on the basis of (4.11), (4.13), (5.14) and (5.16) we obtain

$$p = \rho_0 \frac{R_0^2}{\tau^2 r} g(x), \quad x = \frac{\bar{t}}{\tau}, \quad \bar{t} = t - \frac{r}{c_0}, \tag{5.20}$$

where $g(x) = \frac{f(x)}{y^3}$.

$$v = \frac{\partial\Phi}{\partial r} = \frac{R_0^2}{\tau^2 r} y^2\dot{y} + \frac{R_0^3}{\tau^2 c_0 r}(2y\dot{y}^2 + y^2\ddot{y}). \tag{5.21}$$

We emphasize that the formulas given, based on a solution of the energy balance equation (5.14), describe only the leading part of the wave radiated in the active stage of the discharge, when current flows along its channel and energy is released.

Knowing the pressure profile of the radiated compression wave we find the acoustic energy removed by this wave

$$W_{ac} = 4\pi r^2 \int_0^\infty \frac{p^2}{\rho c} dt = \frac{4\pi p_0 R_0^6}{c t^3} J. \qquad (5.22)$$

where

$$J = \int_0^\infty \left(\frac{f(x)}{x^3}\right)^2 dx.$$

In calculating the acoustic energy integration may be taken up to $\bar{x} \approx 1$ in view of the rapid decrease of the integrand. In addition, for the function f(x) given in Fig. 3.13 , J ≈ 1.

It is useful to turn our attention to the following feature of the above, given formulas for the hydrodynamic characteristics of a discharge: according to their structure they consist of a dimensional constant and a dimensionless function of time. In addition it proves to be the case that the orders of magnitude that can be described by these formulas in practice are determined by the dimensional coefficients.

The dimensionless functions of time in the area of the maximum differ from unity insignificantly. The peculiarities of calculation noted are connected with the choice of the scales characteristic for the processes under consideration as units of time and length.

In principle the formulas presented above, (5.16)--(5.19) and (5.20)--(5.22), make it possible to calculate the hydrodynamic characteristics of a discharge if the mode of energy released characterized by the function f(x) is known.

In particular, for all discharges close to critical, as was mentioned in Chapter III, the standardized law of energy release is identical and is described by a function, a graph of which is presented in Fig. 3.13.

Correspondingly, the dimensionless functions entering into the formulas for the hydrodynamic quantities also are identical for such discharges.

Therefore, for calculating the characteristics of such discharges it is sufficient to know only two parameters--the discharge duration τ and the total energy released during this time, E, determining, according to formula (5.12), R_0, and together with it, the dimensional coefficients of the formulas cited above. Also it is possible to eliminate R_0 and to rewrite these formulas directly in terms of the parameters τ and E.

In this case the hydrodynamic quantities are described by the formulas:

channel radius

$$R = a\rho_0^{-\frac{1}{5}}\tau^{\frac{2}{5}}E^{\frac{1}{5}}y, \tag{5.23}$$

pressure in the channel

$$P = a^2\rho_0^{\frac{2}{5}}E^{\frac{2}{5}}\tau^{-\frac{6}{5}}\left[\frac{f(x)}{y^3} - \frac{1}{2}\frac{x^4}{y^4}\right], \tag{5.24}$$

pressure in the radiated compression wave

$$p = \rho_0^{\frac{2}{5}}\frac{a^2}{r}E^{\frac{2}{5}}\tau^{-\frac{4}{5}}\frac{f(x)}{y^3}, \tag{5.25}$$

radiated acoustical energy

$$W_{ac} = 4\pi\rho_0^{-\frac{1}{5}}a^4E^{\frac{4}{5}}C_0^{-1}\tau^{-\frac{2}{5}}J, \tag{5.26}$$

where

$$a = \left[\frac{8}{4\pi}(\gamma - 1)\right]^{\frac{1}{5}}.$$

It is interesting to note that the time scale τ enters into (5.23) to the same power as in problems of an intense explosion or the slamming of a bubble in a liquid.

In turn, in the case of discharges close to critical, the parameters τ and E may be approximately determined according to the formula

$$\tau = \pi\sqrt{LC}, \quad E \approx \frac{CU^2}{2} \tag{5.27}$$

(see Table 3.5), which makes it possible to calculate the dependence of the hydrodynamic characteristics of a discharge on the parameters of the electrical circuit. For example, the pressure in a compression wave, in order of magnitude, is determined by the formula

$$p \approx 10^{-3}\frac{1}{r}\left(\frac{CU^2}{L^2}\right)^{\frac{1}{2}} \text{atm},$$

if r expressed in cm, C in f, U in V, and L in H.

An important characteristic of a discharge is the amount of its electroacoustic efficiency, which is understood as being the ratio of the acoustical energy radiated during the discharge, to the total energy introduced into the channel,

$$\eta = \frac{W_{ac}}{E} = 3(\gamma - 1)\frac{R_0}{c_0\tau} J \approx 4\pi\rho_0^{-\frac{1}{5}} a \frac{E^{\frac{1}{5}}}{c\tau^{\frac{3}{5}}} J. \tag{5.28}$$

It is obvious that the efficiency is proportional to the rate of expansion of the channel R_0/τ, depends on the value of the effective adiabatic index for the plasma of the discharge, weakly depends on the amount of energy released E, and increases

with a decrease in discharge duration.

For the discharges of moderate intensity under consideration here, $\eta \sim 10\%$ (values of the parameter, typical for such discharges, are given in Table 3.5). In experimental conditions it is convenient to perform a discharge along the surface of a rigid reflector. The influence of this surface also may be considered in a calculation. We shall examine, for example, a discharge taking place immediately on a rigid plane surface.

If as before the electrode gap is small in comparison with the characteristic channel radius (and the latter is small in relation to the wave length), then the shape of the channel will be close to hemispherical.

Correct to the effects connected with the formation of a boundary layer, such a discharge is equivalent to half a spherical discharge in free space.

Hence, it is clear that the hydrodynamic characteristics of a discharge near a plane will coincide with the corresponding characteristics of a free discharge of double the energy.

They may be calculated according to the formulas for a discharge in free space if in calculating the quantity R entering this formula, instead of E in formula (5.12), we substitute 2E, and in addition, we divide in half the amount of work of the channel, the intrinsic energy of the plasma, and the acoustic energy, in the same way considering the energy found only in one of the half spaces.

Section 3. Short Cylinder Model

If the length of the electrode gap is great in comparison with the radius of the channel, but small in comparison with the wave length, that is $R_0 \ll l \ll \lambda$, then in the discharge process

the channel has an elongated shape, which makes it possible to use a uniform model of a short (in comparison with the wave length) cylinder for describing such a discharge.

The calculation is similar to that performed in the preceding section (see [1] and [3]).

The energy E(t) released in the channel basically is expended in increasing the intrinsic energy of the plasma

$$W = \frac{PSl}{\gamma - 1} \tag{5.29}$$

and in the work of expanding the channel

$$A = \int_{S_0}^{S} P l dS, \tag{5.30}$$

where P is the pressure in the channel; S is the cross sectional area of the channel; l is its length.

The pressure on the surface of a short cylinder, expanding with a speed which is small in comparison with the speed of sound in a liquid, was calculated approximately in Chapter IV, formula (4.48). Ignoring the equilibrium pressure in comparison with the pressure in the channel it is possible to rewrite this formula in the form

$$P = \rho_0 \frac{\dot{S}}{2\pi} \ln \frac{l}{R} - \frac{\gamma_1}{2} \rho_0 \frac{\dot{S}^2}{4\pi^2 R^2}. \tag{5.31}$$

Substituting (5.31) into (5.30) and bearing in mind that

$$P \frac{dS}{dt} = \frac{d}{dt} \rho_0 \frac{\dot{S}^2}{4\pi} \ln \frac{l}{R},$$

we find

$$A = l\rho_0 \frac{\dot{S}^2}{4\pi} \ln \frac{l}{R}. \qquad (5.32)$$

Then substituting (5.29), (5.31) and (5.32) into (5.1) and cancelling l, we obtain the energy balance equation in a calculation for a unit length of a channel

$$2\ddot{S}S \ln \frac{l}{R} + \frac{\dot{S}^2}{2}\left[(\gamma - 1) 2 \ln \frac{l}{R} - 1\right] = 4\pi \frac{(\gamma - 1)}{\rho_0} \frac{E(t)}{l}. \qquad (5.33)$$

We introduce the dimensionless variables

$$x = \frac{t}{\tau}, \quad f(x) = \frac{E(t)}{E}, \quad y = \frac{R}{R_0},$$

where τ, E, and R_0 are respectively the discharge duration, the total energy released in a channel during the time τ, and the characteristic unit length.

In the new variables equation (5.33) acquires the form

$$\frac{d}{dx} y\dot{y} + \dot{y}^2 \left[(\gamma - 1) - \frac{1}{2 \ln \frac{l}{R_0 y}}\right] = \frac{(\gamma - 1)\tau^2 E}{\pi \rho_0 R_0^4 l} \frac{f(x)}{y^3 \ln \frac{l}{R_0 y}}. \qquad (5.34)$$

If the length of the discharge gap is chosen as the characteristic unit length R_0, then this equation may be rewritten in the following way:

$$\frac{d}{dx} y\dot{y} + \dot{y}^2 \left[(\gamma - 1) + \frac{1}{2 \ln y}\right] = \bar{l} \frac{f(x)}{y^3 \ln \frac{l}{R_0 y}}. \qquad (5.35)$$

The dimensionless coefficient $\bar{l} = \frac{(\gamma - 1)}{\rho_0} \cdot \frac{\tau^2 E}{\pi l^5}$ may be considered as a similitude criterion in the sense that discharges characterized by $\bar{l}$ and f(x) will be described by identical equations.

In practice, however, in a caculation of the process of expansion of a channel it is more convenient not to choose l as the unit length R_0, but a quantity, which makes the coefficient

in the right hand part of equation (5.34) equal to one and has the sense of the characteristic radius of the channel

$$R_0^4 = \frac{(\gamma-1)}{\pi\mu_0}\tau^2\frac{E}{l}. \qquad (5.36)$$

From a comparison of (5.34) and (5.36) it is easy to establish that the dimensionless similitude criterion $\bar{l}$ is no other than the fourth power of the ratio of the characteristic radius of the channel to its length, that is, this is a criterion of the geometrical similarity of discharges.

Selection of the dimensional scale of length in correspondence with formula (5.36) leads to the following form of the energy balance equation:

$$\frac{d}{dx}y\dot{y} + \dot{y}^2\left[(\gamma-1) - \frac{1}{2\ln\frac{l}{R_0 y}}\right] = \frac{f(x)}{y^3\ln\frac{l}{R_0 y}}. \qquad (5.37)$$

An estimate shows that the second term in the left hand part of this equation is small and may be omitted.

It is possible to verify the correctness of this approximation by means of a comparison of the terms of equation (5.37), performed on the basis of the results of numerical integration of this equation.

Thus, from (5.37) we obtain

$$\frac{d}{dx}y\dot{y} = \frac{f(x)}{y^3\ln\frac{l}{R_0 y}}, \qquad (5.38)$$

which may be rewritten in the form of two first-order equations

$$\frac{dz}{dx} = \frac{f(x)}{y^3 \ln \frac{l}{R_0 y}},$$
$$\frac{dy}{dx} = \frac{z}{y}. \qquad (5.39)$$

From physical considerations we select the boundary conditions in the form:

$$x = 0, \quad y = y_0, \quad \dot{y} = 0, \quad z = y\dot{y} = 0, \qquad (5.40)$$

where y_0 is the initial radius of the channel.

If the mode of energy release in the discharge channel characterized by the function f(x) is known, then integration of equation (5.38) makes it possible to determine the law of expansion of the channel, and together with it, the other hydrodynamic quantities.

We shall now cite the appropriate formulas.

Radius of the channel

$$R = R_0 y. \qquad (5.41)$$

Pressure in the channel

$$P = \rho_0 \frac{R_0^2}{t^2} \zeta_1(x), \qquad (5.42)$$

where

$$\zeta_1(x) = \frac{f(x)}{y^3} - \frac{z^2}{2y^2}.$$

Work performed by the channel during expansion

$$A = l\rho_0 \pi \frac{R_0^4}{t^2} z^2 \ln \frac{l}{R}. \qquad (5.43)$$

Intrinsic energy of the plasma in the channel

$$W = \frac{1}{\gamma - 1} p_0 \frac{\pi R_0^4 l}{\tau^3} \left[f(x) - \frac{x^2}{2} \right]. \qquad (5.44)$$

It is possible to use formula (4.58) for a calculation of the acoustic energy of a discharge.

The first term in this formula, which may be rewritten in the following fashion,

$$p = p_0 \frac{R_0^2}{\tau^2} \frac{l}{2r} g_1(x),$$
$$x = \frac{1}{\tau}\left(t - \frac{r}{c}\right), \quad g_1(x) = \frac{f'(x)}{y^2 \ln \frac{l}{R_0 y}} \qquad (5.45)$$

describes the shape of the wave emitted in the direction perpendicular to the axis of the discharge ($\theta = \pi/2$).

The second term in formula (4.58), providing correction for the first where $\theta \neq \pi/2$, being proportional to the small parameter of the model of a short cylinder $l/c_0\tau$, is small, which reflects the fact that the wave radiated by a cylinder that is short in comparison with the characteristic wave length differs little from a spherically symmetrical wave.

The acoustic energy emitted during a discharge is obtained by integration of the energy flow with respect to a spherical reference surface and with respect to time

$$W_{ac} = 2 \oint_0^{\pi/2} \int_0^{\infty} \frac{p^2}{\rho c} dt 2\pi r^2 \sin\theta d\theta = \pi \rho_0 \frac{p R_0^4}{c_0 \tau^3} \left[J_1 + \frac{1}{12} \frac{R}{c_0^2 \tau^2} J_2 \right], \qquad (5.46)$$

where

$$J_1 = \int_0^1 \left[\frac{f'(x)}{y^2 \ln \frac{l}{R_0 y}} \right]^2 dx, \quad J_2 = \int_0^1 \left[\frac{d}{dx} \frac{f'(x)}{y^2 \ln \frac{l}{R_0 y}} \right]^2 dx.$$

The second term in brackets in formula (5.46) takes into account the deviation of the shape of the wave from a spherically symmetrical

one. Formula (5.46) is applicable if this term is small in comparison with the first.

Using (5.36) and (5.46) we find the electroacoustic efficiency of the discharge

$$\eta = \frac{W_{ac}}{E} = \frac{l}{c_0 \tau}(\gamma - 1) J_1. \qquad (5.47)$$

In order to avoid misunderstandings we emphasize again that all the findings of this section, including formula (5.47), are correct only under the condition $R_0 \ll l \ll c_0 \tau$.

We note also that, as was done in the case of a spherical model of a discharge, it is possible to eliminate R_0 from the formulas for the hydrodynamic characteristics of a discharge with the aid of relationships (5.36), in this way expressing these values in terms of three parameters of the discharge--the total energy released in the channel, the time of its release, and the length of the electrode gap.

In addition, in rough estimates for discharges close to the critical, it is possible to say that the energy released in the channel and the discharge duration are determined by formulas (5.27).

Correspondingly, it is possible to obtain estimating formulas for the different hydrodynamic characteristics of a discharge.

For example, the peak pressure in a compression wave in a plane perpendicular to the discharge axis and passing through the center of the channel is determined by the formula

$$p_\perp \approx 10^{-4} \frac{U}{r} \sqrt{\frac{\tau}{L}} \text{ atm} \qquad (5.48)$$

if U, r, l, and L are expressed correspondingly in V, cm and H.

Section 4. Long Cylinder Model

In an approximation based on smallness of density disturbances long cylinders also may be examined under the condition that the characteristic channel radius remains small in comparison with the wave length: $R_0 \ll \lambda \ll l$ [4].

The pressure on the surface of a cylindrical cavity, the length of which is great in comparison with the wave length, is determined approximately by relationship (4.54)

$$P \approx \rho_0 \frac{\ddot{S}}{2\pi} \ln \frac{2c_0 l}{R} - \rho_0 \frac{\dot{S}^2}{8\pi^2 l^2}.$$

Substituting this expression into the formulas for the intrinsic energy of the plasma (5.29) and the work of channel expansion (5.30), and the result obtained into the energy balance equation (5.1), we obtain the following equation in an approximation:

$$\left(\rho_0 \frac{\ddot{S}}{2\pi} \ln \frac{2c_0 l}{R} - \rho_0 \frac{\dot{S}^2}{8\pi^2 l^2}\right) S + \rho_0 \frac{S^2}{4\pi} \left(\ln \frac{2c_0 l}{R}\right)' (\gamma - 1) = (\gamma - 1) E/l. \tag{5.49}$$

Turning to the dimensionless variables, $x = t/\tau$, $y = R/R_0$, and $f(x) = E/E_0$, we obtain, ignoring the second and third terms of this equation in view of their smallness,

$$\frac{dx}{dx} y^2 \ln \frac{2c_0 \tau}{R_0} \frac{x}{y} = \frac{(\gamma - 1)}{\pi \rho_0} \frac{\tau^2 E}{R_0^4} f(x). \tag{5.50}$$

Selecting as a new unit of length the quantity defined by the relationship

$$R_0^4 = \frac{(\gamma - 1)}{\pi \rho_0} \tau^2 E \tag{5.51}$$

which has the sense of the characteristic channel radius, we arrive at the equation

$$\frac{dz}{dx} = \frac{f(x)}{y^2 \ln \frac{2c_0 \tau}{R_0} \frac{z}{y}}, \qquad (5.52)$$

where $z = yy$.

In the given case it is convenient to choose the intial conditions in the form

$$x \to 0,\ y \to 0,\ \dot{y} \to 0$$

In practice, in virtue of the insensitivity of the calculation for the initial values of the quantities it proves to be possible to use as initial conditions values of the channel radius and rate of expansion which are quite small in comparison with the characteristic values.

The hydrodynamic characteristics are expressed by the solution of this system in the following way.

Channel radius

$$R = R_0 y. \qquad (5.53)$$

Pressure in the channel

$$P = \rho_0 \frac{R_0^2}{\tau^2} \zeta_1(x). \qquad (5.54)$$

Work of channel expansion

$$A = \pi \rho_0 l \frac{R_0^4}{\tau^2} \cdot z^2 \ln \frac{2c_0 \tau}{R_0} \frac{z}{y}. \qquad (5.55)$$

Intrinsic energy of the plasma in the channel

$$W = \pi l r_0 \frac{H_0^4 l}{\rho^3}\left[I(x) - \frac{\pi^2}{2}\right]. \qquad (5.56)$$

As in the case of a short cylinder we find the acoustic energy by summation of the signals of the elementary sources according to formulas (4.56) and (4.57).

In the direction transverse to the axis of the channel ($\theta = \pi/2$, Fig. 4.8) we obtain immediately

$$p_\perp = \rho_0 \frac{H_0^2 l}{2\pi\rho r} g_0(x), \qquad (5.57)$$

where

$$g_0(x) = \frac{I(x)}{y^2 \ln \frac{2c_0\tau}{H_0}\frac{x}{y}}.$$

In the longitudinal direction ($\theta = 0$) from formula (4.56) we obtain

$$p_\parallel = \frac{\rho c_0 H_0^2}{2r\tau}\int_{x_1}^{x_2} \frac{dz}{dx}\,dx; \quad x_{1,2} = x - \frac{r_0}{c_0\tau} \pm \frac{l}{2c_0\tau}. \qquad (5.58)$$

Bearing in mind that the integrand differs from zero only in the interval $0 \leq x \leq 1$ (the duration of the signal is small in comparison with the time required for it to "travel" along the length of the cylinder l/c_0), it is easy to establish that the maximum value of the longitudinal signal is determined by the formula

$$p_\parallel = \frac{\rho c_0 H_0^2}{2r\tau}\int_0^1 \frac{dz}{dx}\,dx = \frac{\rho c_0 H_0^2}{2r\tau} z(1). \qquad (5.59)$$

The ratio of the amplitudes of the transverse and longitudinal signals, $p_\perp/p_\parallel = l/c_0\tau z(1)$, to within the coefficient $1/z(1)$ close to unity (see Chapter VI), is equal to the ratio of the length of the channel to the length of the pulse, thus reflecting the fact that the transverse signal is obtained by

summation of the amplitudes, and the longitudinal by summation of the durations of the elementary pulses, the number of which is proportional to the length of the radiator l.

The total energy radiated by the channel during a discharge

$$W_{ac} = \frac{4\pi r^2}{\rho c_0} \int_0^{\pi/2} \sin\theta d\theta \int_0^{\tau} p^2 dt \qquad (5.60)$$

may be calculated by using the results of Chapter IV, formulas (4.65) and (4.67).

If we consider quite roughly that an elementary pulse is of rectangular form, then, on the basis of formula (5.57) taking as approximation $p_1 = \rho_0 R_0^2 \dot{l}/2\tau^2 r$ and using (5.51), from formula (4.65) we obtain

$$W_{ac} = (\gamma - 1) E \left[\frac{1}{8} \frac{c\tau}{l} + \frac{1}{2} - \ln \frac{c\tau}{l} \right]. \qquad (5.61)$$

whence the electroacoustic efficiency of a discharge also may be determined without difficulty

$$\eta = (\gamma - 1) \left[\frac{1}{8} \frac{c\tau}{l} + \frac{1}{2} - \ln \frac{c\tau}{l} \right]. \qquad (5.62)$$

If we approximate the shape of the radiated compression wave in the direction perpendicular to the channel axis by a Gauss curve with a decay constant $\tau_0 = 0.7\tau$ and an amplitude, in correspondence with (5.57), expressed by the formula

$$p_\perp = \frac{\rho_0 R_0^2 \dot{l}}{2\tau^2 r}, \qquad (5.63)$$

(that is, we represent approximately the dimensionless function of formula (5.57) as an error function), which, as will be seen later, in a calculation of the hydrodynamic characteristics

of discharges better corresponds to experiment, then calculation with the use of formulas (4.67), (5.51) and (5.63) leads to the following formulas for the acoustic energy and the electroacoustic efficiency:

$$W_{ak} = (\gamma - 1)\left(\frac{r_0}{r}\right)^3 E\left[0{,}25\frac{c_0\tau}{l} + 0{,}42 + \ln\frac{l}{c_0\tau}\right]. \qquad (5.64)$$

$$\eta = \left(\frac{r_0}{r}\right)^3 (\gamma - 1)\left[0{,}25\frac{c\tau_0}{l} + 0{,}42 + \ln\frac{l}{c\tau_0}\right]. \qquad (5.65)$$

We note that the hydrodynamic characteristics may be expressed as functions of the basic parameters of the discharge E, τ, and l by means of omitting R_0 from the corresponding formulas with the aid of relationship (5.51).

In turn, these values are expressed, as previously, by the parameters of the discharge circuit. In addition, a formula is obtained exactly coinciding with formula (5.48) for estimating the pressure in the compression wave.

Section 5. Spherical Model of a Discharge. High Rates of Channel Expansion.

In order of magnitude the rate of expansion of the channel of a point electrical discharge is determined by a relationship derived from Formula (5.12),

$$\frac{R_0}{\tau} \sim \frac{E^{\frac{1}{3}}}{\tau^{\frac{2}{3}}}.$$

Evidently, the rate of expansion is proportional to the energy density in the discharge channel and increases with a decrease in the period of energy release.

If a sufficiently large amount of energy is introduced into the discharge channel for short intervals of time, then the expansion of the channel may take place at speeds close to or even exceeding the speed of sound in the liquid.

The density disturbances prove to be significant and it is necessary to consider the compressibility of the liquid in examining such discharges.

We shall limit ourselves to investigation of a point discharge characterized by the following relationships of the dimensional scales [5]:

$$l \ll R_0 \approx \lambda.$$

As before we shall ignore the influence of magnetic pressure, considering it to be small in comparison with the pressure of hydrodynamic origin. We shall consider the fluid pressure created by the expansion of the channel to be isentropic, which makes it possible to use the equation of state (4.3)

$$p = A\left(\frac{\rho}{\rho_\infty}\right)^n - B,$$

where A = 3001 atm, B = 3000 atm, n = 7 for water.

In calculating the hydrodynamic characteristics of a discharge it is convenient to isolate two successive problems to be solved: 1) calculation of the channel expansion with a given mode of energy release; 2) determining the compression wave radiation by a channel expanding according to a known law.

The process of channel expansion may be described approximately by the system of equations

$$P\frac{dV}{dt}+\frac{1}{\gamma-1}\frac{d}{dt}PV=\dot{E}(t),$$

$$R\frac{d^2R}{dt^2}\left(1-\frac{U}{c}\right)+\frac{3}{2}\left(1-\frac{U}{c}\right)U^2=\left(1+\frac{U}{c}\right)H+\frac{R}{c}\left(1-\frac{U}{c}\right)\frac{dH}{dt},$$

$$H=\int_{P_0}^{P}\frac{dP}{\rho}=\frac{c_0^2}{n-1}\left[\left(\frac{P+B}{A}\right)^{\frac{n-1}{n}}-1\right]. \qquad (5.66)$$

the first of which expreses the law of the conservation of energy during a discharge, and the second and third may be considered as relationships determining the pressure on the surface of an expanding sphere equal to the pressure inside the channel P as a function of the radius of the channel and its derivatives with respect to time. The last two equations are the consequence of the hydrodynamic equations and the equation of state of the liquid obtained in the Kirkwood-Bethe approximation (see [6] and formula (4.76)).

The following symbols are introduced in fromula (5.66) in addition to those already used: $\dot{E}$ --the power released in the channel; H--the enthalpy of the liquid along the surface of an expanding sphere; $c = c(\rho)$--the local speed of sound, being a variable quantity, as opposed to the preceding quantity.

We choose the initial conditions in the form $\bar{t} \to 0$, $R \to 0$, $\dot{R} \to 0$.

In practice, as was mentioned already, it proves to be sufficient where $\bar{t} = 0$ to assign values of the radius of the channel and the rate of its expansion which are quite small in comparison with the characteristic values of these quantities. For performing a numerical calculation it is convenient to represent system of equation (5.66) in dimensionless form.

We introduce the dimensionless variables

$$x=\frac{\bar{t}}{\tau},\quad y=\frac{R}{R_0},\quad z=\frac{\dot{R}}{c_0},\quad \zeta=\frac{P}{P_0\frac{R_0^3}{\tau^2}},$$

$$\eta=\frac{H}{\frac{R_0^2}{\tau^2}},\quad M=\frac{H_0}{c_0^2}, \qquad (5.67)$$

where τ and R_0 are new units of time and length, c_0 is the equilibrium speed of sound, M is the Mach number.

If we choose the discharge duration as the unit of time, and the characteristic channel radius, determined by relationship (5.12) as the unit of length, it is possible to obtain the following system of equations from (5.66):

$$\frac{d\zeta}{dx} = \frac{j(x)}{y^3} - 3\gamma\frac{\zeta}{y}\frac{dy}{dx}, \tag{5.68}$$

$$\frac{d^2y}{dx^2} = \frac{1+M\frac{\dot y}{z}}{1-M\frac{\dot y}{z}}\frac{\eta}{y^3} + M\frac{1}{z}\frac{d\eta}{dx} - \frac{3}{2}\frac{1-\frac{1}{3}M\frac{\dot y}{z}}{1-M\frac{\dot y}{z}}\frac{\dot y^2}{y}, \tag{5.69}$$

$$\eta = \frac{1}{M^2(n-1)}\left[\left(nM^2\zeta + \frac{B}{A}\right)^{\frac{n-1}{n}} - 1\right], \tag{5.70}$$

$$z = \left(M^2 n\zeta + \frac{B}{A}\right)^{\frac{n-1}{2n}}, \quad \dot y = \frac{dy}{dx}, \quad M = \frac{R_0}{c_0 t}. \tag{5.71}$$

relative to the unknown functions y(x), ζ(x), z(x), η(x). A, B and n are constants of the equation of state of the liquid; f(x) is the dimensionless power characterizing the mode of energy release in the channel. In dimensionless form the initial conditions are formulated as follows:

$$x \to 0, \quad y \to 0, \quad z \to 1, \quad \zeta \to 0, \quad \eta \to 0.$$

We note that system of equations (5.68)--(5.71) describing the process of channel expansion contains a single similitude criterion--the Mach number (M).

In the limiting case as $M \to 0$ this system, as should be expected, transforms into a system of equations describing the process of the expansion of the channel of a spherical model with slow rates of expansion of the channel (see Section 2 of the present chapter.

Numerical integration of system of equations (5.68)--(5.71) makes it possible to determine the dependence of the channel radius on time, the rate of expansion of the channel, the pressure in the channel, and also the values of the functions

$$G(\bar{t}) = R(H + U^2/2) = (R_0^2/\tau^2)\,y\left(\eta + \frac{1}{2}\dot{y}^2\right) = \frac{R_0^2}{\tau^2}\,g(x)$$

on the surface of the expanding sphere.

Determining these functions is the initial point of solving the problem of radiation in the Kirkwood-Bethe theory, assuming that the values of the function G = r(h + 1/2 v^2), where h is the enthalpy of the liquid at the point r and v is the hydrodynamic speed, remain constant at points traveling at a speed of c + v, which makes it possible to determine this function at any point in space according to known values of it on the surface of the sphere.

In practice it proves to be more convenient to calculate a function, the inverse of G(t, r) [7], according to formulas obtained from (4.86)--(4.91) by reducing them to dimensionless form

$$\xi = \frac{t}{\tau} = x(g) + M^2\frac{n+1}{4}g\left[\frac{1+2\beta v}{\beta v(1+\beta v)} - \frac{1+2\beta U}{\beta U(1+\beta U)} - 2\ln\frac{(1+\beta v)\beta U}{\beta v(1+\beta U)}\right]. \tag{5.72}$$

$$\beta v = \frac{1}{2}\left[\left(1+(n+1)\frac{R_0}{r}M^2 g\right)^{\frac{1}{2}} - 1\right], \tag{5.73}$$

$$\beta U = \frac{1}{2}\left[\left(1+(n+1)M^2\frac{g}{y}\right)^{\frac{1}{2}} - 1\right], \quad \beta = \frac{n+1}{4c_0}. \tag{5.74}$$

In the case of small disturbances, when $M \ll 1$ and, consequently, $\beta U \ll 1$ and $\beta v \ll 1$ these formulas transform into a solution

$$t - \frac{r-R}{c_0} = \tau x(g). \tag{5.75}$$

corresponding to an approximation of linear acoustics.

Consideration of the next term in the expansion of formulas (5.72)--(5.74) in M leads to the formula

$$t-\frac{r-R}{c_0}=\tau x(g)-\tau g M^2\frac{n+1}{2}\ln\frac{r}{R}. \qquad (5.76)$$

This approximate formula graphically demonstrates the influence of nonlinear effects in the propagation of a wave: points of the wave profile corresponding to great values of g approach the point of observation with shorter times t, that is, they travel faster than points with smaller values of g.

According to known values of the function G it is easy to determine the hydrodynamic speed (5.73) and the pressure

$$p=A\left[\frac{2}{n+1}+\frac{n-1}{n+1}\left(1+\frac{n+1}{r}R_0M^2\right)^{\frac{1}{2}}\right]^{\frac{2n}{n-1}}-B \qquad (5.77)$$

and to find the profile of the compression wave at any point in space.

This formula is simplified in the area where $(n+1)M^2R_0/r\ll 1$, acquiring the following form:

$$p=p_0\frac{R_0^2}{r^2}g(t). \qquad (5.78)$$

At a sufficient distance from the discharge the solution for the compression wave profile may become ambiguous which, as is known [8], signifies the formation of shock fronts.

Their behavior and the magnitude of the discontinuity are determined by means of joining the solution obtained with the Rankine-Hugoniot relationships on a shock front, which for shock waves of low intensity reduces to the simple rule of

"equality of areas" [8].

At great distances from the discharge, where nonlinear effects lead to great distortion of the original wave profile, the shock wave acquires a form which is weakly dependent on the detailed features of the function G on the surface of the channel. This makes it possible to obtain simple asymptotic expressions, describing the shock wave at a distance from the discharge and, in particular, making it possible to clarify the nature of its damping. Two cases are possible here.

If the rate of expansion of the channel is equal to or exceeds the speed of sound, then shock waves arise in the immediate vicinity of the discharge.

In this case it is possible to use the asymptotic expressions of the theory developed by Kirkwood and Bethe for describing shock waves from an explosion and applicable at a great distance from it [6].

According to this theory, the form of a wave is assumed to be approximately exponential

$$p = p_m \exp(-t/\tau_0), \qquad (5.79)$$

and the quantities p_m and τ_0 are determined according to the following formulas

$$p_m = \rho_0 G_m / r, \quad G_m = \alpha G_0,$$

where G_0 is the maximum value of the function G on the surface of the sphere, and α is quantity characterizing the damping of the shock wave,

$$\alpha = \frac{2}{1 + \sqrt{1 + 4\beta \frac{G_0}{c_0^2 \tau} \ln \frac{r}{R_0}}}, \qquad (5.80)$$

where R_0 and τ are the characteristic values of the radius of the channel and the time of its expansion;

$$\tau_0 = \frac{2\beta G_0}{c_0^2} \ln \frac{r}{R_0}. \tag{5.81}$$

Formulas (5.79)--(5.81) are applicable in the case of the fulfillment of the conditions

$$2\beta G_0/\tau c_0^2 > 1, \tag{5.82}$$

$$\ln \frac{r}{R_0} \gg 1, \tag{5.83}$$

the first of which expresses the condition of the formation of a discontinuity near the discharge and the second makes it possible to use the asymptotic formulas of the Kirkwood-Bethe theory. As is seen, the parameters of the shock wave at great distances are determined simply by the maximum value of the function G under the condition that the characteristic values of R_0 and τ are known.

In turn, for rough estimates it is possible to assume that $G_0 \approx R_0^3/\tau^2$, that is, to consider that the maximum value of g is close to unity, which, as will be seen below, agrees with the results of numerical calculation.

Thus, it is possible to find the order of magnitude of the pressure in the shock wave radiated by an intensive discharge according to a given discharge duration τ and the total energy released in the channel E.

By using the estimate given above for G_0 is is possible to rewrite inequality (5.82) in the following way:

$$\frac{2\beta G_0}{c_0^2 \tau} = \frac{1}{2} M^2 = \left(\frac{E/R_0^3}{\rho c_0^2}\right)^{1/2} \approx \left(\frac{E}{\rho c_0^2 \tau^3}\right) > 1. \tag{5.84}$$

From this formula, in particular, it follows that the possibility of the formation of a shock wave depends on the ratio of the energy density in the channel proportional to the pressure in it and to the characteristic pressure in the liquid $\rho_0 c_0^2$.

If the rate of expansion of the channel is less than the speed of sound, which occurs in the case where instead of (5.84) the inverse inequality is fulfilled

$$4M^3 = \frac{2\beta G_0}{v c_0^2} < 1, \tag{5.85}$$

then shock waves may be formed as a result of cumulative nonlinear effects at a certain distance from the discharge. Consideration of this factor, performed in approximation of nonlinear acoustics [5], leads to the following formula for p_m

$$p_m = \rho_0 \frac{G_m}{r}, \beta G_m^2/c_0^2 = \frac{5}{6} G_0 \tau \left[\ln \frac{r}{R_0}\right]^{-1}. \tag{5.86}$$

This formula is valid if $\ln \frac{r}{R_0} > \frac{c_0 \tau}{2\beta G_0}$. Fulfillment of this condition signifies that a shock wave was formed at the distance r.

Section 6. Approximate Calculation of the Electrical and Hydrodynamic Characteristics of a Discharge According to Given Parameters of the Electrical Circuit.

The models of an electrical discharge examined in the preceding sections are incomplete in the respect that the mode of energy released, determined by the electrical characteristics of the process, must be given for a calculation of the hydrodynamic characteristics of a discharge.

Meanwhile, if we include the electrical circuit in our examination, it is possible to obtain a closed system of equations,

describing both the electrical and the hydrodynamic phenomena during a discharge. An approximate calculation corresponding to this approach is made by A. I. Ioffe in [9], which we follow in the presentation below.

The principle difficulty which arises in an examination of such a closed model is connected with determining the channel resistance which is variable in time and depends on the particle density and temperature in the channel.

We shall consider that the electrical circuit of a discharge is an oscillatory circuit with a given inductance L, a capacitance C, and a resistance determined by the resistance of the discharge channel which varies with time.

Then the electrical characteristics of the process are described by the equation of an oscillatory circuit

$$\frac{d^2U}{dt^2} + \frac{R_e}{L}\frac{dU}{dt} + \frac{U}{LC} = 0, \; R_e = \frac{l}{\eta_{ei} S}. \tag{5.87}$$

Here U is the condenser voltage; R_e is the ohmic resistance of the discharge channel; $1/\eta_{ei}$ is the resistivity; S is the cross sectional area of the channel.

In agreement with that which was stated in Chapter III we shall consider approximately that the conductivity of the plasma is determined only by the interaction of electrons with ions and is described by formula (3.29) (where Z = 1)

$$\eta_{ei} = 1{,}52 \cdot 10^{-4} \frac{T^{3/2}}{\ln \Lambda} \frac{1}{\text{ohm} \cdot \text{cm}}, \tag{5.88}$$

where

$$\Lambda = \frac{3 (kT)^{3/2}}{2 (4\pi)^{1/2} e^3 n_e^{1/2}}.$$

For practical reasons in our calculation lnA which varies slightly with a change in electron configuration was assumed to be constant. Here e is the electron charge; T is the temperature; n_e is the number of electrons in a unit volume.

For specificity we shall consider a discharge corresponding to the short cylinder model, that is, we shall consider that the length of the electrode gap is great in comparison with the characteristic channel radius, but much less than the characteristic wave length $R_0 \ll l \ll \lambda$, $\lambda = c_0\tau$, where τ is the discharge duration.

Then the energy balance equation with respect to a unit of length of the channel may be written in the form

$$P\frac{dS}{dt} + \frac{1}{\gamma - 1}\frac{dPS}{dt} = \sigma^0\left(\frac{dU}{dt}\right)^0 \frac{1}{\eta S} - I^2 R_0,$$
$$I = C\frac{du}{dt}. \qquad (5.89)$$

and the pressure on the surface of the expanding cylinder is determined by formula (4.48), which it is convenient to write in the following way

$$P = \frac{\mu_0}{2\pi} \ddot{S} \ln\left(\frac{\pi^{\frac{1}{2}} l}{S^{\frac{1}{2}}}\right) - I^2 \frac{\dot{S}^2}{8\pi}. \qquad (5.90)$$

Estimates show that the length of the radiation path in a plasma at a temperature of $T \approx 2 \cdot 10^{4}$° K and with a density $n_e \approx 10^{20}$ cm^{-3} is approximately $l_v \sim 10^{-1}$ cm and is small in comparison with the characteristic channel radius (see Chapter III). Therefore, the plasma of the channel may be considered to be a black body radiating the radiant flux $q = \sigma T_{ef}^4$ from a a unit of its surface.

If, therefore, we assume that the radiated energy flux q is

absorbed in a thin layer of water and goes only to evaporate the water within the channel, then for the particle density in the channel it is possible to write the following equation:

$$\frac{d}{dt}nS = \frac{2\pi R s T^4}{D}, \qquad (5.91)$$

where D is the evaporation energy on a molecule.

Together with the equation of state of an ideal gas

$$p = nkT, \qquad (5.92)$$

approximately applicable for a slightly ionized discharge plasma, relationship (5.91) closes the system of equations, consisting, therefore, of the five equations (5.87)--(5.92).

This system may be integrated numerically with the appropriate initial conditions. Several of these are obvious: at the initial moment the condenser is charged to a given voltage U_0, and there is no current in the circuit, which leads to the condition dU/dt = 0. The remaining conditions are not so specific; for practical purposes in our calculations it was assumed that the initial value of the channel cross section was 0.1 cm^2, the rate of expansion was zero, and the intial temperature and particle density were chosen as approximately equal to 10^4 K and 10^{19} cm^{-3}. Variations of 10-30% in the initial values had an insignificant effect on the results of calculation.

The results of a calculation, describing the electrical and hydrodynamic characteristics of a discharge with respect to four given parameters: initial condensor voltage, the inductance L and capacitance C of the discharge circuit, and the length of the discharge gap L are compared with experimental data in the following chapter.

Section 7. Similarity of Electrical Discharges in a Liquid.

As was mentioned, the relationship between the three dimensional scales--the length of the discharge gap L, the characteristic channel radius R_0, and the characteristic wave length λ is an important characteristic of the hydrodynamic phenomena during a discharge; it is precisely this relationship that determines, in particular, the choice of one or another of the discharge models examined above.

This relationship may be characterized by two dimensionless parameters: $M = R_0/\lambda$ and $N = l/\lambda$, the first of which is equal to the ratio of the characteristic rate of channel expansion to the speed of sound, $M = R_0/c\tau = U/c$, and therefore may be called the Mach number, and the second characterizes the length of the channel in comparison with the length of the radiated wave. Different discharges correspond to different values of the parameters; on the other hand, identical values of them correspond to identical, in a hydrodynamic respect, discharges, that is, they play the role of hydrodynamic similitude criteria.

The meaning of these parameters becomes more clear if we turn to the dimensionless equations describing the different discharge models [see, for example, formulas (5.13), (5.28) (5.38), (5.47), (5.52), (5.62) and (5.69)]. In spite of the differences in these equations, the common factor is that the parameters M and N (or their ratios) are the coefficients which enter these equations.

Hence it follows that discharges with identical values of the parameters M and N are described by equations which may differ only in the form of the dimensionless function f(x), characterizing the mode of energy release in the channel.

It is not difficult, however, to verify the fact

that the nature of this function, determined by the time dependence of the power I^2R_{ohm}, depends both on M and on only one other parameter $Z = R_{ef}/\sqrt{L/C}$, entering as a coefficient into the equation for the discharge current

$$\frac{d^2I}{dx^2} + \pi Z \frac{d}{dx}\bar{R}(x)I + \pi^2 I.$$

Here I is the discharge current, R_{ohm} is the ohmic resistance of the circuit; it is assumed that it is due, basically, to the resistance of the channel; R_{ef} is the effective value of this quantity, equal to $l/\eta S$ for a cylindrical model and $1/\eta R$ for a spherical model; L and C are the inductance and capacitance of the circuit; $\bar{R}(z) = R_{ohm}/R_{ef}$ is the dimensionless "resistance," which may be considered an identical function for similar discharges x, $x = t/\tau$, $\tau = \pi\sqrt{LC}$.

Thus, it is obtained that discharges with identical values of the parameters M, N, and Z are described by identical equations, that is, these parameters are similitude criteria.

We shall represent them in a different form. First we shall examine discharges corresponding to cylindrical models. In this case the parameter Z, being a similitude criterion of the electrical (and energy) characteristics of the discharge may be written as such:

$$Z = R_{ef}\sqrt{\frac{C}{L}} = \sqrt{\frac{C}{L}}\frac{l}{\eta S} \sim \sqrt{\frac{C}{L}}\frac{l}{\eta_{ef}\frac{I_0^2}{\tau^2 c^2}\tau^2 c^2}, \qquad (5.93)$$

where S is the cross sectional area of the channel.

Bearing in mind that the amount of plasma conductivity is determined by the temperature and pressure in the channel, which

are identical for similar discharges*, and therefore omitting η_{ef} and also the combination of parameters equal to M^2, constant for similar discharges, we obtain

$$Z \sim \sqrt{\frac{C}{L}} \frac{l}{\tau c^2}. \tag{5.94}$$

In examining the similarity of discharges in one and the same liquid it is possible to consider the speed of sound c to be constant, so that

$$M \sim R_0/\tau, \quad N \sim l/\tau, \quad Z \sim \sqrt{\frac{C}{L}} \frac{l}{\tau^2}. \tag{5.95}$$

Now we shall express these similitude criteria with the parameters C, U, L, and l usually given in an experiment.

We have according to (5.36)

$$M = R_0/\tau \sim \left(\frac{E}{l\tau^2}\right)^{\frac{1}{4}} \sim \left(\frac{U^2}{lL}\right)^{\frac{1}{4}}, \quad N \sim \frac{l}{\sqrt{LC}}, \quad Z \sim \frac{l}{L^{3/2}C^{1/2}}.$$

Hence it follows that for similarity of discharges it is necessary that the quantities U^2/lL, $l\sqrt{LC}$, $l/L^{3/2}C^{1/2}$ be constant which leads to the following condition for the similarity of two cylindrical discharges in one and the same liquid:

$$\frac{u_1^2}{u_2^2} = \frac{l_1}{l_2} = \frac{C_1^{\frac{1}{2}}}{C_2^{\frac{1}{2}}}, \quad L_1 = L_2. \tag{5.96}$$

We note that relationships (5.93)--(5.96) coincide with the

---

* In agreement with formula (3.43) for discharges corresponding to a cylindrical model, the temperature $T \sim (E/\tau^2 l)^{3/20} \sim M^{3/5}$ and therefore is identical for discharges with an identical value of M; for discharges corresponding to a spherical model, $T \sim M^{3/5}\tau^{1/5}$, that is, it changes slightly with a change in τ in the case of constant M. The amount of pressure in the channel $\sim M^2$ and therefore is identical for similar discharges.

results in [10], obtained on the basis of general methods of similitude theory.

Bearing in mind also that the equations for a spherical model do not depend on the parameter N we obtain that in this case discharges are similar under the condition that the following two parameters are constant

$$M = \frac{R_0}{c\tau}, \quad Z = \sqrt{\frac{C}{L}}\frac{1}{\eta R_0} \sim \sqrt{\frac{C}{L}}\frac{1}{\eta\frac{R_0}{c\tau}c\tau} \sim \sqrt{\frac{C}{L}}\frac{1}{c\tau}. \tag{5.97}$$

For discharges in one and the same liquid these criteria may be rewritten in different form

$$M \sim (E/\tau^3)^{1/5} \sim u^3/L^{3/5}C^{1/5},$$
$$Z \sim \sqrt{\frac{C}{L}}\frac{1}{\tau} \sim 1/L^{3/5}C^{1/5}. \tag{5.98}$$

Hence we obtain that, for example, two discharges, corresponding to spherical models, are similar under the condition

$$\frac{u_1^3}{u_2^3} = \frac{L_1^{3/5}}{L_2^{3/5}} = \frac{C_1}{C_2}. \tag{5.99}$$

Similarity of discharges signifies not only agreement of the dimensionless functions entering into formulas (5.16)--(5.19) and (5.20)--(5.22) and formulas similar to them, but also equality of the absolute values of the quantities characterizing the process of channel expansion (pressure, rate of expansion, etc.), taken at corresponding moments of time (identical x).

In addition, the characteristics of the compression wave, determined at corresponding points (with identical l/r or R_0/r) at the corresponding moments of time, also prove to be equal.

LITERATURE

1. *Иоффе А. И., Наугольных К. А., Рой Н. А.*— ПМТФ, 1964, № 4, 108.
2. *Наугольных К. А., Рой Н. А.*— ПМТФ, 1967, № 4, 137.
3. *Наугольных К. А., Рой Н. А.*— Докл. АН СССР, 1966, 168, № 3, 550.
4. *Иоффе А. И., Кожетунова И. Г., Наугольных К. А., Рой Н. А.*— Акуст. ж., 1967, 13, вып. 2, 208.
5. *Иоффе А. И., Наугольных К. А.*— ПМТФ, 1968, № 1, 134.
6. *Кокс Р.* Подводные взрывы. М., ИЛ, 1950.
7. *Акуличев В. А., Бочковский Ю. И., Иоффе А. И., Наугольных К. А.*— Акуст. ж., 1967, 13, вып. 3, 321.
8. *Ландау Л. Д., Лифшиц Е. М.* Механика сплошных сред. М., ГИТТЛ, 1954.
9. *Иоффе А. И.*— ПМТФ, 1966, № 6, 69.
10. *Окунь И. З.* Теоретическое и экспериментальное исследование импульсного разряда в жидкости. Канд. дисс., Политехнический ин-т. Л., 1969.

CHAPTER VI

HYDRODYNAMIC CHARACTERISTICS OF DISCHARGES. COMPARISON WITH EXPERIMENTS

Section 1. Introduction

The theory of electrical discharges in a liquid presented in the preceding chapter makes it possible to calculate their hydrodyamic characteristics if the mode of energy release in the discharge channel is known. If we characterize the mode of energy release by the dimensionless function $f(x) = E(t)/E(\tau)$, where $x = \frac{t}{\tau}$ and τ is the discharge duration, then, as experimental results show, the form of this function proves to be practically identical for discharges close to critical. This circumstances imparts a certain universality to the calculation of the dimensionless hydrodynamic characteristics of a discharge, performed for one form of the function $f(x)$. The results of such a numerical calculation, performed with the use of formulas (3.1) and (3.2), approximating the conditions of the release of energy in the case of a critical discharge, are given below.

We note that these results may be used approximately in calculating not only discharges close to critical, but also aperiodic and periodic discharges, if in the first case we introduce a correction for the increase in discharge duration in comparison with the value $\pi\sqrt{LC}$ and in the second case a correction for the fact that only part of the stored energy $CU^2/2$ is released during the first half-period. Examples of the application of the approximation theory for calculating the hydrodynamic characteristics of specific discharges presented above are given below.

We emphasize that we are speaking here only of the phenomena during the condenser discharge, where electrical current flows along the channel.

The hydrodynamic phenomena in the subsequent stages of the

discharge are not examined in this study. We note only that the pulsating bubble formed as a result of a discharge in many regards is similar to the gas bubbles formed in the case of underwater explosion or in case of cavitation [1], [2].

In particular, the pulsation process of a spherical bubble at a great distance from the boundaries is described by the formulas in Section 2 of Chapter IV from which follows the simple relationship (4.28), connecting the pulsation period of the bubble with the pulsation energy.

In the process of the pulsations, compression waves which are easily recorded experimentally are emitted when the bubble slams shut. This make it possible to determine the pulsation period and then, by using formula (4.28), the energy of the pulsating bubble in the case of a spherical discharge model.

Discharges corresponding to cylindrical models create a gas bubble differing from a spherical one and similar in form to a cylinder with hemispherical ends. In the subsequent stages of expansion such a bubble gradually acquires a shape close to spherical. The slamming of nonspherical bubbles, as motion picture photography shows, is accompanied by losses in stability of form. The bubble breaks up into several separate bubbles of different dimensions, slamming shut at different moments of time and as a result creating several compression pulses. The instability of the slamming process is expressed also by the significant fluctuation of the pulsation periods of the bubbles created by discharges, identical with respect to electrical characteristics. Naturally, the connection between the energy of a bubble and the pulsation period determined by formula (4.28) is very approximate for cylindrical models of discharges.

The pulsation energy of a bubble, being equal to the product of its maximum volume by the amount of hydrostatic pressure, also may be determined by measuring photographs taken by filming the

bubble against an illuminated background. According to experimental data, the pulsation energy of a bubble, which arose as the result of an electrical discharge, amounts to around 30% of the total energy released in the channel.

Of the three principle hydrodynamic characteristics of a discharge--the dependence of the channel radius on time, the pressure in the channel and the pressure the compression wave--the last two values are the most sensitive to accuracy of calculation, since they depend not only on the radius of the channel, but also its derivatives with respect to time.

Measurement of the pressure in the channel, is, however, quite a complex experimental problem due to the presence of high electrical voltage in the area of measurement. It is signicantly simpler to measure the pressure in the compression wave radiated by the discharge. Therefore this value is used in comparing theoretical and experimental results.

Measurement of the pressure in a compression pulse usually is performed with the aid of broad-band pressure receivers. They may be of two types: receivers in which the sensing element is directly subjected to the action of the pressure to be measured, and waveguide type receivers, in which the sensing element reacts to the deformation wave arising in a long metal rod upon the action of the pressure to be measured on its end; the lateral surface of the rod in this case is acoustically insulated from the external medium with a metal tube.

Sensing elements of the piezoelectric type, made of piezoceramic of ferro-electric compositions, for example of barium titanate with the addition of cobalt, or of TsTS-200 piezoceramic, are the most suitable. If the pressure on the piezocell exceeds several

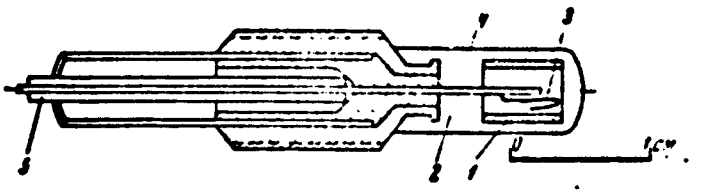

Fig. 6.1. Diagram of the construction of a hydrophone.
1 - cylinder of piezoceramic; 2 - resin filling; 3, 4 - leads to electrodes; 5 - single strand wire.

hundred atmospheres, it is necessary to apply protective sheathing of the piezocell in order to avoid nonlinear distortions. Piezocells in the form of cylinders around 3 mm in diameter and with a wall thickness of 0.3 mm have a capacitance of around 1000 nf and very low natural frequency of around 0.5 mHz. In the case of an input resistance of the oscillograph of megachms, the receiving channel makes it possible to reproduce pressure pulses lasting from 10^{-3} to 10^{-5} second on the oscillograph screen without significant distortions.

In receivers of the first type (Fig. 6.1) the piezocell is attached to the end of a coaxial holder with the aid of an elastic resin. The elastic attachment is necessary in order that the elastic waves which arise in the holder upon the action of the compression pulse on it are not transmitted to the piezocell. It is necessary to turn our attention to the following factor. The displacment speeds of liquid particles are great in a compression pulse of great amplitude. The drag on the piezocell by the liquid causes the appearance of mechanical stresses of inertial origin in the piezocell. If the piezocell has less sensitivity in the case of cubic compression than in the case of unilateral compression, the result of pressure measurement proves to be inaccurate in the case where calibration of the piezocell was performed in the absence of unilateral compression. Because of its axial symmetry, a cylindrical piezocell is not sensitive to compression

in the direction perpendicular to its axis. Therefore, in the case of the action of a compression pulse in this direction it reacts only to cubic compression. A piezocell in the form of a piezoceramic cube or disc may give incorrect information on the pressure in a compression pulse if it is calibrated by cubic compression.

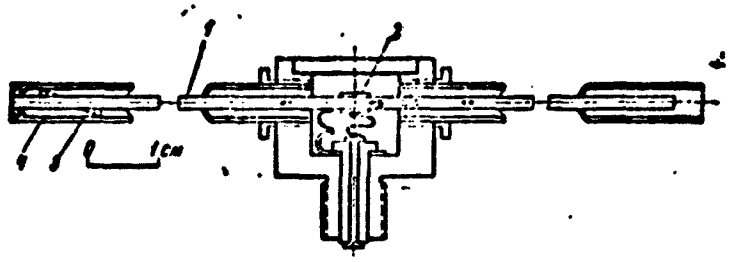

Fig. 6.2. Diagram of the construction of a waveguide type hydrophone.

1 - waveguide; 2 - piezocell; 3 - screening tube; 4 - filament.

In receivers of the waveguide type (Fig. 6.2) the cylindrical piezo element is mounted on the waveguide and rigidly attached to it. The distance between the free end of the waveguide and the piezocell must be no less than half the length of the pulse in the material of the waveguide in order that a reflected pulse not be superimposed on a direct one. It is necesary to create a good acoustical coupling between the waveguide and the screening tube. For this it is sufficient, for example, to wind the waveguide with a half millimeter wool thread at a spacing of 1 cm. The stuffing box at the working end of the waveguide blocking water from entering the screening tube and at the same time not creating a strong acoustical connection between the screening tube and the waveguide, is an important element. The absence of transmission of compression pulses to the waveguide when a metal object strikes the screening tube and the end of the stuffing box serves as a measure of the smallness of this connection. A sketch of a stuffing box is shown in Fig. 6.3.

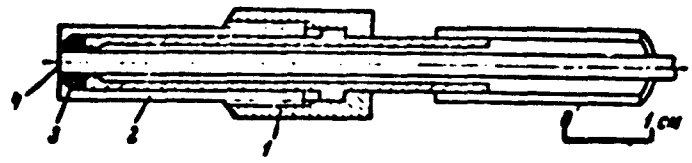

Fig. 6.3. Sketch of stuffing box.

1 - Union nut; 2 - moveable sleeve; 3 - rubber ring; 4 - end of waveguide.

Calibration of receivers of the first type may be performed in air, for example by the action of stepwise pressure pulses of known value on the piezocell. For this the piezocell is placed in a chamber of as small diameter as possible, separated with the aid of a breakable diaphragm from a chamber of large volume in which there is air under a known pressure.

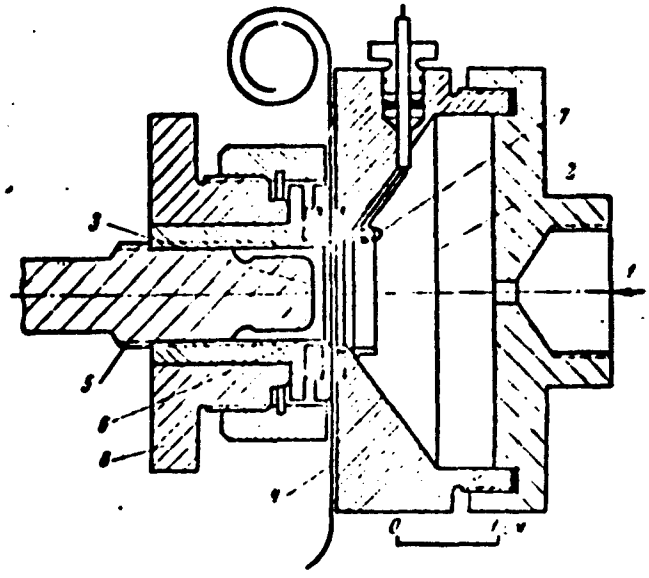

Fig. 6.4. Sketch of calibrating device.

1 - Insertion opening; 2 - large chamber; 3 - small chamber; 4 - film dividing the chambers; 5 - pressure receiver to be calibrated; 6 - knife cutting film upon the rotation of nut 8;7 - ring-shaped piezocell for the moving oscillograph.

Fig. 6.4 shows a sketch of a device for calibrating pressure receivers of the first type. Fig. 6.5 shows an example of a pressure oscillogram recorded during calibration. The damped oscillations superimposed on the exponential component of the electrical voltage are seen in the oscillogram. These oscillations are connected with the transition process which appears when the diaphragm breaks. These oscillations must be averaged in determining the sensitivity of the receiver. The constant of the exponent is determined by the size RC of the receiving channel . For a piezocell of 1000 nf capacitance and the input resistance of an IO-4 oscillograph it amounts to around 10 msec. A typical value of the sensitivity of receivers of the first type with a piezocell sheathed with a filling of epoxy resin is usually around 0.3 V/atm.

It is convenient to perform calibration of waveguide receiver by the method of rod collisions. For the calibration a rod-calibrator is made of the same material as the waveguide. The ends of the waveguide and the rod are polished so that the maximum pressure upon collision is reached as rapidly as possible.

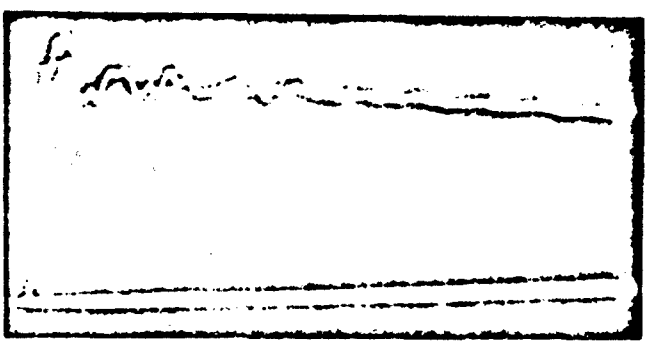

Fig. 6.5. Calibration oscillogram for a hydrophone.

The maximum pressure acting on the ends of the waveguide and rod is determined according to the formula

$$p = \rho c \frac{v}{2},$$

(6.1)

where ρc is the wave resistance of the material of the rod and the waveguide; v is the collision speed determined according to the formula

$$v = \sqrt{2gh}, \tag{6.2}$$

where g is the acceleration of the force of gravity; h is the height from which the rod is dropped.

The length of the rod is chosen so that the maximum pressure at the point of contact of the rod with the waveguide is set during the collision. Usually the setting time for steel rods 2 mm in diameter is around 10^{-5} sec. Fig. 6.6 shows an example of a calibration oscillogram for a waveguide receiver.

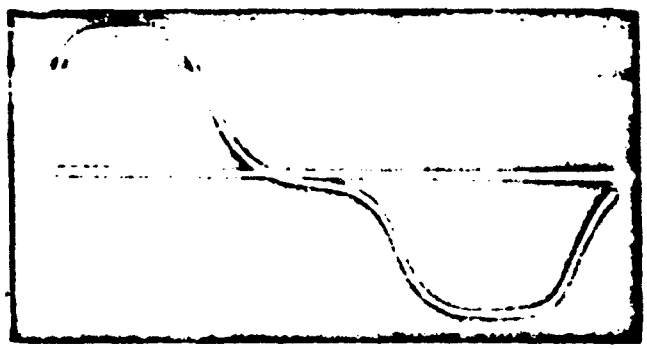

Fig. 6.6. Calibration oscillogram of a waveguide receiver.

The first pressure pulse arising upon the collision of the rods, and the rarefaction pulse following it reflected from the free end of the waveguide, are seen in the oscillogram. In order to separate these pulses it is necessary to move the piezocell from the free end of the waveguide to a distance greater than the length of the rod. Sometimes small disturbances caused by the reflection of pulses passing along the waveguide from nonuniformity of the cross section of the waveguide caused by the piezocell

are seen on oscillograms. The sensitivity of waveguide receiver amounts to several hundredths of a volt in the atmosphere.

The accuracy of measuring pressure with receivers of the types described above is 10%.

Section 2. Discharges corresponding to a spherical model.

The function f(x) (curve 1, Fig. 3.12), corresponding to an approximation of the power of an isosceles triangle, was used for integrating the system of equations (5.14) describing the expansion of the channel of a spherical model.

The initial conditions were chosen out of the following considerations.

The photograms of channel expansion examined show that the initial values of the channel radius and the rate of its expansion are at least one order of magnitude smaller than the characteristic values of these quantities in the discharge process. Therefore, numerical integration of system (5.14) was performed for different initial values of y_0 and z_0, small in comparison with unity. It proved to be the case that an arbitrary selection of the initial values of these quantities does not have a significant influence on the results of integration under the condition that $y_0 \ll 1$ and $z_0 \ll 1$. Physically this is explained by the fact that the law of channel expansion is determined chiefly by the conditions of energy release in the channel, and not by the initial conditions. The results of a calculation for $y_0 = 0.03$ and $z_0 = 0.00001$ are presented below.

Table 6.1 gives values of the functions necessary for calculating the hydrodynamic characteristics according to formulas (5.16)--(5.22).

We recall that $y(x)$, $g = f(x)/y^2$, and $\tau = (f(x)/y^3) - z^2/2y^4$ represent the time dependences of the channel radius, pressure in the compression pulse, and pressure in the channel in dimensionless form.

The results of the calculation, presented in Table 6.1, also are depicted in Figures 6.7, 6.8, and 6.9 by curves 1. As was mentioned in Section 2 of Chapter III, the normalized functions of energy release $f(x)$ differ somewhat from each other. The difference between them is approximately the same as that between the curves obtained as a result of integration of the time dependencies of power, approximated by an isosceles triangle and a triangle the height of which is displaced from the reference point along the x axis by one-third of the base.

TABLE 6.1.

x	f(x)	y	v	g	τ
0	0	0	0	0	0
0,1	0,020	0,045	0,178	0,632	2,52
0,2	0,080	0,119	0,310	0,831	1,91
0,3	0,180	0,210	0,428	0,978	1,63
0,4	0,320	0,314	0,540	1,09	1,45
0,5	0,500	0,429	0,645	1,20	1,33
0,6	0,680	0,551	0,746	1,22	1,15
0,7	0,820	0,671	0,843	1,15	0,92
0,8	0,920	0,781	0,935	1,05	0,73
0,9	0,980	0,881	1,020	0,939	0,56
1,0	1,000	0,968	1,100	0,821	0,43

In order to explain what the degree of applicability of the approximation of the function $f(x)$ used is, Figs. 6.7, 6.8, and 6.9 represent graphic depictions of the curves 2 of the functions $y(x)$, $(f(x)/y^3) - z^2/2y^4$, and $f(x)/y^2$, calculated with the use of an

approximation of the power curve by a non-isosceles triangle.

In Fig. 6.7 it is obvious that y(x) where x = 1, that is, when t = τ, is close to 1.1 with any of the approximations of f(x) taken and, consequently, to within this coefficient, according to (5.16), the radius of the channel at the end of the discharge is equal to R_0.

In exactly the same way the function $f(x)/y^2$ is not very sensitive to the choice of approximation. At the maximum it is equal to approximately 1.2—1.3. Thus, the maximum pressure in the compression pulse, according to (5.12), is equal to the product of this coefficient by the value $\rho_0 R_0^3/\tau^2 r$, determined by the square of the mean rate of expansion of the channel, taking account of the spherical divergence.

In contrast to the dimensionless radius and the pressure in the compression pulse, the pressure in the channel proves to be highly dependent on the choice of approximation for f(x) in the case of small values of the arguments (x<0.2) due to the presence of the term $f(x)/y^3$ in the expression for the pressure in the channel. This factor makes calculation of the pressure in the channel at the beginning of the discharge unreliable and, in particular, does not permit determining the maximum pressure possible in the channel. In view of this the pressure in the channel was calculated using other, more precise approximations of f(x) for a spherical model of a discharge. An approximation of the experimental dependence of energy on time with a tenth power polynomial was taken as the first such approximation. The result is shown in Fig. 6.8, curve 3. In the same place curve 4 shows the pressure in the channel calculated according to f(x), obtained from an approximation of the power curve by a compound curve: by the parabola to x = 0.3 and by an isosceles triangle from x = 0.1 to x = 1. On the basis of the data obtained it is possible to conclude that the maximum value of the dimensionless function determining the pressure in the channel is close to 2.

It is necessary to know the value of the integral in formula (5.23) in order to determine the amount of efficiency. Calculations show that for any of the approximations of f(x) used this integral is practically equal to unity.

Now we shall present several examples of the calculation of the hydrodynamic characteristics of discharges, the parameters of which are given in Table 3.5.

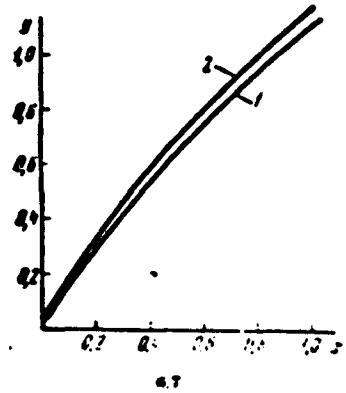

Fig. 6.7. Dimensionless radius of a channel as a function of time.

Curve 1 corresponds to an approximation of the energy release conditions by the function f(x), formula (3.1); curve 2--by the function $f_1(x)$ (formula 3.2).

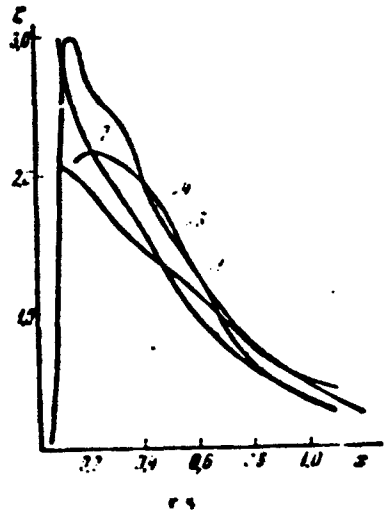

Fig. 6.8. Dimensionless pressure in a channel as a function of time.

Curves 1, 2 and 3, 4 correspond to an approximation of the energy release conditions by the functions f(x), and $f_1(x)$ and empirical relationships respectively.

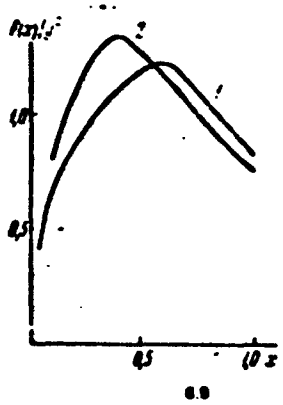

Fig. 6.9. Dimensionless profile of the pressure in a compression wave radiated by a channel.

Curves 1 and 2 correspond to an approximation of the energy release conditions by the functions f(x) and $f_1(x)$.

As is seen from the Table, discharges Nos. 1, 2 and 3 satisfy the condition of applicability of the model of a spherical discharge ($l \ll R_0 \ll \lambda$); discharge No. 4 is at the limit of applicabiltiy of this model.

Discharges Nos.1, 2,and 3 were produced on the surface of a rigid plate on electrodes made flush with its surface; the shape of the channel in the discharge process in these cases is close to hemispherical, which must be considered in a calculation (see the footnote at the end of Section 2 of Chapter V). Discharge No. 1 was initated with a corona discharge in the electrode gap created by an auxiliary electrode. In this case in a gap of $l = 0.3$ cm for $50 \cdot 10^6$ sec, $E = 510$ J of energy was released. By using formulas (5.16)-(5.22) and Table 6.1 we obtain that the radius of the channel at the end of the discharge was $R \approx 1.2$ cm, which means that the mean rate of its expansion is equal to $U \approx 2.4 \cdot 10^4$ cm/sec. The pressure in the discharge channel P reached approximately 1000 atm., and the maximum pressure in the compression wave at a distance of 50 cm from the discharge was 13 atm; a theoretical profile of the compression wave is depicted in Fig. 6.10 by curve 1. Curve 2 in the same figure shows the experimentally determined shape of the signal. The broken nature of this curve is due, evidently, to the excitation of oscillations of the reflecting plate and the pressure pickup under the action of the compression pulse. The energy of the compression wave, according to formula (5.28), is approximately 12% of the energy released in the channel.

Fig. 6.11 shows the distribution of the hydrodynamic velocity v in the compression wave calculated according to formula (5.21). Curves 1 and 2 of the figure correspond to the first and second terms in this formula.

Fig. 6.12 shows the time dependences of the energy of the plasma in the channel, the expansion work A, and the acoustic energy removed by the compression wave A_{ac} calculated according to the

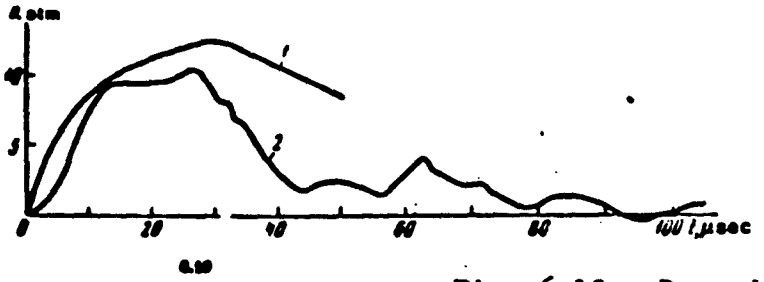

Fig. 6.10. Dependence of the pressure in a compression pulse on time for discharge No. 1, Table 3.5.

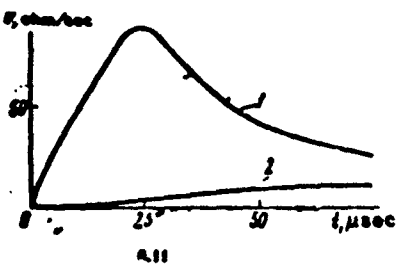

Fig. 6.11. Distribution of hydrodynamic velccity in the compression wave, the pressure profile of which is shown in 6.10.

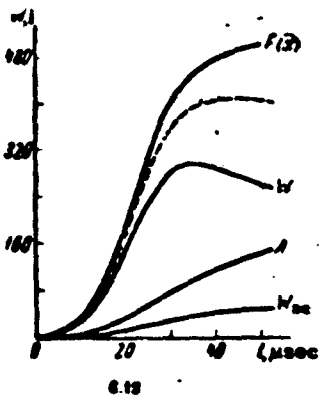

Fig. 6.12. Energy balance for discharge No. 1.

W_{ac} is the emitted acoustic energy; A is the expansion work of the channel; W is the intrinsic energy in the channel; F(x) is the total energy released in the channel. The sum of A and W is represented by the dotted curve.

formulas (5.18), (5.19),and (5.22), and also the time dependence of the energy released in the channel, assuming for purposes of calculation $E(x) = f(x)E$.

The sum W + A is represented by the dotted line and its difference from E(x) characterizes the error of calculation resulting from the approximate nature of the solution of the initial

energy balance equation. As is seen the amount of error does not exceed 20%.

Discharges Nos.2 and 3 differ from discharge No. 1 by the smaller length of the discharge gap, which broke down directly with the working voltage. As is seen from Table 3.5, 376 J of energy was released in discharge channel No. 2 after $30 \cdot 10^{-6}$ sec. The channel radius at the end of the discharge was equal to $R \approx 0.9$ cm, the characteristic rate of expansion of the channel was $U \approx 2.8 \cdot 10^4$ cm/sec and the maximum pressure in the channel $P \approx 1600$ atm. The maximum pressure in the compression wave p at a distance of 100 cm from the discharge was approximately equal to 8 atm. A profile of the compression wave at this distance is shown in Fig. 6.13. Curve 1 is theoretical and curve 2 experimental. The energy of the compression wave is around 13% of the energy released in the channel.

The hydrodynamic characteristics of discharge No. 3 are close to those cited above for discharge No. 2. A profile of the compression wave at a distance of 100 cm from this discharge is shown in Fig. 6.14. The calculated electroacoustic efficiency of the discharge is 13%, and the efficiency determined according to the experimentally recorded signal shape is 10%.

In conclusion we shall examine discharge No. 4 (Table 3.5) which differs by the great amount of energy stored in the condensors--169 kJ [1]. The discharge was initiated with a wire 7.5 cm long. The discharge duration and the amount of energy released in the channel are not mentioned in [1]. If we assume that all the energy of the condensor battery was released during a time of $400 \cdot 10^{-6}$ sec in agrreement with the experimental duration of the compression wave, then for a discharge No. 4 we obtain: $R \approx 7.5$ cm, $U \approx 1.7 \cdot 10^4$ cm/sec, $P \approx 600$ atm, $p \approx 26$ atm, and the efficiency is 9%. Theoretical (curve 1) and experimental (curve 2) profiles of the compression wave at a distance of 90 cm from the discharge are shown in Fig. 6.15.

The dependences of the maximum pressure in the compression pulse on the initial voltage and on the capacitance of the condenser battery, expressed by the number of condensers in the battery, were calculated for the same discharge. The theoretical dependence of the maximum pressure on voltage is shown in Fig. 6.16 by the solid line; the results of measurement are indicated with crosses.

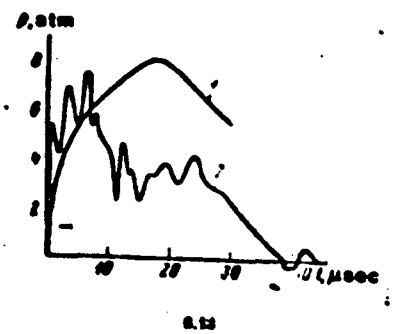

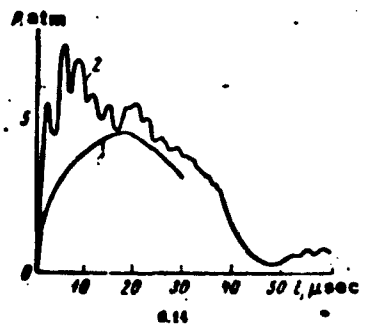

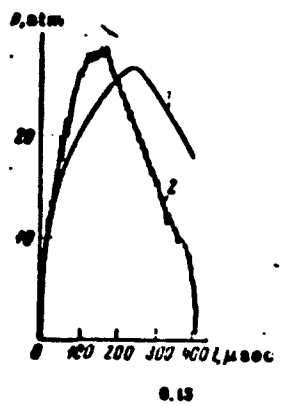

Fig. 6.13. Compression wave pressure profiles for discharge No. 3.

Fig. 6.14. Theoretical (1) and experimental (2) compression wave pressure profiles for discharge No. 3.

Fig. 6.15. Theoretical (1) and experimental (3) compression wave pressure profiles for discharge No. 4.

The solid line in Fig. 6.17 depicts the dependence of the maximum pressure in the compression pulse on the number of condensers in the battery; experimental data are indicated with the crosses and circles.

We shall now turn our attention to a factor common to all

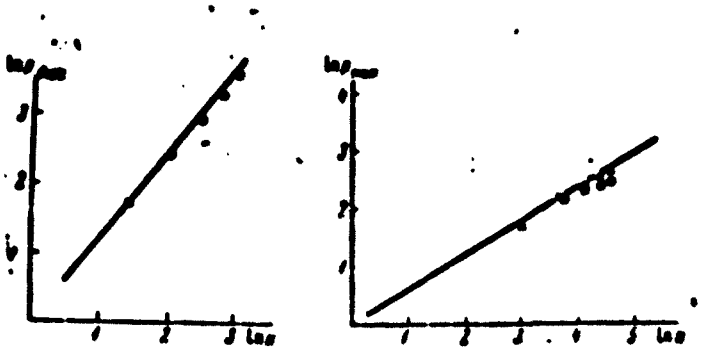

Fig. 6.16. Dependence of maximum pressure in the compression pulse on the initial voltage. Solid line--theoretical dependence; Circles--experimental data.

Fig. 6.17. Dependence of maximum pressure in the compression pulse on condenser capacitance.

cases examined. While the absolute value of the maximum pressure in compression pulses is in quite good agreement with the calculated value, it is impossible to say this relative to the final stage of the compression pulses. Here it is always observed that the calculated pressure significantly exceeds, by approximately two times, the experimental pressure for corresponding moments of time. Rapid cooling of the plasma in the discharge channel may be a possible cause of the phenomenon.

Section 3. Discharges Corresponding to a Short Cylinder Model.

In order to go from spherical discharges to discharges corresponding to a short cylinder model, it is necessary to increase the length of the channel so that it, while remaining shorter than the length of the compression pulse, exceeds the radius of the channel. Discharges Nos.5-10 in Table 3.5 satisfy these requirements. The relatively great length of the channels of these discharges, while still remaining shorter than the emitted compression pulse, is achieved as a result of using relatively low voltage discharges with a working pressure of several kilovolts, initiated

with thin tungsten wires 0.04 mm in diameter. All discharges mentioned were produced in free space, that is, far from the tank walls and without the use of any reflecting elements. The electrodes had a small diameter in comparison with the length of the compression pulse and could not introduce any significant distortions in the acoustic field created by the discharge.

The acoustic field created by discharges corresponding to a short cylinder model no longer have spherical symmetry; the compression pulse emitted by the channel in the longitudinal direction relative to the channel axis is of less amplitude and greater duration than for the transverse direction due to the spatial lag of the disturbances created by separate sections of the channel. Therefore, comparison of experimental and theoretical results will be performed for the direction perpendicular to the axis of the channel. The results of numerical integration of system (5.39) are no longer completely universal, as it was in the case of spherical discharges. Universality is lost because of the presence of the ratio l/R_0, occurring after the logarithm sign, in the first equation of system (5.39). However, the slight dependence of the solution of system (5.39) on the ratio l/R makes it possible to apply the results of integration obtained for a specific value of this ratio to discharges with another value of l/R_0 without significant error. The results of integration of system (5.39) for $l/R_0 = 6$, $y_0 = 0.1$, and $z_0 = 0$ are presented in Table 6.2. The experimentally investigated discharges, corresponding to a short cylinder model, had a value of l/R_0 close to that indicated above. As in the case of spherical discharges, an arbitrary choice of the initial value of y_0 under the condition that $y_0 < 1$ has an insignificant influence on the results of calculation.

The function $y(x)$ is shown in Fig. 6.18 by the solid line and the symbols here refer to the experimental dependences of the channel radius on time, recorded on an SFR-1 high speed photographic

recorder and reduced to dimensionless form.

TABLE 6.2

0	0	0	0	0	0
0,1	0,02	0,016	0,104	0,50	1,84
0,2	0,08	0,085	0,145	1,02	3,60
0,3	0,18	0,202	0,225	1,06	3,15
0,4	0,32	0,319	0,319	1,07	2,67
0,5	0,50	0,417	0,418	1,07	2,36
0,6	0,68	0,523	0,518	1,03	2,02
0,7	0,82	0,622	0,619	0,942	1,63
0,8	0,92	0,711	0,719	0,839	1,29
0,9	0,98	0,790	0,817	0,737	1,00
1,0	1,00	0,858	0,912	0,638	0,78

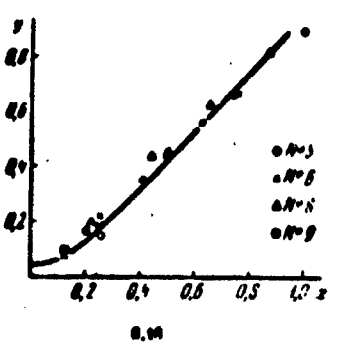

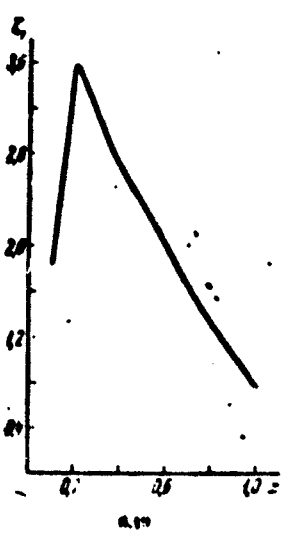

Fig. 6.18. Dimensionless channel radius as a function of time. Solid curve - theoretical dependence; symbols - experimental data for discharges No. 5, 6, 8, 9 Table 3.5.

Fig. 6.19. Dimensionless pressure in the channel as a function of time.

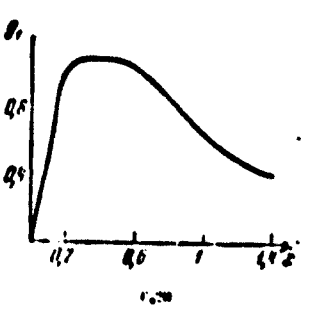

Fig. 6.20. Dimensionless pressure on the compression wave.

Graphs of the functions $[f(x)/y^2 - z^2/2y^2]$ and $f(x)/y^2 \ln(l/R_0 y)$, characterizing the shape of the radiated compression pulse in the direction perpendicular to the channel axis and the pressure in the channel in relation to time are plotted in Figs. 6.19 and 6.20. These functions must be multiplied by the corresponding dimensional coefficients according to formulas (5.42) and (5.45) in order to obtain absolute values of the hydrodynamic quantities.

We note that the dimensionless functions depicted in Figs. 6.18, 6.19 and 6.20 are little sensitive to the choice of the approximation for f(x) both in the case of the short cylinder under consideration as in the case of a long cylinder which will be examined in the next section.

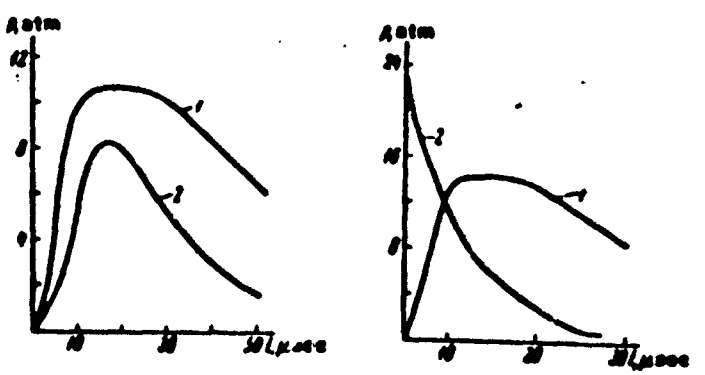

Fig. 6.21. Theoretical (1) and experimental (2) compression wave pressure profiles for discharge No. 7, Table 3.5 in the direction perpendicular to the channel axis.

Fig. 6.22. Theoretical (1) and experimental (2) compression wave pressure profiles for discharge No. 10, Table 3.5 in the direction perpendicular to the channel axis.

We shall now give some examples of the calculation of the hydrodynamic characteristics of discharges corresponding to a short cylinder model. For discharge No. 7 we have (see Table 3.5): length of the discharge gap $l = 6$ cm, discharge duration $\tau = 53 \cdot 10^{-6}$ sec, energy released $E = 2260$ J. Using the formulas in Section 3 of Chapter V and Table 6.2 we obtain that the channel radius at the end of

the discharge R ≈ 0.9 cm, the characteristic rate of expansion $U \approx 1.8 \cdot 10^4$ cm/sec, and the pressure in the channel reaches a value of P ≈ 1200 atm. The maximum pressure in the compression wave in the perpendicular direction at a distance of 100 cm from the channel amounts to P ≈ 12 atm. A profile of the compression wave at this point is shown in Fig. 6.21.

The electroacoustic efficiency of a discharge may be calculated according to formulas (5.46) and (5.47) if we bear in mind that the integrals in these formulas, calculated according to the data in Table 6.2, respectively are $J_1 = 0.83$; $J_2 = 6.6$. For discharge No. 7 we obtain: $\eta_{theor} = 14\%$; $\eta_{ex} = 12\%$. As a second example we shall examine discharge No. 10. The great power of discharge No. 10 in comparison with discharge No. 7 is achieved with the use of a low inductance discharge circuit (IMM-5-150 condenser and a supply circuit of seven parallel type RK-6 cables 120 cm long) and with the use of a channel up to 3 cm in length, which shortened the duration of the discharge to $3 \cdot 10^{-6}$ sec with almost the same amount of total energy released in the channel--approximately equal to 2500 J as in the case of discharge No. 7. The channel radius at the end of the discharge R = 0.8 cm, the characteristic rate of its expansion $U = 2.9 \cdot 10^4$ cm/sec and the maximum pressure in the channel P = 3000 atm.

The peak pressure in the compression wave at a distance of 100 cm from the discharge in the direction perpendicular to the channel axis p ≈ 14 atm. A profile of the compression wave at this point of observation is shown in Fig. 6.22.

It is obvious that the experimentally recorded shape of the profile, as opposed to the theoretical shape, has a shock front and a higher peak pressure. Several possible causes of this difference may be mentioned.

In the first place, for discharge No. 10 the ratio l/R is approximately two times less than the value of this parameter

taken in calculating Table 6.2 to be used for calculation. This circumstance led to an underestimation of the calculated amount of pressure in the compression wave of approximately 1.2.

In the second place, the form of the function f(x) used in the calculation only roughly approximates the real law of energy release.

Further, the higher value of the effective adiabatic index in comparison with the mean value $\gamma = 1.26$ used in calculation corresponds to the comparatively high pressures and temperatures in discharge channel No. 10. As is clear from the formula for the pressure in a compression pulse, higher pressures correspond to higher values of γ. This is another reason why the calculated compression pulse turns out to be smaller than the experimental value.

The hydrodynamic characteristics of discharge No. 10, as of all preceding ones, were calculated under the assumption of a slow rate of channel expansion in comparison with the speed of sound. An estimate of the rate of expansion as the ratio R_0/τ gives for discharge No. 10 a value of $0.2c_0$, where c_0 is the speed of sound. Judging by the experimental results for such rates of channel expansion it is already necessary to take account of the compressibility of the liquid in calculating the channel expansion and to consider nonlinear effects in describing the propagation of compression pulses. In Section V we shall compare the results of a calculation, performed taking account of nonlinear effects, with experimental data obtained for discharge No. 10.

Discharge No. 10 has one more peculiarity. As an analysis of the photograms showed, the rate of expansion of the sections of the channel near the electrodes is higher than in the central part of the channel. Time-lapse filming with the SFR-1 revealed

that the shape of the channel of discharges with a short channel length resembles a dumbbell formed by the merging spherical electrode sections. Fig. 3.15 shows one of the frames of a photograph of this type of channel corresponding to the final stage of the discharge.

Section 4. Discharges Corresponding to a Long Cylinder Model.

High voltage discharges fed from storage devices of comparatively low capacitance usually correspond to long cylinder models. The working voltages amount to no less than several tens of kilovolts, the condenser capacitance is on the order of several microfarads, the length of the electrode gap is no less than several centimeters, and the inductance is several microhenries.

With such parameters of the discharge circuit, as is shown by experiment, the discharge proceeds in close to critical conditions. The length of the compression pulse radiated in the direction perpendicular to the channel axis does not exceed the length of the channel, and the radius of the channel at the end of the discharge does not exceed the length of the compression pulse, that is, the inequality $R < \lambda < l$, characteristic of a long cylinder model, is fulfilled.

Discharges of this type in poorly conducting water are initiated by the high voltage breakdown of the electrode gap, and in highly conducting water by wire bridges.

Discharges corresponding to a long cylinder model create a spatially very nonuniform acoustic field: the shape of the emitted compression pulse, its duration and amplitude, greatly depend on the angle between the axis of the channel and the direction to the point of observation.

We shall now turn to an examination of the results of the numerical integration of system (5.52). A solution of this system, as in the case of a short cylinder, depends on the parameter characterizing the geometry of the model, in the given case on the value $c\tau/R_0 = a$.

TABLE 6.3

a	f(a)	s	v	a_k	t_k
0	0	0,01	0,03	0	0
0,1	0,02	0,08	0,09	1,02	2,06
0,2	0,08	0,16	0,18	0,98	1,85
0,3	0,1[illegible]	0,24	0,26	0,95	1,77
0,4	0,[illegible]	0,37	0,38	0,94	1,73
0,5	0,50	0,46	0,48	0,93	1,71
0,6	0,68	0,56	0,56	0,88	1,59
0,7	0,82	0,61	0,67	0,78	1,37
0,8	0,92	0,71	0,77	0,67	1,14
0,9	0,96	0,77	0,87	0,57	0,93
1,0	1,00	0,82	0,95	0,47	0,74

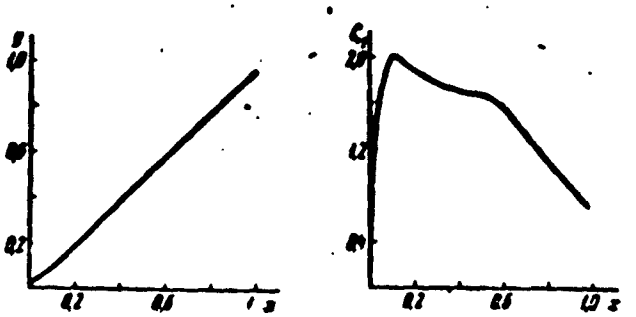

Fig. 6.23. Dimensionless channel radius as a function of time.

Fig. 6.24. Dimensionless channel pressure as a function of time.

However, this dependence is not great, since this parameter also is found under the logarithm sign. Changing it by two times causes practically no change in the solution of system (5.52). Integration of the system (5.52) was performed for the initial vlaues $y_0 = 0.03$ and $z_0 = 0.01$. The value $2c\tau/R_0$ is chosen as equal to 10 in agreement with difficult experimental results.

Table 6.3 presents values of the dimensionless functions $y(x)$, $[f(x)/y^2 - z^2/2y^2]$, and $f(x)/y^2 \ln(2c\tau x/R_0 y)$, characterizing the time dependence of the channel radius, the pressure in the compression pulse radiated by the channel in the transverse direction, and the pressure in the channel. These functions are represented graphically in Figs. 6.23, 6.24 and 6.25.

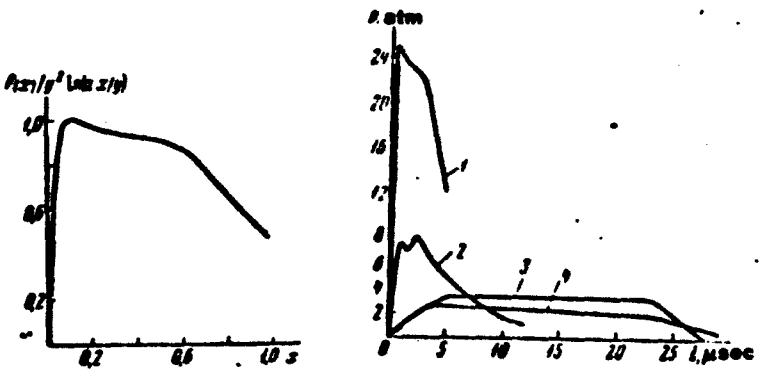

Fig. 6.25. Dimensionless profile of the pressure in the direction perpendicular to the channel axis.

Fig. 6.26. Calculated (1, 3) and experimental (2, 4) compression wave profiles for discharge No. 16 in the directions perpendicular (1, 3) and longitudinal (2, 4) to the channel axis.

Discharge No. 16 (see Table 3.5) is a discharge corresponding to a long cylinder model.

In this case an energy of E = 160 J was released in a discharge channel of the length = 4.5 cm after $5 \cdot 10^{-6}$ sec. The channel radius at the end of the discharge was R ≈ 0.16 cm, the rate of expansion U = $3.3 \cdot 10^{4}$ cm/sec, and the maximum pressure in the channel P ≈ 2300 atm.

Fig. 6.26 shows the shape of a compression wave, calculated 1 and measured experimentally 2, corresponding to the direction perpendicular to the channel axis and to a distance equal to 100 cm from the channel. Calculated 3 and experimental 4 compression pulses for the longitudinal direction also are shown here. As should be expected, the greatest discrepancy occurs between the theoretical and experimental pulses corresponding to the direction perpendicular to the axis (respectively 24.5 and 8.1 atm), while the pulses for the longitudinal direction do not differ so significantly (3.4 and 2.5 atm). The cause of the great difference between the theoretical and experimental pulses for the transverse direction, as was mentioned, is the crookedness of the channel and, in addition, possibly, the influence of the increased absorption due to the quite high pulse amplitude.

We calculate the electroacoustic efficiency of discharge No. 16 according to formula (5.65). If as an approximating curve for the transverse pulse we choose a Gauss curve with a constant decay, equal to 0.7τ, where τ is the discharge duration, then η ≈ 29%. The experimental value of the electroacoustic efficiency is found in the following way. Oscillography of the compression pulses is performed for different angles of observation relative to the channel axis and the compression pulse energy per unit area for each direction is determined. Then, considering the axial symmetry of the compression pulse field, the energy which has passed through the spherical belts encompassing the chosen directions is found. The sum of these energies, relative to the energy released in the channel, gives the experimental value of the electroacoustic efficiency. Usually, the experimental value of the efficiency amounts to 15-20%. As was seen in examining the spherical model and the

short cylinder model, the experimental values of the electro-acoustic efficiency always were less than the theoretical values. In the case of a long cylinder model this difference is much more noticeable. Here again the effect of the crookedness of the channel adds to inaccuracy of calculation. "Mis-phasing" the elementary compression pulses lowers the amplitude of the compression pulses. In this case the area of the combined pulses is retained, but their energy is reduced significantly because of the quadratic dependence on its pressure. Because of the reduction of the acoustic part of the work performed by the channel, the kinetic energy of the diverging flow of liquid increases.

Section 5. Spherical Model of a Discharge with High Rates of Expansion of the Channel

The basic equations describing a spherical model of a discharge with high rates of expansion of the channel, when it is necessary to consider the influence of the compressibility of the liquid, were presented in Section 5 of the preceding chapter (formulas 5.68-5.74).

In this section we shall examine the results of numerical integration of these equations. In integrating, as before, it is assumed that the mode of energy release is described by function (3.1), corresponding to a "triangular" approximation of the dimensionless power f(x), in the right hand part of equation (5.68)

$$f(x)=\begin{cases} 4x & 0\leqslant x\leqslant \frac{1}{2} \\ 4(1-x) & \frac{1}{2}\leqslant x\leqslant 1 \\ 1 & 1\leqslant x \end{cases} \qquad (6.3)$$

First of all we note that the system of equations (5.68)-(5.71), describing the process of channel expansion, contains one dimensionless parameter--the M number. In addition to this, the equation (5.72)-(5.74) describing the compression waves contain another

parameter--the reduced distance to the point of observation R_0/r. These two parameters may be considered to be similitude criteria in the sense that all discharges corresponding to a spherical model, taking account of compressibility characterized by identical values of these two parameters, are described by identical equations. This circumstance imparts a certain universality to the calculation.

The results of calculation for three values of the M number where $R_0/r = 10^{-2}$ are shown in Table 6.4 and in the graphs in Figs. 6.27-6.29.

Fig. 6.27 shows the dependences of the dimensionless channel radius $y = R/R_0$ on the dimensionless time $x = t/\tau$ for $M = 0.12$ (curve 1) and $M = 2$ (curve 2). As is seen, the result of calculation changes little with a change in the M number, which indicates that the influence of compressibility is small. This property of the calculation also is manifested in calculating the pressure in the discharge channel; the dimensionless value of this quantity as a function of the dimensionless time for $M = 0.12$ (1), $M = 1$ (2), and $M = 2$ (3) is shown in Fig. 6.28.

Fig. 6.29 shows the results of a calculation of the function $g(x)$ which plays an important role in calculating the compression wave emitted by a discharge. Actually, the pressure in a compression wave is described by formula (5.78), $p = \rho_0 \frac{R_0^2}{\tau^2 r} g(\bar{x})$, so that it is obvious that the function $g(\bar{x})$ characterizes the profile of the wave radiated by a discharge.

It is significant to note that, although the form of the function $g(x)$, as is seen from Fig. 6.29, changes comparatively slightly with an increase in the M number, which points to the insignificant influence of the compressibility of water on the process of the expansion of a channel even in the case of supersonic rates of its

TABLE 6.4

$\varepsilon_0 = 0{,}03$; $\beta_0 = 0$.

M = 0,12

x	v	ψ	ζ	t	σ
0,10	0,186	1,50	2,49	12,7	1,665
0,20	0,321	1,29	1,89	12,8	0,876
0,30	0,418	1,19	1,61	12,9	1,03
0,40	0,504	1,12	1,45	13,	1,10
0,50	0,573	1,07	1,32	13,1	1,27
0,60	0,778	1,02	1,15	13,2	1,30
0,70	0,877	0,962	0,947	13,3	1,23
0,80	0,971	0,903	0,761	13,4	1,13
0,90	1,06	0,845	0,609	13,5	1,02
0,00	1,14	0,792	0,479	13,6	0,899
1,1	1,22	0,743	0,382	13,7	0,796
1,2	1,29	0,701	0,313	13,8	0,715
1,3	1,36	0,661	0,262	13,9	0,622
1,4	1,42	0,632	0,223	14,0	0,596
1,5	1,48	0,603	0,193	14,1	0,551

M = 1,0

0,1	0,183	1,48	2,62	117	0,557
0,2	0,321	1,30	1,95	115	0,750
0,3	0,445	1,20	1,61	114	0,892
0,4	0,562	1,13	1,35	113	1,01
0,5	0,673	1,09	1,32	112	1,11
0,6	0,779	1,03	1,15	112	1,14
0,7	0,877	0,951	0,945	112	1,08
0,8	0,969	0,877	0,765	113	1,00
0,9	1,05	0,806	0,619	114	0,901
1,0	1,13	0,739	0,491	115	0,799
1,1	1,20	0,683	0,402	116	0,711
1,2	1,27	0,636	0,337	117	0,642
1,3	1,33	0,598	0,288	117	0,586
1,4	1,39	0,565	0,251	118	0,541
1,5	1,44	0,536	0,221	118	0,503
1,6	1,49	0,5	0,198	119	0,471
1,7	1,54	0,490	0,178	119	0,443
1,8	1,59	0,471	0,162	119	0,419
1,9	1,64	0,454	0,148	120	0,398
2,0	1,68	0,438	0,137	120	0,380

M = 2,0

0,1	0,177	1,43	2,91	210	0,497
0,2	0,310	1,26	2,16	201	0,673
0,3	0,431	1,16	1,81	196	0,802
0,4	0,544	1,10	1,60	192	0,909
0,5	0,651	1,06	1,45	189	1,00
0,6	0,754	0,997	1,26	188	1,03
0,7	0,851	0,926	1,04	190	0,981
0,8	0,939	0,851	0,842	193	0,912
0,9	1,02	0,776	0,678	195	0,827
1,0	1,1	0,720	0,550	199	0,755

1,1	1,17	0,665	0,439	213	0,656
1,2	1,23	0,621	0,378	206	0,594
1,3	1,29	0,582	0,314	208	0,545
1,4	1,35	0,550	0,273	210	0,501
1,5	1,40	0,522	0,241	212	0,470
1,6	1,45	0,498	0,215	214	0,441
1,7	1,50	0,476	0,191	215	0,416
1,8	1,55	0,458	0,177	216	0,391
1,9	1,59	0,441	0,162	218	0,375
2,0	1,61	0,425	0,149	219	0,356

expansion, the compression wave profile, observed at a fixed distance from the discharge, changes markedly with an increase in the rate of expansion of the channel.

This is due to the difference in the process of the propagation of waves of low amplitude emitted by discharges of low intensity, and of waves of finite amplitude emitted in the case of near or supersonic modes of channel expansion.

Formally this difference is due to the fact that in the case of small M numbers the time t at the point of observation differs, according to formula (5.75), from x only by the constant value $\frac{r-R}{c_0}$, identical for all points of the profile and considering the time of wave propagation. In this case the wave propagates without changing the profile. A graph of the function g(t) where $M = 0.12$ and $r/R_0 = 10^{-2}$ is shown in Fig. 6.30.

With an increase in M the connection between t and x becomes different [see formulas 5.72 and 5.76], for different values of t the propagation time becomes different, whereby, as is easily seen from formula (5.86), a shorter propagation corresponds to a larger g.

As a result the wave profile is highly distorted. This case is illustrated in Fig. 6.31, where a graph of the function with

$M = 0.4$ and $r/R_0 = 10^2$ is shown.

As already was mentioned, "entanglement" of the profile signifies the formation of a shock front, the position of which may be determined approximately according to the rule of "equality of areas" [3] (Fig. 6.31).

Now we shall use the theoretical information discussed for describing individual experimental results.

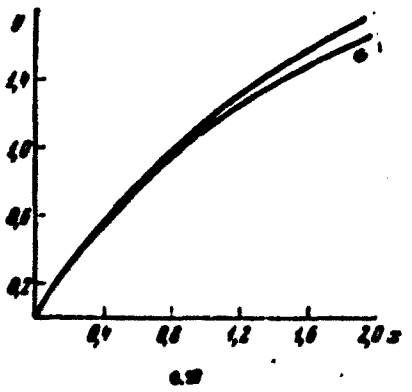

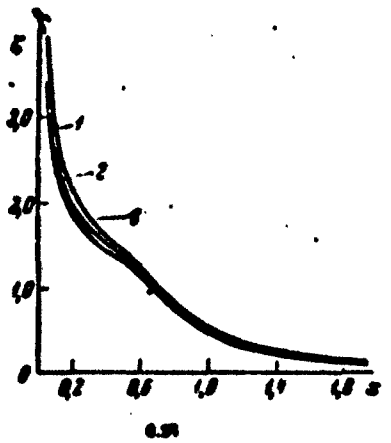

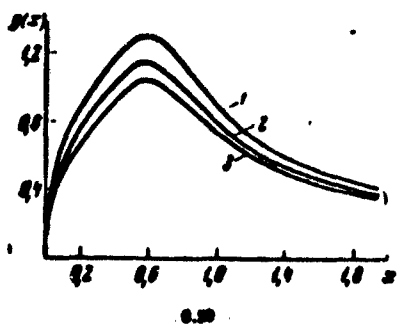

Fig. 6.27. Dimensionless channel radius as a function of time.

Fig. 6.28. Dimensionless pressure in a discharge channel as a function of time.

Fig. 6.29. Dimensionless kinetic enthalpy on the surface of an expanding sphere as a function of time where $M = 0.12$ (1), $M = 1$ (2), and $M = 2$ (3).

Let us examine the propagation of the compression wave emitted by discharge No. 10 (see Table 3.5).

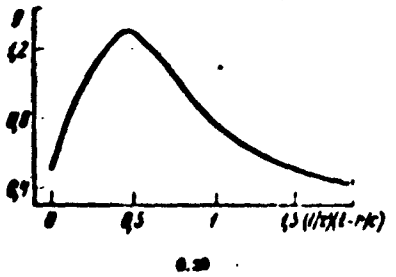

Fig. 6.30. Dimensionless kinetic enthalpy at the point of observation as a function of time where M = 0.12.

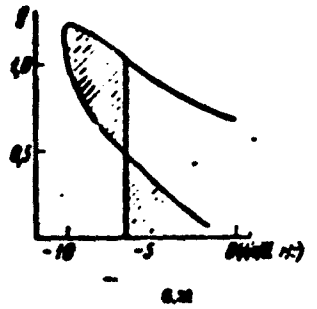

Fig. 6.31. Dimensionles kinetic enthalpy at the point of observation as a function of time where M = 0.4.

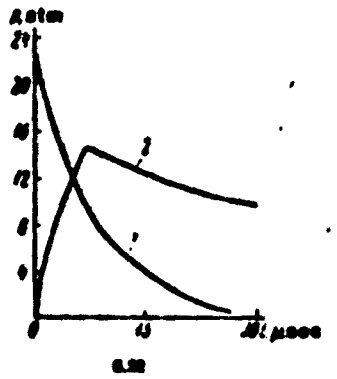

Fig. 6.32. Calculated (2) and experimental (1) profiles of the pressure in the compression wave from discharge No. 10, Table 3.5.

Let us examine the propagation of the compression wave emitted by discharge No. 10 (see Table 3.5).

The signal from this discharge, in the direction perpendicular to the channel axis, recorded with a hydrophone is shown in Fig. 6.32, curve 1, and clearly indicates that there is a shock wave at the leading edge of the signal.

The characteristic channel radius of discharge No. 10, R_0 = 0.837, is small in comparison with its length, therefore direct application of the spherical model considered in this section is inconvenient for calculating the compression wave emitted by discharge No. 10. It is possible, however, to examine a discharge equivalent to discharge No. 10 in the sense that it, possessing spherical symmetry, in all directions radiates a compression wave of the same amplitude and duration as discharge No. 10 radiates in the direction perpendicular to the channel axis, that is, to determine the characteristic ra-

dius of this discharge $\bar{R}_0$ from the condition $\rho \frac{\bar{R}_0^3}{\tau^2} = \rho \frac{R_0^2 l}{2\tau^2}$, hence $\bar{R}_0 = 1.18$ cm. Assuming according to Table 3.5, $\tau = 30.10^{-6}$ sec, we obtain $M = \frac{\bar{R}_0}{c\tau} = 0.26$.

The result of integrating equations (5.68)-(5.74), where $M = 0.26$ and $r/R_0 = 10^2$, is shown in Fig. 6.32, curve 2.

As is seen, the theoretical profile of the compression wave also reveals a tendency toward increasing the steepness of the leading edge. In conclusion we note that experimental investigations of electrical discharges in liquid have been conducted recently by a number of authors (see, for example, [5-7]). The data on the hydrodynamic characteristics of discharges obtained in these studies also agree with the results of calculation conducted in accordance with the approximation theory presented above.

Section 6. Comparison of Electrical Discharges in Water with Underwater Explosions

The results presented above show that the hydrodynamic phenomena accompanying electrical discharges to a significant degree are similar to the corresponding phenomena which occur in the case of explosions of solid explosives in a liquid medium. It is of interest to compare the quantitative characteristics of these two processes.

We shall begin with the energy values. Trinitrotoluene, the energy capacity of which is around 4200 J/g, usually is used as the explosive. The constant nature of energy capacity makes it possible to characterize the energy of the explosive in weight units. The range of variation of the charge weights used in practice is very wide. The charge weights used, for example, in oceanic investigations, in industrial engineering, etc., are measured in values of from tens of grams to tens of kilograms.

In energy values this range extends from several tens of kilojoules to several tens of megajoules. In view of the small energy capacity of condensers, amounting to around 0.1 J/cm^3, it is difficult to create discharges of great energy. The maximum of electrical discharges in a liquid, according to the data in the literature, does not exceed several tens of kilojoules, and requires a condenser volume of no less than several cubic meters for its accumulation.

We shall now compare an electrical discharge with the explosion of an explosive of identical energy. The rate of energy release in the case of explosions of solid explosives is determined by the rate of detonation, which is around $7 \cdot 10^5$ cm/sec. Considering that the density of the explosive is equal to approximately 1.5 g/cm^3, it is easy to find that the typical linear dimensions of charges are within the range from several centimeters to several tens of centimeters and, consequently, the energy release times are within the limits of from several microseconds to several tens of microseconds. Electrical discharges in water usually take place during times of tens to hundreds of microseconds. Thus, a significantly slower rate of energy release than occurs in the case of the explosions of solid explosives is characteristic of electrical discharges. This, of course, does not mean that in the case of electrical discharges it is fundamentally impossible to obtain a high rate of release of large amounts of energy. However, achieving rates of energy release corresponding to explosions of explosives in this case is connected with specific technical difficulties.

Because of the high rate of energy release the compression pulse emitted in the process of the explosion of an explosive has an energy reaching 60% of the energy of the charge. The pressure in it amounts to several tens of thousands of atmospheres and therefore the pulse has a shock front. The intense energy dissipation leads to a rapid drop in pressure in the compression pulse. In addition, thanks to the increased rate of propagation of the shock

wave, the duration of the compression pulse increases At distances reduced to a unit weight, on the order of 100 cm/g and more, the compression pulse created by an explosion is described, according to the data of R. Koul [1], by the formulas

$$p = p_m \exp(-t/\theta)$$
$$p_m = 7200(W^{1/3}/r)^{1.13}\ [\text{atm}]; \quad \theta = 5.68 \cdot 10^{-6} W^{1/3}(r/W^{1/3})^{0.22}\ [\text{sec}],$$

where W is the weight of the charge (in g); r is the distance (in cm).

According to these data it is easy to find that the ratio of the energy of the compression pulse to the energy of the charge at reduced distances, on the order of 100 cm/g, proves to be equal to 20%, which is close to the electroacoustic efficiency of electrical discharges in water.

The pulsation energy of the gas bubble formed by the explosion of an explosive is approximately equal to 40% of the energy of the charge, while in the case of electrical discharges it amounts to 25-30% of the energy f the discharge. The difference is explained by the fact that discharges are accompanied by significantly greater energy losses, since the matter in the discharge channel has a temperature on the order of several tens of thousands of degrees, while in the case of explosions it amounts to only several thousands of degrees.

LITERATURE

1. *Кирк Р.* Подводные взрывы. М., ИЛ, 1950.
2. *Флинн Х. Г.* Физика акустической кавитации в жидкостях. Физическая акустика, IIБ. М., изд-во «Мир», 1967.
3. *Перселл Дж.*—Сб. «Электрический взрыв проводников». М., изд-во «Мир», 1965.
4. *Ландау Л. Д., Лифшиц Е. М.* Механика сплошных сред. М., ГИТТЛ, 1954.
5. *Арсентьев Л. В.* К теории мощных электрических разрядов в жидкой среде. Канд. дисс. Гос. ун-тет, Ростов-н-Дону, 1966.
6. *Филиппов Н., Журин В., Сулаев Н.* ПФЖ, 1962. 2, № 4, 311.
7. *Окунь И. З.*— ЖТФ, 1967, 37, вып. 9, 1729—1738.